

SYSTEM-LEVEL SEISMIC PERFORMANCE OF CONCENTRICALLY BRACED FRAMES
WITH REPLACEABLE BRACE MODULES

**SYSTEM-LEVEL SEISMIC PERFORMANCE OF CONCENTRICALLY BRACED
FRAMES WITH REPLACEABLE BRACE MODULES**

By

Vahid Mohsenzadeh

B.Sc., M.Sc.

A Thesis Submitted to the School of Graduate
Studies in Partial Fulfilment of the Requirements for
the Degree

Doctor of Philosophy

McMaster University
Hamilton, Ontario, Canada
April 2020

© Copyright by Vahid Mohsenzadeh, 2020

Doctor of Philosophy (2020) (Civil Engineering)

McMaster University Hamilton, Ontario

TITLE: **System-Level Seismic Performance of Concentrically
Braced Frames with Replaceable Brace Modules**

AUTHOR: **Vahid Mohsenzadeh, B.Sc., M.Sc.**

SUPERVISOR: **Dr. Lydell Wiebe, Ph.D., P.Eng.**

NUMBER OF PAGES: **xxi, 195**

*This thesis is dedicated to my mom and dad for their love, endless support and sacrifices.
My heart pounds for you every second!*

Abstract

Current seismic design procedures are expected to result in acceptable solutions in terms of protecting people's lives during an earthquake. However, the capacity of buildings to maintain or regain functionality after an earthquake is another critical factor that has recently attracted increased attention. A recent report published by the Insurance Bureau of Canada concluded that a realistic large earthquake off the west coast of Vancouver Island would cause losses of \$75 billion, while one in eastern Quebec would cost \$61 billion. Therefore, it is crucial to consider ways to reduce the extent of damage caused by an earthquake and to design more resilient buildings that can promote functional recovery of buildings after an earthquake.

This thesis examines concentrically braced frames (CBFs) with replaceable brace modules (RBMs), where the RBMs dissipate energy through tensile yielding and in-plane compressive buckling and post-buckling behaviour. RBMs are intended to improve the constructability of braced frames by using bolts instead of field welding, and to make the brace unit more easily replaceable by confining all damage to the RBM until brace fracture.

In CBFs with RBMs, the modular brace connection allows for either simple or moment-resisting beam-column connections. Both are permitted by current design codes, but practical design considerations result in many beam-column connections in modern braced frames behaving as moment-resisting. Therefore, this thesis begins by investigating what level of fixity is required to ensure adequate collapse capacity of special concentrically braced frames (SCBFs) in accordance with the FEMA P695 methodology. Three different conditions (pinned, shear tab, and fixed) are modelled for connections within the braced bay, without and with a model to represent the contribution of the gravity framing, for three archetype buildings ranging from three to 12 storeys. The fragility curves are constructed, and the collapse capacity is assessed using the FEMA P695 methodology. The results show that the influence of gravity framing is so strong in the low- and mid-rise buildings that the connection fixity within the braced bay does not significantly influence the collapse

capacity of the system. However, the connection fixity is more influential for taller structures (12 storeys).

In the next phase of this research, the seismic demands on the columns of SCBFs with or without RBMs are investigated. The results show that current design methods lead to frequent column yielding (above the base) in flexure that is contrary to the intent of capacity design, even though the eccentricity of load on the columns when using RBMs does not significantly increase the flexural demands on the columns. Therefore, three new design methods for predicting moment demands on the columns of SCBFs are proposed and assessed. By applying these methods, columns can safely resist the seismically induced axial and flexural demands, with the additional benefit of reducing residual drifts, thus increasing the likelihood of simplified structural repairs.

Based on the knowledge gained through the initial numerical studies, this thesis culminates with large-scale substructure experimental testing to examine the seismic performance of a 70%-scale one-storey one-bay concentrically braced frame system with RBMs. Three specimens were tested to investigate three potential beam-column connections, and after testing each specimen to fracture of at least one RBM, the specimen was repaired by replacing the RBMs and the test was repeated. The results revealed that the specimens performed well, where the strength was not compromised by the RBM connections, the storey drift range was comparable to previous results for concentrically braced frames with more commonly used gusset plate connections, and the damage was confined to the intended locations. In addition, all three specimens with replaced brace modules could sustain their initial stiffness and strength after successive load reversals.

In summary, based on the current work, the recently proposed concept of replaceable brace modules, accompanied by the recommended methods for designing columns and detailing beam-column connections, appears to be a promising approach. The fabrication and installation are simpler, the seismic performance is similar to that of SCBFs with currently accepted connection detailing, and the approach can increase the post-earthquake reparability of steel concentrically braced frames.

Acknowledgements

My sincere gratitude goes to my supervisor Dr. Lydell Wiebe for his continuous support, his patience, encouragement, and guidance throughout the course of my PhD. Dr. Wiebe selflessly and patiently helped me in many different ways to become a research scientist and a free thinker I am today. I have been very lucky to be supervised by him.

Special thanks are due to my supervisory committee members, Dr. Michael Tait and Dr. Ken Sivakumaran, for their valuable comments and suggestions. I would like to thank Dr. Dawn Lehman for reviewing my work and providing insightful comments as the external examiner.

One of the significant aspects of this project was a large-scale testing program in the Applied Dynamic Laboratory (ADL) at McMaster University. I am thankful for the work provided by summer research interns Berg Ellemers and Anirban Kundu (Mitacs Globalink Research Intern). This experimental study would not have been possible without the help of technical staff (Kent Wheeler and Paul Heerema) at the ADL.

My gratitude extends to all my friends and colleagues whom I met during my journey at McMaster University for their moral supports and helpful discussions. Also, I would like to, in particular, thank Daniel Stevens, who started this research. Many thanks to my former Master's supervisor at University of Tehran, Dr. Mohammad Khanmohammadi, who taught me a lot about structural and earthquake engineering.

I would also like to appreciate the Canadian Institute of Steel Construction (CISC) and the National Sciences and Engineering Research Council (NSERC) for the financial support, Salit Steel and Atlas Tube for donating wide flange sections and HSS sections, respectively. I want to thank Walters Inc. for fabrication services.

At last, but by no means the least, I want to give a big thank you from the bottom of my heart to my parents, my lovely sisters and brother, for their love, spiritual support, and prayers as I completed this research.

Co-Authorship

This thesis has been prepared in accordance with the regulations for a ‘Sandwich’ thesis format or as a compilation of papers stipulated by the Faculty of Graduate Studies at McMaster University. Chapters 2 through 4 have been published or submitted to be considered for publication in peer-reviewed journals, for which the numerical, analytical, and experimental work was carried out solely by the author of this thesis. The work was all completed under the supervision, guidance, and review of Dr. Lydell Wiebe.

Chapter 2: Effect of beam-column connection fixity on the seismic collapse risk of special concentrically braced frames.

Authors: Vahid Mohsenzadeh and Lydell Wiebe

Published in *Soil Dynamics and Earthquake Engineering*, 115 (2018), 685-697.

Chapter 3: Seismic design of braced frame columns with and without replaceable brace modules

Authors: Vahid Mohsenzadeh and Lydell Wiebe

Submitted for Review to the *Journal of Constructional Steel Research*.

Chapter 4: Experimental investigation of a concentrically braced frame with replaceable brace modules.

Authors: Vahid Mohsenzadeh and Lydell Wiebe

Submitted for Review to the *ASCE Journal of Structural Engineering*.

Contents	
Abstract	v
Acknowledgements	vii
Co-Authorship	viii
Table of Contents	ix
List of Tables	xiv
List of Figures	xv
1 Introduction	1
1.1 Motivation	1
1.2 Seismic Design of Concentrically Braced Frames	2
1.2.1 Gusset Plate Design	2
1.2.2 Knife Plate Connection	4
1.2.3 Current Brace Connection Drawbacks	4
1.3 Overview of Previous Experimental Studies	5
1.3.1 Brace Behaviour	5
1.3.2 Gusset Plate Behaviour	6
1.3.3 Full Braced Frame System Behaviour	8
1.4 Overview of Previous Analytical Studies	10
1.4.1 Simulation of Brace	10
1.4.2 Simulation of Gusset Plate	12
1.4.3 Simulation of Full System	12
1.5 New Proposed Connection and Previous Study	13
1.6 Impetus and Research Objectives	15

1.7 Thesis Organization	17
References	19
2 Effect of Beam-Column Connection Fixity and Gravity Framing on the Seismic Collapse Risk of Special Concentrically Braced Frames	23
Abstract	23
2.1 Introduction	23
2.1.1 Motivation	23
2.1.2 Background	25
2.1.3 Paper Organization	27
2.2 Details of Archetype Buildings	27
2.3 Numerical Modelling	29
2.4 Ground Motion Selection and Scaling	34
2.5 Example Near-Collapse Response of Six-Storey Building	36
2.5.1 Models without Gravity Framing	36
2.5.2 Models with Gravity Framing	39
2.6 Collapse Risk Assessment	40
2.6.1 Influence of Connection Fixity on Collapse Risk without Modelling Gravity Framing	41
2.6.2 Influence of Gravity Framing on Collapse Risk	43
2.6.3 Influence of Gravity Columns Alone on Collapse Risk	44
2.6.4 Influence of Damping Model on Collapse Risk	48
2.7 Inter-Storey Drift Response	49
2.8 Summary and Design Recommendations	52
Acknowledgments	54

References	54
3 Seismic Design of Braced Frame Columns with and without Replaceable Brace Modules	59
Abstract	59
3.1 Introduction	60
3.1.1 Brace Connection Design	60
3.1.2 Column Design	61
3.1.3 Objectives	63
3.2 Design of Reference SCBFs	64
3.3 Nonlinear Modelling	66
3.4 Ground Motion Selection and Scaling	70
3.5 Column Demand in SCBFs	71
3.5.1 Models with Elastic Columns	71
3.5.2 Models with Inelastic Columns	76
3.6 Alternative Column Design Provisions	79
3.7 Application to Example Structures	83
3.7.1 Influence of Modified Design Procedures on Collapse Risk of SCBFs	84
3.7.2 Column Strength Utilization	87
3.7.3 Residual Drifts	89
3.8 Summary and Design Recommendations	91
Acknowledgments	92
References	93
4 Experimental Investigation of a Concentrically Braced Frame with Replaceable Brace Modules	97

Abstract	97
4.1 Introduction	98
4.2 Experimental Program	100
4.2.1 Reference Structure	100
4.2.2 Test Setup	101
4.2.3 Test Specimens	103
4.2.4 Beam-Column Connection Details	105
4.2.5 Loading Protocol and Control	107
4.3 Experimental Observations	109
4.3.1 Specimen 1 with Single Shear Tab Connections (STC)	109
4.3.2 Specimen 2 with End Plate Connection (EPC)	113
4.3.3 Specimen 3 with Bolted Unstiffened Extended End Plate Connection (BUEEPC)	116
4.3.4 General Observations	118
4.4 Brace Behaviour	119
4.5 Contribution of Frame Action	121
4.6 Connection Behaviour	122
4.7 Conclusions	125
Acknowledgments	126
References	127
5 Conclusion and Recommendations	130
5.1 Summary	130
5.2 Conclusions	131

5.2.1 Effects of Beam-Column Connections Fixity and Gravity Framing on Collapse Capacity of Special Concentrically Braced Frames	131
5.2.2 Seismic Design of Braced Frame Columns	132
5.2.3 Large-Scale Experimental Testing of a Concentrically Braced Frame with Replaceable Brace Modules	133
5.3 Recommendations for Further Research	134
References	135
Appendix A New Connection Design Examples	136
A.1 Material Properties	136
A.2 Brace Overstrength Resistance and Predicted Yield Drift	136
A.3 Hinge Plate Design	139
A.3.1 Hinge Plate Dimensions	139
A.3.2 Design of Bolts between Hinge Plate and Support Plate	140
A.3.3 Hinge and Support Plate Thickness	141
A.3.4 Hinge Plate Buckling	143
A.3.5 Hinge Plate to Brace Weld	143
A.3.6 Brace Slot Cover Plates	144
A.3.7 Support and Stiffener Plates	145
A.3.8 Bearing Strength of the Beam	146
A.4 Beam-Column Connections	147
A.4.1 Single Shear Tab Connection	148
A.4.2 End Plate Connection	151
A.4.3 Bolted Unstiffened Extended End Plate Connection	153
Appendix B SCBF with RBMs Subassembly Shop Drawings	161

Appendix C Experimental Study Instrumentations	186
C.1 Hinge Plate Rotation	187
C.2 Brace Center Displacement	188
C.3 Frame Inter-Storey Drift	190
C.4 Beam-to-Column Connection Rotation	190
C.5 Strain Gauges	191
C.5.1 Brace Axial Force	191
C.5.2 Column Forces	192
C.6 Data Acquisition System	192
C.7 Actuator and Reaction Frame	193

List of Tables

Table 2.1 Seismic design parameters -----	28
Table 2.2 Section sizes for SCBFs -----	29
Table 2.3 Fundamental periods for models with different modelling assumptions (s) ---	34
Table 2.4 Collapse results for all SCBF models -----	45
Table 3.1 Seismic design parameters -----	65
Table 3.2 Section sizes-----	66
Table 3.3 Collapse analysis results for frames designed considering only axial demands -----	79
Table 3.4 Fundamental periods -----	84
Table 3.5 Column sections from different design methods-----	85
Table 3.6 Collapse analysis results for frames designed considering flexural demands using proposed methods-----	87
Table 4.1 Details of braces -----	105
Table 4.2 Summary of frame behaviour-----	119
Table 4.3 Summary of frame behaviour-----	121

List of Figures

Figure 1.1 Brace connection details: (a) liner offset, (b) elliptical offset and (c) midspan gusset plate offset, (d) knife plate configured for in-plane buckling.-----	4
Figure 1.2 Test setup schematic [17] -----	7
Figure 1.3 Test setup schematic [9]-----	10
Figure 1.4 Schematic illustration of proposed multi-element beam-column element (a) initial imperfection (b) monitored integration points (c) ability to model multiple cross sections (d) uniaxial material model [9] -----	12
Figure 1.5 Replaceable brace module connection details-----	14
Figure 1.6 Experimental setup [29] -----	15
Figure 1.7 Dissertation flowchart -----	17
Figure 2.1 Brace connection details; a) Linear hinge zone b) Elliptical hinge zone c) Knife plate configured for in-plane buckling d) Proposed replacement/modular connection-----	25
Figure 2.2 a) Plan configuration of three- and six-storey buildings b) Plan configuration of 12-storey building -----	28
Figure 2.3 a) Schematic of numerical model for six-storey SCBF. b) Leaning column without or with the simulation of lateral load resisting contribution of gravity framing. c) Composite shear-tab connection behaviour (compared to [15]). d) Global hysteretic behaviour of two-storey SCBF (compared to [10])-----	30

Figure 2.4 Scaled mean 5%-damped spectra for considered stripes, compared with DBE and MCE code-based spectra, for a)3-storey b)6-storey c)12-storey building	36
Figure 2.5 Dynamic response of the 6-storey SCBF for the Nishi-Akashi record from the Kobe 1995 ground motion at a scale factor of 3.8 (1.25MCE)	38
Figure 2.6 Sequence of damage during Nishi-Akashi record from the Kobe 1995 ground motion at a scale factor of 3.8	38
Figure 2.7 Collapse fragility curves for three-, six-, and 12-storey SCBF a)without gravity framing contribution b)with gravity framing contribution	42
Figure 2.8 Collapse fragility curves for a) three-, b) six-, and c) 12-storey SCBF considering only the contribution of gravity columns	48
Figure 2.9 Collapse fragility curves for a) three-, b) six-, and c) 12-storey SCBF without gravity framing contribution and fixed connections	49
Figure 2.10 Peak inter-storey drift ratios for (a) 3-storey building (b) 6-storey building (c) 12-storey building	50
Figure 2.11 DCF index values at MCE level for different models considering a) connection fixity and gravity framing effects b) connection fixity and gravity column effects	52
Figure 3.1 Brace to frame elements connection details: Typical gusset plate with a) linear hinge zone, b) elliptical hinge zone; proposed connection with c) single shear tab, and d) bolted unstiffened extended end plate connection	61
Figure 3.2 Plan configuration of a) three- and six-storey buildings b)12-storey building	65

Figure 3.3 a) Schematic of the numerical model for six-storey SCBF b) Connections in SCBF with conventional connection c) Connections in SCBF with RBMs -----	69
Figure 3.4 Scaling of the selected ground motions for a)three-storey building b)six-storey building c)12-storey building-----	71
Figure 3.5 Median demand-to-capacity ratios of columns of three-storey SCBF with and without RBM -----	72
Figure 3.6 Median demand-to-capacity ratios of columns of six-storey SCBF with and without RBM -----	74
Figure 3.7 Median demand-to-capacity ratios of columns of 12-storey SCBF with and without RBM -----	75
Figure 3.8 Median peak inter-storey drift ratio for: a & b) three-storey, c & d)six-storey, e & f)12-storey SCBFs -----	77
Figure 3.9 Collapse fragility curves a) three-storey b)six-storey c)12-storey SCBF -----	79
Figure 3.10 Analysis procedure to determine column moment demand a) bending moment diagram on braced bay columns from ETABS, b) Method 3 approximation for finding column moments -----	82
Figure 3.11 Storey shear demand-to-capacity ratio for a) three-storey and b)six-storey and c)12-storey SCBFs -----	84
Figure 3.12 Collapse fragility curves for SCBFs with different column sections: a, b)three-storey, c, d)six-storey, and e, f)12-storey SCBFs -----	86

Figure 3.13 Demand-to-capacity ratios of columns of three-, six- and 12-storey SCBF with and without RBMs using modified design methods at MCE -----	89
Figure 3.14 Fragility curves for maximum inter-storey residual drift ratios over all storeys for SCBFs with RBMs -----	91
Figure 4.1 Replaceable brace module connection details-----	100
Figure 4.2 Reference building in Vancouver, BC: (a) plan, (b) considered bay, (c) schematic deformed shape and associated column moment diagram, (d) prototype specimen -----	101
Figure 4.3 Overview of the experimental setup: (a) annotated drawing, (b) photograph -----	103
Figure 4.4 Tested connection details: (a) specimen 1 with shear tab connection (STC), (b) specimen 2 with end-plate connection (EPC), and (c) specimen 3 with bolted unstiffened extended end-plate connection (BUEEPC)-----	106
Figure 4.5 Loading protocol -----	108
Figure 4.6 Normalized lateral force versus inter-storey drift hysteresis loops: (a) and (b) Specimen 1 (with shear tab connection), (c) and (d) Specimen 2 (with end plate connection), (e) and (f) Specimen 3 (with bolted unstiffened extended end plate connection) -----	111
Figure 4.7 Specimen 1 (with STC): (a) initial north brace in-plane buckling; (b) south brace local cupping; (c) south brace fracture; (d) north brace bottom hinge plate; (f) north brace top hinge plate -----	112

Figure 4.8 Specimen 2 (with EPC): (a) north brace in-plane buckling; (b) column web yielding in the lower north beam-column connection at the end of the first phase; (c) added a diagonal stiffener -----	115
Figure 4.9 Specimen 3 (with BUEEPC) after completion of loading cycles beyond brace fracture: (a) north column yielding; (b) bottom south beam-column connection panel zone; (c) bottom south beam-column connection-----	117
Figure 4.10 Frame contribution to storey shear: (a) Specimen 1 (with STC); (b) Specimen 2 (with EPC); (c) Specimen 3 (with BUEEPC)-----	122
Figure 4.11 Connection rotation vs inter-storey drift: (a) Specimen 1 (with STC); (b) Specimen 2 (with EPC); (c) Specimen 3 (with BUEEPC)-----	124
Figure 4.12 (a) STC connection at 0.032 rad rotation; (b) EPC connection at 0.022 rad rotation; (c) BUEEPC connection at 0.02 rad rotation -----	124
Figure A-1 Axial Force-deformation relation for used braces -----	138
Figure A-2 Applied forces in tension and compression-----	139
Figure A-3 Hinge plate detail-----	141
Figure A-4 Block shear failure modes-----	143
Figure A-5 Proposed connection details -----	148
Figure A-6 Connection free body diagram -----	149
Figure A-7 Shear tab connection details -----	151
Figure A-8 End plate connection details -----	153
Figure A-9 Bolted Unstiffened End plate connection free body diagram -----	154
Figure A-10 Bolted Unstiffened End plate connection details-----	160

Figure C-1 Instrumentation setup (Dimensions are in mm)-----	186
Figure C-2 Lower-south hinge plate connection-----	188
Figure C-3 Parallel brace displacement string pots and pivot plate setup-----	188
Figure C-4 Brace center displacement method-----	189
Figure C-5 Connection rotation setup -----	190
Figure C-6 Connection rotation setup pictures -----	191
Figure C-7 Column force determination figure -----	192
Figure C-8 Loading frame beam-column connections -----	194
Figure C-9 Out-of-plane implement cylinder details-----	194
Figure C-10 End connection details of the out-of-plane implement cylinder -----	195

1 Introduction

1.1 Motivation

Current seismic design procedures are able to control effectively the casualties caused by earthquakes. However, the economic loss and the social influence are still enormous. After the 2011 Christchurch earthquake in New Zealand, a preliminary damage assessment of buildings found that 1933 of 3621 buildings checked within Central Business District were collapsed or in need of demolition, while 826 were in need of significant repair [1]. The 2010 and 2011 Christchurch earthquakes caused reconstruction costs of over 40 billion NZD [2]. Considering seismic design in Canada, a recent report published by the Insurance Bureau of Canada [3] concluded that a realistic large earthquake (with a probability of occurrence of 1-in-500 years) off the west coast of Vancouver Island would cause losses of \$75 billion CAD, while one in eastern Quebec would cost \$61 billion CAD. These significant economic losses clearly show that engineers need to consider alternative ways to mitigate damage and develop more resilient and sustainable cities for the future.

While damage to buildings and infrastructure causes direct economic loss due to an earthquake, an earthquake also results in indirect economic loss because of temporary suspension or reduced use of the structures. This indirect loss can be reduced if the structures can regain their functionality quickly after the earthquake. For that reason, the study of earthquake resilient structures has become one of the new promising directions in the earthquake engineering. An earthquake resilient structure is a structure that can rapidly restore its structural functionality after a severe earthquake without significant repair [4]. One way of making more earthquake resilient structures is by using replaceable structural components, where the damage due to the earthquake will concentrate on these components that can be easily replaced after the earthquake. This allows the structures to be more easily repairable after the earthquake.

With this in mind, the concentrically braced frame (CBF) with replaceable brace modules (RBMs) is a system that reduces the time and cost of initial installation and allows for quick and cost-efficient repairs after an earthquake. This thesis focuses on the system level performance of a CBF with RBMs, and proposes some design recommendations and detailing for real-life applications.

1.2 Seismic Design of Concentrically Braced Frames

Concentrically braced frames (CBFs) are one of the most common lateral force resisting systems as they can economically provide significant amounts of lateral strength and stiffness, which increases the likelihood of buildings being serviceable after small-to-moderate and frequent earthquakes. A special concentrically braced frame (SCBF) is a category of concentrically braced frame (CBF) system that is capable of providing significant inelastic deformation capacity, as defined in AISC 341-16 [5]. In Canada, CSA S16-14 refers instead to moderately ductile concentrically braced frames (MD-CBFs), which have generally similar design requirements to SCBFs and can also be used in regions of high seismicity [6]. During a moderate to a severe earthquake, the braces are expected to experience considerable inelastic deformation through tensile yielding, buckling and post-buckling behaviour of braces. Gusset plate connections need to be deformation compatible by permitting brace buckling. The structure should tolerate this large inelastic deformation without loss of life or building collapse. To ensure that SCBFs will achieve these large inelastic deformations without premature failure, the capacity design of beams, columns and gusset plate connections is necessary. In this way, braces will be able to yield and buckle without undesirable and unpredicted failure modes, maximizing energy dissipation and displacement capacity prior to brace fracture.

1.2.1 Gusset Plate Design

Seismic behaviour and performance of the gusset plate, which joins the brace to the beam and column, can play a critical role in the seismic behaviour of the CBFs. Improper design

of this connection will result in poor performance, less energy dissipation and low ductility capacity [7]. Current AISC seismic provisions [5] and CSA S16-14 [6] require that adequate strength in the connection be provided such that the yielding and buckling of the brace can be achieved. AISC seismic provisions and CSA S16-14 also require that the brace-to-frame connection should either resist the flexural resistance of the brace or provide a condition to permit end rotation of the brace to accommodate brace buckling. Out-of-plane buckling of the brace is accommodated using geometrical limits on the gusset plate relative to the end of the brace to permit brace rotation. A $2t_p - 4t_p$ linear clearance distance, proposed by Astaneh-Asl et al. [8], between the end of the brace and the hinge line is commonly employed (Figure 1.1(a)). Satisfying this requirement with rectangular gusset plates leads to very large plates, which can result in uneconomical seismic design [7]. Moreover, premature toe weld fractures can occur at the gusset plate welds due to opening and closing moments on the connections, which can negatively affect the ductility and of energy dissipation of the system [9].

Lehman et al. [7] conducted tests on single-storey single-bay specimens to investigate the performance of the frame while considering two different brace clearance requirements (a linear clearance or an elliptical clearance) (Figure 1.1(a-b)). It was observed that elliptical clearance using a balance design procedure [10] provides equal or better performance than the linear clearance. The gusset plates are also more compact relative to gusset plates with linear clearance which improves the constructability of braced frames. According to their test results, using an elliptical clearance distance for the corner gusset plate will permit the frame to experience acceptable displacement capacity, which exceeds that of achieved in frames with current linear clearance for gusset plates. As shown in Figure 1.1(c), this clearance for the midspan gusset plate was proposed to be $6t_p$ [11]. The elliptical clearance and the linear clearance are the same for plates tapered to Whitmore width.

1.2.2 Knife Plate Connection

When using the typical connection details shown in Figure 1.1 (a-c), the plastic hinges that form in the gusset plates cause the brace to buckle in the out-of-plane direction. Out-of-plane buckling can cause damage to the interior partitions or exterior cladding, creating a potential hazard for building residents [12]. In order to limit the brace buckling in the plane of the frame and to avoid toe weld fracture, a knife plate can be used perpendicular to the gusset plate (Figure 1.1(d)) [11]. The knife plate is commonly slotted and directly welded to the gusset plate. Experimental studies have shown that the proposed knife plate to gusset and brace connection performed satisfactorily and it would sustain the peak force to large drifts during the ground motions [13].

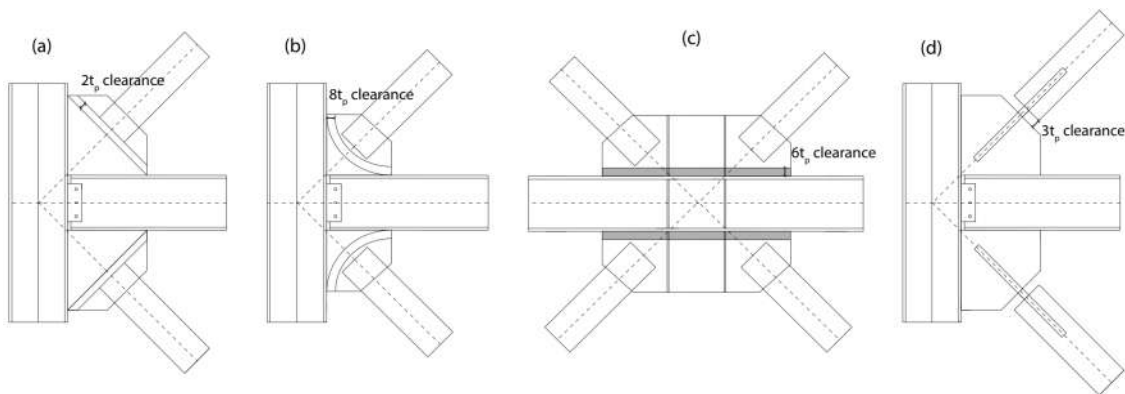


Figure 1.1 Brace connection details: (a) liner offset, (b) elliptical offset and (c) midspan gusset plate offset, (d) knife plate configured for in-plane buckling.

1.2.3 Current Brace Connection Drawbacks

There are a few issues with all the connections shown in Figure 1.1. The first is that field welding is required for connecting the brace to the gusset plate, which is relatively time-consuming. Next, in addition to the need to replace a brace after significant inelastic excursions, a gusset plate that yielded to accommodate brace buckling may also need to be replaced out of concern for its remaining low-cycle fatigue life; this is expected to be a relatively time-consuming process as it would require removing the welds to replace the

plate. Furthermore, significant local yielding deformation in the beam and column adjacent to the gusset plate have been observed as a result of frame action induced by the rigidity of the gusset plates [7], further increasing the number of elements that would need to be repaired or replaced after an earthquake.

1.3 Overview of Previous Experimental Studies

Many experimental tests have been done to better understand the behaviour of SCBFs and predict more accurately the failure modes of these systems. The focus of these experimental studies can be categorized into three groups: brace behaviour, gusset plate behaviour and full braced frame system.

1.3.1 Brace Behaviour

Investigation of inelastic response of steel brace elements under cyclic loading was the topic of many physical tests (e.g. [14,15]). A survey of past experimental studies on hysteretic behaviour of diagonal braces under cyclic loading was presented in a paper by Tremblay [16]. In this study, the author gathered information from nine experimental studies, including 76 specimens. The following parameters were investigated: buckling strength of braces, maximum tensile resistance, post-buckling compressive capacity, lateral deformation of braces and fracture life of hollow structural sections (HSS). Using these test results, some equations were proposed to determine the minimum post-buckling strength of brace at different ductility demands. The author also proposed an equation to compute the lateral deformation of braces, which should be accounted for in design if it can damage the adjacent walls or non-structural elements.

Shaback and Brown [15] investigated the behaviour of full-scale HSS braces with typical gusset plates under cyclic loading. In this study, nine HSS specimens of various sizes with rectangular gusset plates were considered. A regular slotted connection was used to join the brace to the gusset plate. The specimen slenderness ratio varied from 69 to 93, and

width to thickness ratios were between 11.9 and 15.1. The predetermined hinge length in the gusset plate ranged from 1.25 to 2.00 times the thickness of the plate. The following conclusions were made according to these experiments:

- The effective slenderness ratio is the most critical parameter influencing the hysteresis of the specimens. It was seen by reducing the slenderness ratio the brace members exhibited greater energy dissipation.
- Hollow structural sections tend to concentrate yielding deformations at corners of the section. These corners are located where the crest of primary local buckle had previously formed on the compressive side of the brace.
- Local buckling in compression followed by tension loading is required for fracture of HSS bracing elements to happen.
- The width to thickness ratio of the HSS sections is the most critical parameter that can affect the fracture life. The slenderness of the element and strength of the material are less important.
- Slender braces can experience a higher ductility ratio before fracture. The reason most likely refers to the fact that strain demand in the plastic hinge reduces in braces with higher slenderness.

1.3.2 Gusset Plate Behaviour

To develop new strategies for improving SCBF seismic behaviour and improve gusset plate design, 32 single-storey single-bay full-scale diagonal braced frames were tested at the University of Washington ([17-20]). Figure 1.2 shows the general test setup. In these tests, various gusset plate connection design parameters were investigated including shape and thickness of the gusset plate, weld type, types and sizes of clearance on the plate and beam-column connection. Based on this investigation, two main design recommendations were proposed for the seismic design of SCBFs. The first is the elliptical clearance model instead of the commonly used linear clearance model proposed by Astaneh-Asl et al. [8]. The

second one is a balanced design procedure (BDP) for special concentrically braced frames. In this procedure, in order to maximize the drift capacity, instead of limiting the displacement capacity to the yielding/buckling of braces, a balance between all yield mechanisms (including brace yielding/buckling and gusset plate yielding) and all failure modes of the system is considered. This procedure will result in promoting the ductility of the system and preventing undesirable failure modes [10].

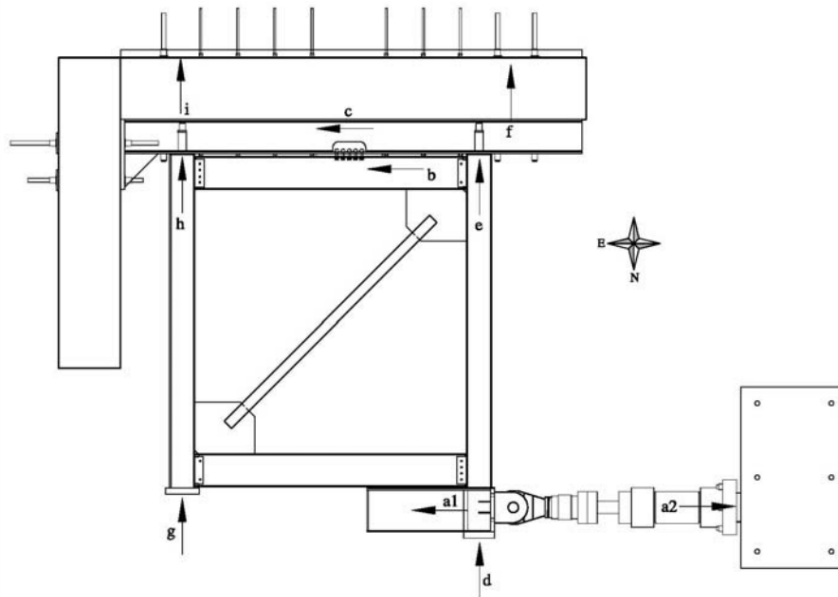


Figure 1.2 Test setup schematic [17]

The University of Washington test program enhanced the understanding of the seismic behaviour of concentrically braced frames by providing the following conclusions (among others):

- The gusset plate connection and the brace cross-section can significantly influence the seismic performance of concentrically braced frames.
- Gusset plate flexural yielding will occur after brace initial buckling, which reduces local brace buckling, damage to the welds at the intersection of the gusset and beam and

column, and local yielding deformation in the beam and column adjacent to the gusset plate.

- Gusset plates should be detailed following capacity based design. However, excess strength and stiffness will shorten the inelastic length of the brace and cause early brace fracture.
- Gusset plates with the elliptical clearance are smaller and more compact relative to gusset plates with linear clearance. They also increase the deformation capacity of the system.
- The system response is highly dependent on the inclusion of beams and columns.

Researchers at University of Washington also studied the deficiencies of bolted connections which were used in older CBFs built prior to 1988 [21]. In this study, bolted gusset plate to column and beam connections, representative of older construction, were tested using eight specimens and the test setup shown in Figure 1.2. It was found that generally the bolted connections are more robust compared to welded connections.

1.3.3 Full Braced Frame System Behaviour

In some other studies the seismic performance of full-scale multi-storey concentrically braced frames was investigated ([9,11,22]). Uriz and Mahin [9] tested a full-scale two-storey braced frame with HSS elements as braces and tapered gusset plates (Figure 1.3). Their objectives were to improve understanding of the seismic performance of concentrically braced frames and to gather some information to improve analytical tools to predict the dynamic behaviour while considering damage due to low cycle fatigue. The specimen was designed in compliance with AISC seismic design provisions [23], and columns were designed using the amplified lateral load corresponding to Ω_0 (the overstrength factor) times the nominal ultimate design load for the frame. All the damage concentrated in the lower storey immediately after the brace buckled in the first storey. Figure 1.3 shows that the specimen was loaded from the top beam, which means that the

shear force was equal for the two stories. From this, researchers concluded that probably braced frames are more susceptible to soft stories than other lateral systems. Large inelastic local deformation and force demand on the beam and column adjacent to the gusset plate connection were observed. Yielding in the column base and column fracture at the beam-column connection were seen. This implies that the behaviour of the braced frames is highly system dependent and in order to predict the performance accurately, the interaction between frame elements must be considered. In this research, the uniform force method and conventional detailing requirements were used for joining the gusset to the frame members. The gusset plate-beam-column connection resulted in considerable moment frame behaviour. Once the braces buckled in the lower storey, the beam-column connections started to contribute to resisting the lateral load, such that the beam and column framing could develop about 30% of the peak lateral resistance. The beam-column connection exhibited complex local behaviour when it transferred the moment from the beam and brace to the column, while this was not considered in the initial design.

Lumpkin [10] tested three full-scale, three-storey, single-bay frames with a two-storey X configuration for the first two storeys and a chevron configuration at the top storey. The cyclic loading was applied through the third storey slab, and the system also included the composite floor slab. The test specimens were designed following the balanced design procedure, where $8t_p$ elliptical clearance model and $6t_p$ linear clearance model were used for the corner gusset plates and midspan gusset plates, respectively. Additionally, the effect of varying brace shape and brace buckling direction were also examined. This study further showed that all of the components and their interaction influence the inelastic response of concentrically braced frame systems.

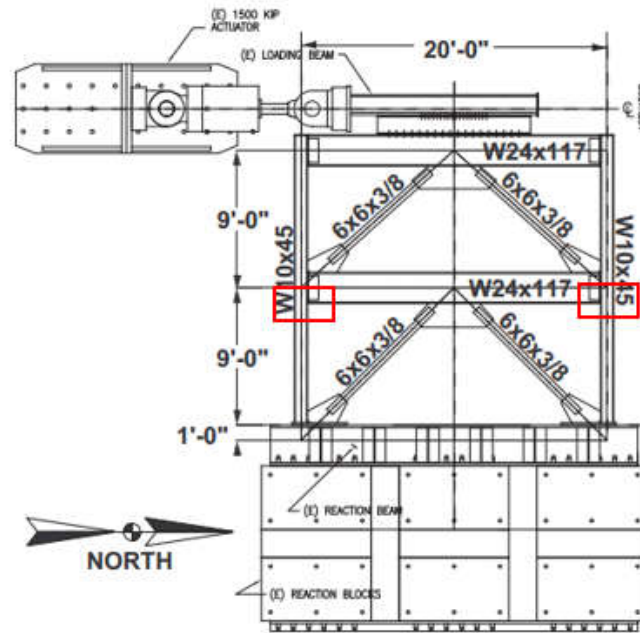


Figure 1.3 Test setup schematic [9]

1.4 Overview of Previous Analytical Studies

1.4.1 Simulation of Brace

In addition to previous experimental investigations, some analytical studies have been conducted to improve analytical models to predict the brace frame response more accurately. The highly nonlinear behaviour of braces can play a major role and strongly influences the overall seismic behaviour of braced frames. Three main types of analytical models have been proposed and used in previous studies to simulate the brace behaviour: (a) phenomenological models, (b) physical-theory models, (c) finite element (FE) models. In phenomenological models, some simplified hysteretic rules are used to imitate experimentally observed axial force-axial displacement behaviour. These analytical models are usually one-dimensional truss elements and hence they are simple. While these models are computationally efficient, their accuracy is often uncertain because some parameters are necessary, which are hard to obtain properly, to be defined to control the

shape of hysteretic behaviour [9]. Physical-theory models are intermediate models between phenomenological and FE approaches and consist of two elastic struts and a plastic hinge model. It is assumed that the inelastic deformation of the brace concentrates in the plastic hinge located at the mid-length of the brace [24]. For using this model, only the material properties and geometric properties of the brace element are needed. While FE models are computationally expensive, they are more and more commonly used as computational capacity increases. Uriz and Mahin [9] proposed an FE brace model using the OpenSees framework to achieve both high accuracy and computational efficiency. This modelling procedure uses fibre beam-column elements to capture the nonlinear cyclic yielding and buckling behaviour of braces, including using a rain-flow counting procedure within individual fibres to model fracture due to low-cycle fatigue. To induce the buckling behaviour of the brace, an initial imperfection of 0.05%-0.1% of brace length is required. This fibre model has some important limitations: cross-section distortion cannot be modelled, local buckling is not considered, and multi-axial stress states are ignored. Figure 1.4 shows the proposed model schematically.

Simulation of brace fracture has been the focus of other previous nonlinear modelling recommendations as well. Hsiao et al. [25] proposed a fracture criterion based on the maximum strain range (MSR) using force-based beam-column elements. More recently, Sen et al. [26] proposed a new brace fracture model based on the MSR approach using displacement-based beam-column elements, which was found to work reasonably well for rectangular HSS braces.

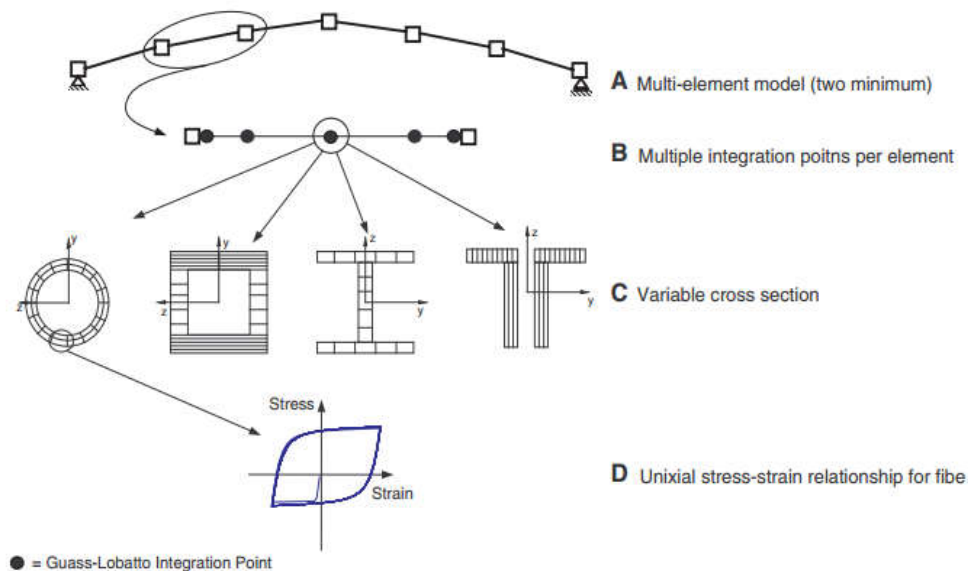


Figure 1.4 Schematic illustration of proposed multi-element beam-column element (a) initial imperfection (b) monitored integration points (c) ability to model multiple cross sections (d) uniaxial material model [9]

1.4.2 Simulation of Gusset Plate

While the gusset plate connection has often been simplified as pinned or fixed (e.g. [7]), experimental results showed that inelastic deformations of the brace place significant secondary yielding deformation demands on beams, columns, and connections, which cannot be captured accurately by pin-ended or rigid end connections for the brace. Hsiao et al. [27] proposed a new connection model to simulate the gusset plate behaviour. The proposed model was able to simulate the global behaviour of the braced frames accurately and provided acceptable predictions for many local behaviours.

1.4.3 Simulation of Full System

Many researchers have investigated the seismic performance of concentrically braced frames through simulation. Uriz and Mahin [9] conducted an analytical study on the risk assessment of low- and mid-rise steel braced frames. Hsiao et al. [28] investigated the appropriate value of reduction factors (R) for the seismic design of steel braced frames.

They suggested that for low-rise SCBFs, smaller R values relative to the current value proposed by the codes is required, whereas the mid- and high-rise SCBFs can still be designed using existing code recommendations.

1.5 New Proposed Connection and Previous Study

More recently, a new connection has been proposed based on a replaceable brace module for the seismic design of concentrically braced frames (see Figure 1.5) [29] which avoids the concerns as mentioned earlier of more conventional gusset plate connections, meeting the following criteria:

- 1- The new alternative connection does not require field welding and bolts are used for connecting the brace to the support plate (shop-welded/ field-bolted connection). This improves the constructability of SCBFs by providing easier and more accurate installation.
- 2- A bolted connection is used for joining the brace to beam, which confines all the damage to an easily replaceable assembly and results in fast repairs in the event of damage.
- 3- The brace buckles in the in-plane of the frame direction. In-plane buckling reduces the damage to partitions and cladding, resulting in less dramatic consequences to the building occupants.

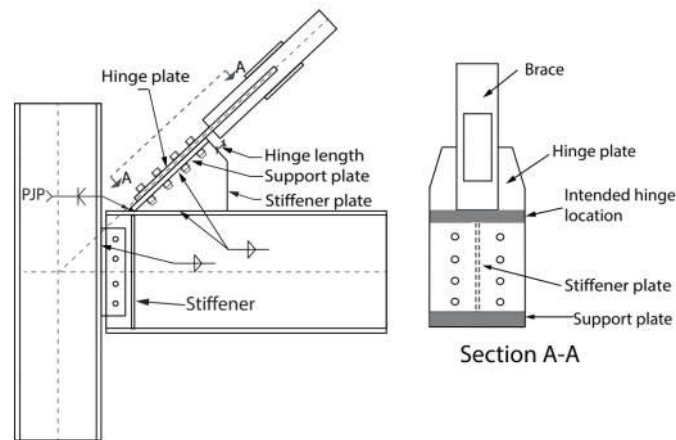


Figure 1.5 Replaceable brace module connection details

Stevens and Wiebe [29] conducted an experimental study at the component level to ensure that a brace with the new alternative connection would be able to provide the desired benefits, and that its seismic performance would be comparable to braces with conventional gusset plate connections. Eight 2:3 scale brace specimens with hollow structural sections were rotated 45 degrees and loaded vertically, and the connections were designed to simulate the end connection in a real braced frame (see Figure 1.6). The brace section, hinge plate thickness, hinge length and single-sided or double-sided splice connection were varied between the specimens. According to the test results, these conclusions were made:

- For all the specimens, the brace buckled in the in-plane direction and connection failure was not observed for any specimen.
- The damage was completely confined to a replaceable assembly.
- The hysteretic behaviour of replaceable brace modules with the new proposed connection was comparable with what would be expected with more conventional practice.
- The drift range of each specimen was primarily influenced by the width-to-thickness ratio of the brace shape used.

- A hinge plate can provide a large amount of rotational stiffness. Hence for determining the effective buckling length, its effect should be considered.
- Bolt slip did not have a considerable effect on hysteretic behaviour.

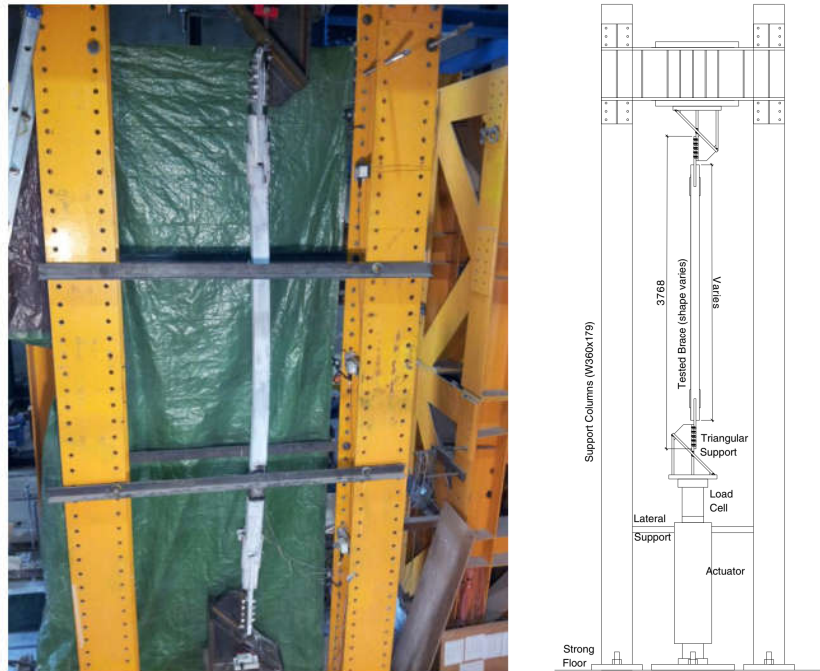


Figure 1.6 Experimental setup [29]

Although this study enhanced the understanding of the seismic behaviour of brace with the new connection, it was not able to explore questions related to replaceability and yielding or damage in the beam and the column.

1.6 Impetus and Research Objectives

Although the experimental study of RBMs at the component level showed a promising alternative connection, braced frame behaviour is highly system dependent and thus requires considering the contribution of frame elements.

The primary objective of this research study is to develop a greater understanding and quantitative characterization of the seismic performance of SCBFs with RBMs. This study evaluates the overall system-level behaviour of a braced frame with this recently proposed connection detail. As shown in Figure 1.7, it was necessary to address two key questions related to the design requirements for SCBFs with RBMs before an experimental program could be designed that would represent how this system would behave in practice. Based on the questions shown in Figure 1.7, the following research objectives were defined:

- 1- Assess the effect of beam-column connection fixity within the braced bay, and of gravity framing, on the collapse capacity of seismically designed concentrically braced frames.
- 2- Assess the influence of the column design parameters on the seismic response of SCBFs with or without RBMs, and propose new methods for considering moment demands for designing the columns to achieve a minimum acceptable margin of safety against collapse.
- 3- Propose and design beam-column connections that can be used in SCBFs with RBMs. Conduct a large-scale system-level experimental study with realistic boundary conditions to validate the seismic performance of braced frames with initial and replaced RBMs, and to examine the replaceability of RBMs.

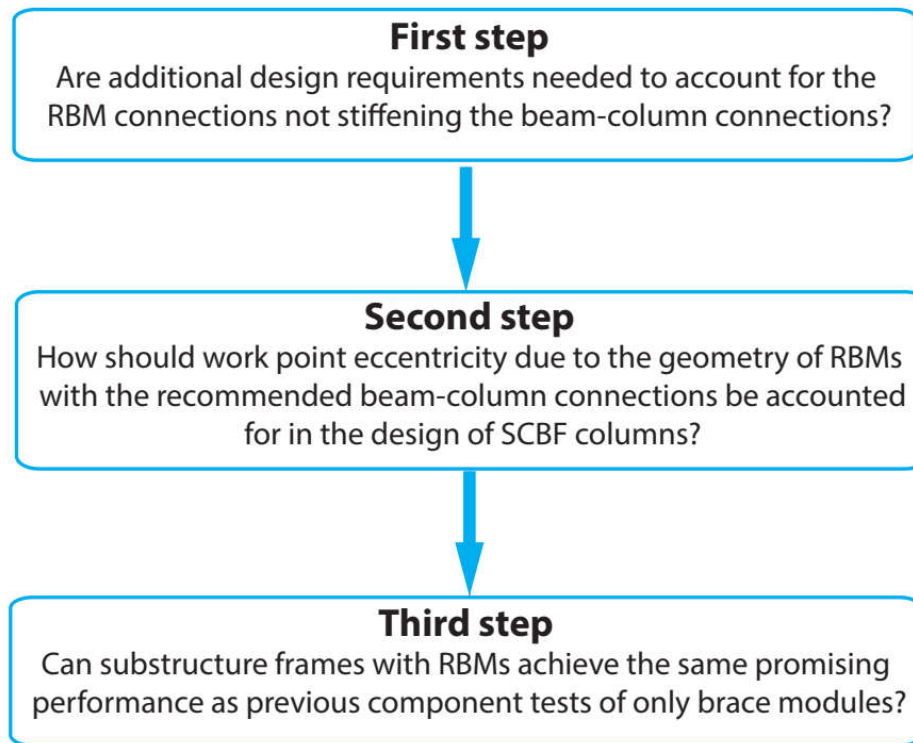


Figure 1.7 Dissertation flowchart

1.7 Thesis Organization

This thesis was prepared in accordance with the regulations of a “sandwich” thesis format containing previously published and prepared material. Since Chapter 2 to Chapter 4 were prepared to become stand-alone journal manuscripts, each chapter has its own introduction, conclusion and bibliography. Some overlap might exist between chapters, mainly in the introduction part of each.

This thesis comprises five chapters:

- Chapter 1 presents the motivation of the research. A literature review of prior experimental and analytical investigations is provided in this chapter, including

the description of the new alternative connection that can be used in SCBFs. Finally, the objectives of the research are stated.

- Chapter 2 contains the seismic collapse risk assessment of three SCBFs with different connection fixity within the braced bay, following the FEMA P695 methodology. In conventional gusset plate connections, the gusset plate can increase the strength and stiffness of the connection significantly. This provides a source of reserve capacity by developing frame action in the beams and the columns at larger drifts, which can prevent the structure from collapse [30]. However, the new alternative connection does not include a gusset plate. Therefore, this chapter examines the effects of connection fixity at the beam-column connections and of gravity framing on the collapse capacity of the SCBF buildings. The influence of the damping model is also investigated.
- Chapter 3 presents a study conducted with the objective of developing provisions for designing the columns in SCBFs. Three SCBFs of different heights are designed following the latest seismic design codes. Two different brace-to-frame connection models are used: conventional gusset plate connection, and the new connection for RBMs. The seismic performance of the structures is discussed in terms of seismic demands on columns and collapse capacity. New design recommendations for considering the flexural demand on columns in braced frames are presented and examined. Collapse fragility curves are constructed after considering the new recommendations for designing the columns.
- Chapter 4 presents a large-scale experimental program that was designed based on the recommendations that were identified in Chapters 2-3 as necessary to ensure that SCBFs with RBMs could have the desired system-level structural performance. It discusses the seismic behaviour and performance of three single-storey SCBF substructures with replaceable brace modules, including a description of the experimental program, building layout, test setup, loading

protocol and instrumentation of the specimens. The design of these specimens is described in greater detail in Appendix A, the shop drawings are given in Appendix B, and additional details related to instrumentation are provided in Appendix C. Three different beam-column connections are considered and designed to be used in SCBFs with RBMs including: a single shear tab connection, end-plate shear connection, and bolted unstiffened extended end-plate moment connection. Recommendations are made for the selection of the beam-column connection based on the experimental results.

- Chapter 5 concludes the thesis. It summarizes the important findings and provides recommendations for the continued research and development of the new connection.

References

- [1] Kam W, Akguzel U, Pampanin S. 4 Weeks On: Preliminary reconnaissance report from the Christchurch 22 Feb 2011 6.3 Mw Earthquake. Christchurch, New Zealand. New Zeal Soc Earthq Eng Inc 2011:1–6.
- [2] Radio New Zealand, 2012. “Christchurch rebuild cost put at \$40b.” Available from: [http://www.radionz.co.nz/news/national/133745/christchurch-rebuild-cost-put-at-\\$40b](http://www.radionz.co.nz/news/national/133745/christchurch-rebuild-cost-put-at-$40b), Accessed January 28, 2014
- [3] Insurance Bureau of Canada. Study of impact and the insurance and economic cost of a major earthquake in British Columbia and Ontario/Québec. 2013.
- [4] Liu Q, Jiang H. Experimental study on a new type of earthquake resilient shear wall. *Earthq Eng Struct Dyn* 2017;46:2479–97.
- [5] American Institute of Steel Construction. Seismic provisions for structural steel buildings, ANSI/AISC 341–16. Chicago, IL: 2016.

- [6] CSA. Design of steel structures, CAN/CSA S16-14. Canadian Standards Association: Mississauga, ON, Canada 2014. Handbook of Steel Construction. 2014.
- [7] Lehman DE, Roeder CW, Herman D, Johnson S, Kotulka B. Improved seismic performance of gusset plate connections. *J Struct Eng* 2008;134:890–901.
- [8] Astaneh-Asl A, Goel SC, Hanson RD. Cyclic behaviour of double angle bracing members with end gusset plates. Research Report UMEE 82R7, Department of Civil Engineering, University of Michigan, Ann Arbor, Michigan. 1982.
- [9] Uriz P, Mahin SA. Toward earthquake-resistant design of concentrically braced steel-frame structures. UCB/PEER-2008/08, Univ. of California, Berkeley, CA.: 2008.
- [10] Roeder CW, Lumpkin EJ, Lehman DE. A balanced design procedure for special concentrically braced frame connections. *J Constr Steel Res* 2011;67:1760–72.
- [11] Lumpkin EJ. Enhanced seismic performance of multi-storey special concentrically brace frames using a balanced design procedure. MSc thesis, University of Washington, 2009.
- [12] Tremblay R, Timler P, Bruneau M, Filiatrault A. Performance of steel structures during the 1994 Northridge earthquake. *Can J Civ Eng* 1995;22:438–51.
- [13] Tsai C-Y, Tsai K-C, Lin P-C, Ao W-H, Roeder CW, Mahin SA, Lin CH, YU YJ, Wang KJ, Wu AC, Chen JC, Lin TH. Seismic design and hybrid tests of a full-scale three-storey concentrically braced frame using in-plane buckling braces. *Earthq Spectra* 2013;29:1043–67.

- [14] Goggins JM, Broderick BM, Elghazouli AY, Lucas AS. Experimental cyclic response of cold-formed hollow steel bracing members. *Eng Struct* 2005;27:977–89.
- [15] Shaback B, Brown T. Behaviour of square hollow structural steel braces with end connections under reversed cyclic axial loading. *Can J Civ Eng* 2003;30:745–53.
- [16] Tremblay R. Inelastic seismic response of steel bracing members. *J Constr Steel Res* 2002;58:665–701.
- [17] Johnson SM. Improved seismic performance of buckling restrained braced frames. MSc thesis, University of Washington, 2005.
- [18] Herman D. Further improvements on and understanding of SCBF systems. MSc thesis, University of Washington, 2006.
- [19] Kotulka BA. Analysis for a design guide on gusset plates used in special concentrically braced frames. MSc thesis, University of Washington, 2007.
- [20] Powell J. Evaluation of special concentrically braced frames for improved seismic performance and constructability. MSc thesis, University of Washington, 2009.
- [21] Sen A, Sloat D, Johnson MJ, Roeder CW, Lehman D, Berman JW. Experimental evaluation of the seismic vulnerability of braces and connections in older concentrically braced frames. *J Struct Eng* 2016; 142(9): 04016052
- [22] Clark K. Experimental performance of multi-storey x-brace systems. MSc thesis, University of Washington, 2009.
- [23] American Institute of Steel Construction. Seismic provisions for structural steel buildings. Chicago, IL: 1997.
- [24] Ikeda K, Mahin SA. Cyclic response of steel braces. *J Struct Eng* 1986;112:342–61.

- [25] Hsiao PC, Lehman DE, Roeder CW. A model to simulate special concentrically braced frames beyond brace fracture. *Earthq Eng Struct Dyn* 2013;42:183–200.
- [26] Sen A, Roeder CW, Lehman D, Berman JW. Nonlinear modeling of concentrically braced frames. *J Constr Steel Res* 2019;157:103–120.
- [27] Hsiao PC, Lehman DE, Roeder CW. Improved analytical model for special concentrically braced frames. *J Constr Steel Res* 2012;73:80–94.
- [28] Hsiao P-C, Lehman DE, Roeder CW. Evaluation of the response modification coefficient and collapse potential of special concentrically braced frames. *Earthq Eng Struct Dyn* 2013;44:657–75.
- [29] Stevens D, Wiebe L. Experimental testing of a replaceable brace module for seismically designed concentrically braced steel frames. *J Struct Eng* 2019;145. 04019012
- [30] Stoakes CD, Fahnestock LA. Cyclic flexural testing of concentrically braced frame beam-column connections. *J Struct Eng* 2011;137:739–47

2 Effect of Beam-Column Connection Fixity and Gravity Framing on the Seismic Collapse Risk of Special Concentrically Braced Frames

Abstract

In concentrically braced frames (CBFs), braces are typically connected at beam-column connections through gusset plates, which also increase the rotational stiffness and moment capacity of the beam-column connection. This fixity provides a reserve lateral force resisting capacity that may improve the seismic collapse capacity of the system, but that is not considered in design. Recently, a new brace connection type has been proposed that does not include a gusset plate that would stiffen and strengthen the beam-column connection. To address the implications of the range of possible connection design alternatives, this paper assesses the effects of the fixity of beam-column connections on the behaviour of three special concentrically braced frames of different heights. The results show that flexural strength and stiffness at the beam-column connections reduces the collapse probability when the gravity framing contribution is ignored, but this influence is minor for low-rise buildings and is typically much less significant than the influence of the gravity framing's stiffness and strength. Simple design recommendations are presented regarding the beam-column connection fixity within the braced bay.

Key words: Earthquake engineering; Steel structures; Special concentrically braced frames; Seismic collapse risk; Nonlinear time history analysis; Connection fixity; Gravity framing; Multiple stripe analysis

2.1 Introduction

2.1.1 Motivation

Steel special concentrically braced frames (SCBFs) are commonly used as lateral force resisting systems in regions of high seismicity. During moderate to severe earthquakes, the

braces are intended to experience inelastic deformation through buckling, post-buckling and tensile yielding. Through this nonlinear behaviour of braces, energy is dissipated and the peak seismic force is limited. In current practice, a gusset plate is used to join the brace to the frame members, and brace rotation due to out-of-plane buckling is accommodated using geometrical limits (linear or elliptical clearance) on the gusset plate (Figure 2.1 (a,b)) [1-3]. The associated out-of-plane buckling displacement can be larger than 400 mm before the brace fractures [4], causing damage to adjacent infill walls or cladding. To reduce toe weld fractures at the gusset plate and avoid damage due to out-of-plane deformation, an alternative detail has been proposed that uses a knife plate perpendicular to the gusset plate (Fig. 1(c)) [5]. More recently, an alternative connection has been developed based on a replaceable brace module (Fig. 1(d)) [6]. This connection is intended to improve the constructability of braced frames by allowing bolts to be used instead of field welding, and to make the brace unit more easily replaceable by confining all damage to the replaceable brace module. An experimental study by Stevens and Wiebe [6] has shown that this proposed connection can provide comparable seismic performance (i.e. yield and failure development, drift range before brace fracture, and cumulative energy dissipated) as current SCBF connections. However, whereas the gusset plate in other connections provides an undesigned level of beam-column fixity that could affect the collapse capacity of braced frames [7], omitting the gusset plate allows the designer to select the beam-column connection fixity. Therefore, there is a need to determine what level of fixity, if any, is required to ensure adequate collapse capacity of an SCBF.

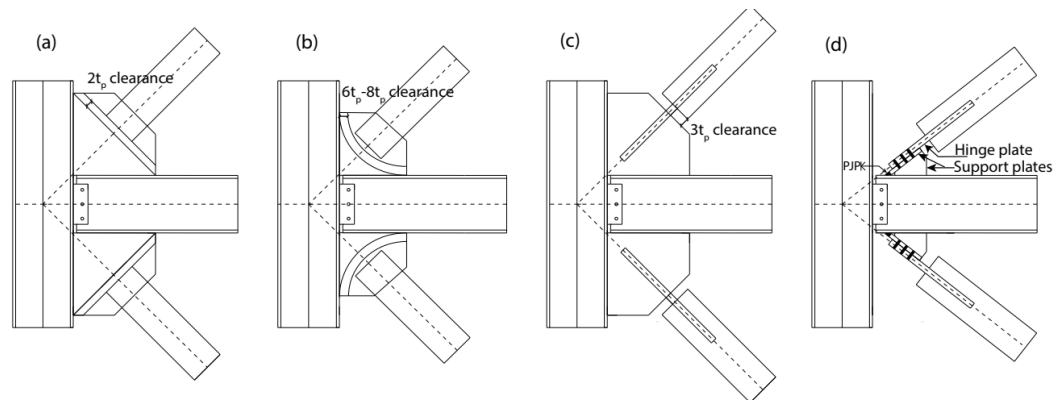


Figure 2.1 Brace connection details; a) Linear hinge zone b) Elliptical hinge zone c) Knife plate configured for in-plane buckling d) Proposed replacement/modular connection

2.1.2 Background

In current practice, designers often model SCBFs by assuming a pinned connection for beam-column connections with gusset plates. This is an attractive assumption as it simplifies the analysis and design process. However, it has been shown that the gusset plate can increase the flexural strength and stiffness of beam-column connections [8,9] enough to develop substantial frame action through bending of beams and columns [5]. Results of an experimental study on a full scale single braced bay by Lehman et al. [2] showed that the gusset plate in an SCBF can induce considerable inelastic deformations into adjacent beams and columns because of bending moments coming from the frame action. Uriz and Mahin [10] investigated the cyclic behaviour of braced frame beam-column connections in a full scale two-storey SCBF test. Conventional detailing requirements (Fig. 1(a)) were used to join the gusset plate to the frame members. After the first-storey braces fractured, the beam and column framing could still develop about 30% of the peak lateral resistance. This reserve capacity can also improve the collapse capacity of CBFs designed for moderate seismicity, becoming especially important after the braces fracture [11-13]. Kanyilmaz [13] investigated the effects of frame action on the global performance of CBF systems that were designed for moderate seismicity. A considerable improvement in the

resistance and ductility capacity was observed in those systems where gusset plates were used to connect the brace to the frame elements relative to the frame with ideally pinned connections.

Outside of braced bays, shear-tab connections are frequently used to join beams to columns in gravity frames. These connections are typically idealized as pinned in design because of their low contribution to the initial stiffness and base shear [14]. However, these connections can provide up to 20% of the plastic flexural capacity (M_p) of the beam in a bare steel frame, and up to 50% of M_p in the presence of the slab [15,16]. Due to the number of shear-tab connections in a building, their collective role may be significant [17]. Moreover, gravity columns can also reduce the drift concentration by providing lateral strength and stiffness that improve the seismic performance after brace fracture [18,19]. Hsiao et al. [20] concluded that modelling gravity framing connections could reduce the drifts significantly in the case of a low-rise (three-storey) SCBF building, assuming fixed beam-column connections within the braced bay. Malaga-Chuquitaype et al. [21] reported an improvement of 40% in the median collapse intensity of a 6-storey CBF after considering the lateral strength and stiffness of gravity framing. More recently, another study conducted by Hwang and Lignos [22] revealed that considering the gravity framing contribution with the composite action provided by the floor slab can significantly increase the collapse capacity of SCBFs and should be considered in the collapse risk studies of SCBFs. Although FEMA P695 [23] does not recommend considering the gravity framing strength and stiffness because they are not designed as part of the seismic-force-resisting system, it does note that the methodology outlined there can be used to investigate the importance of the gravity framing, and Appendix F of that document recommends considering the gravity framing for collapse modelling.

2.1.3 Paper Organization

In light of the above discussion, this paper examines the effects of connection fixity at the beam-column connections and of gravity framing on the collapse capacity of SCBF buildings. Three different conditions (pinned, shear tab and fixed) are considered for connections within the braced bay, without and with the contributions of the gravity framing, for three archetype buildings ranging from three to 12 storeys. After examining a representative example of the modelled behaviour of one frame near the collapse intensity, fragility curves are constructed and the collapse capacity is assessed using the FEMA P695 methodology and simplified design recommendations are presented. The influence of the damping model is also investigated by using the initial stiffness rather than the tangent stiffness to define the damping for one model of each archetype building. Finally, the inter-storey drift response is investigated near the median collapse intensity, so as to highlight the effects of the connection fixity and gravity framing on the collapse mechanism of each frame.

2.2 Details of Archetype Buildings

To represent a range of buildings with potential differences in the importance of force redistribution after brace buckling, three archetype SCBF buildings with heights of three, six and 12 storeys are considered in this study. The buildings were designed by others for a previous study [24] and use a two-storey X-braced configuration. The buildings have a rectangular plan configuration with six 9.14 m bays in one direction and four 9.14 m bays in the other direction, as shown in Figure 2.2, with a constant storey height of 4.57 m. The seismic weight of each floor and roof is 8800 kN and 6800 kN, respectively. Table 2.1 shows the seismic design parameters. The three- and six-storey buildings were designed using the equivalent lateral force (ELF) procedure, while the 12-storey building was designed according to response spectrum analysis (RSA) procedure in compliance with ASCE/SEI 7-05 [25]. The storey drift was limited to 2.5% for the three-storey building and

2.0% for the six- and 12-storey buildings. The braces are circular hollow structural sections (HSS) that satisfy the global and local slenderness ratio limits specified in ANSI/AISC 341-05 [26]. The beams were assumed to be continuously laterally supported, and a fixed-base condition was assumed for the columns, which resist lateral load through strong axis-bending. Table 2.2 shows the structural sections used for the considered buildings.

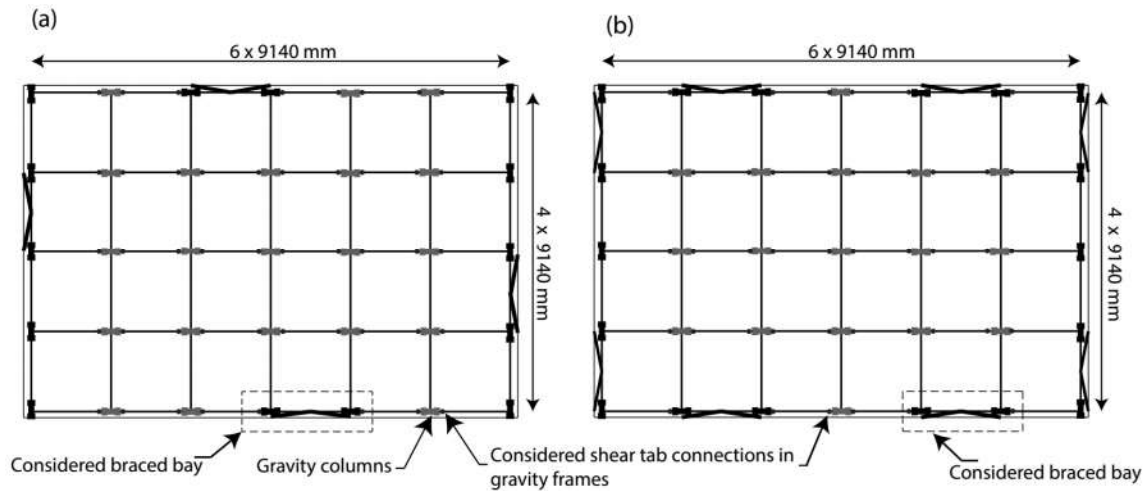


Figure 2.2 a) Plan configuration of three- and six-storey buildings b) Plan configuration of 12-storey building

Table 2.1 Seismic design parameters

Parameters	Value
Importance factor	1
Site class	D
Short-period site coefficient (F_a)	1
Long-period site coefficient (F_v)	1.5
Design spectral acceleration at short periods (S_{DS})	1.0g
Design spectral acceleration at 1-second period (S_{D1})	0.6g
Seismic design category	D
Response modification factor (R)	6.0
System over-strength factor (Ω)	2.0
Deflection amplification factor (C_d)	6.0

Table 2.2 Section sizes for SCBFs

Storey	Braces	Beams	Columns	Gravity Beams	Gravity Columns	α
3-storey						
3	HSS8.75x0.312	W30x173	W12x120	W24x55	W14x90	0.029
2	HSS8.75x0.5	W21x111	W12x120	W24x55	W14x90	0.019
1	HSS9.625x0.5	W18x65	W12x120	W24x55	W14x90	0.017
6-storey						
6	HSS7.5x0.312	W18x97	W14x68	W24x55	W14x48	0.034
5	HSS9.625x0.375	W24x104	W14x68	W24x55	W14x48	0.017
4	HSS9.625x0.5	W24x131	W14x176	W24x55	W14x74	0.027
3	HSS11.25x0.5	W18x76	W14x176	W24x55	W14x74	0.024
2	HSS12.5x0.5	W24x146	W14x342	W24x55	W14x90	0.026
1	HSS12.5x0.5	W21x62	W14x342	W24x55	W14x90	0.026
12-storey						
12	HSS6.625x0.312	W18x55	W12x45	W24x55	W14x48	0.015
11	HSS6.625x0.312	W18x35	W12x45	W24x55	W14x48	0.015
10	HSS8.75x0.312	W18x60	W14x99	W24x55	W14x74	0.019
9	HSS8.75x0.312	W18x35	W14x99	W24x55	W14x74	0.019
8	HSS10x0.375	W18x65	W14x193	W24x55	W14x90	0.018
7	HSS10x0.375	W18x35	W14x193	W24x55	W14x90	0.018
6	HSS10x0.375	W18x65	W14x283	W24x55	W14x120	0.024
5	HSS10x0.375	W18x35	W14x283	W24x55	W14x120	0.024
4	HSS9.625x0.5	W18x71	W14x398	W24x55	W14x145	0.024
3	HSS9.625x0.5	W18x35	W14x398	W24x55	W14x145	0.024
2	HSS9.625x0.5	W18x71	W14x550	W24x55	W14x176	0.030
1	HSS9.625x0.5	W18x35	W14x550	W24x55	W14x176	0.030

2.3 Numerical Modelling

The study frames were all modelled with a similar approach using OpenSees [27]. As an example, Figure 2.3 shows a schematic of the numerical model for the six-storey archetype building. Force-based fiber beam-column elements were used to model the inelastic behaviour of the frame members, with a Gauss-Lobatto integration scheme to account for the distributed plasticity along the length of each element. Fibre beam-column elements were also used to capture the cyclic inelastic behaviour of the braces, following the recommendations of Uriz and Mahin [10]. A uniaxial Giuffre-Menegotto-Pinto steel material with isotropic strain hardening (Steel02) was assigned to each fiber.

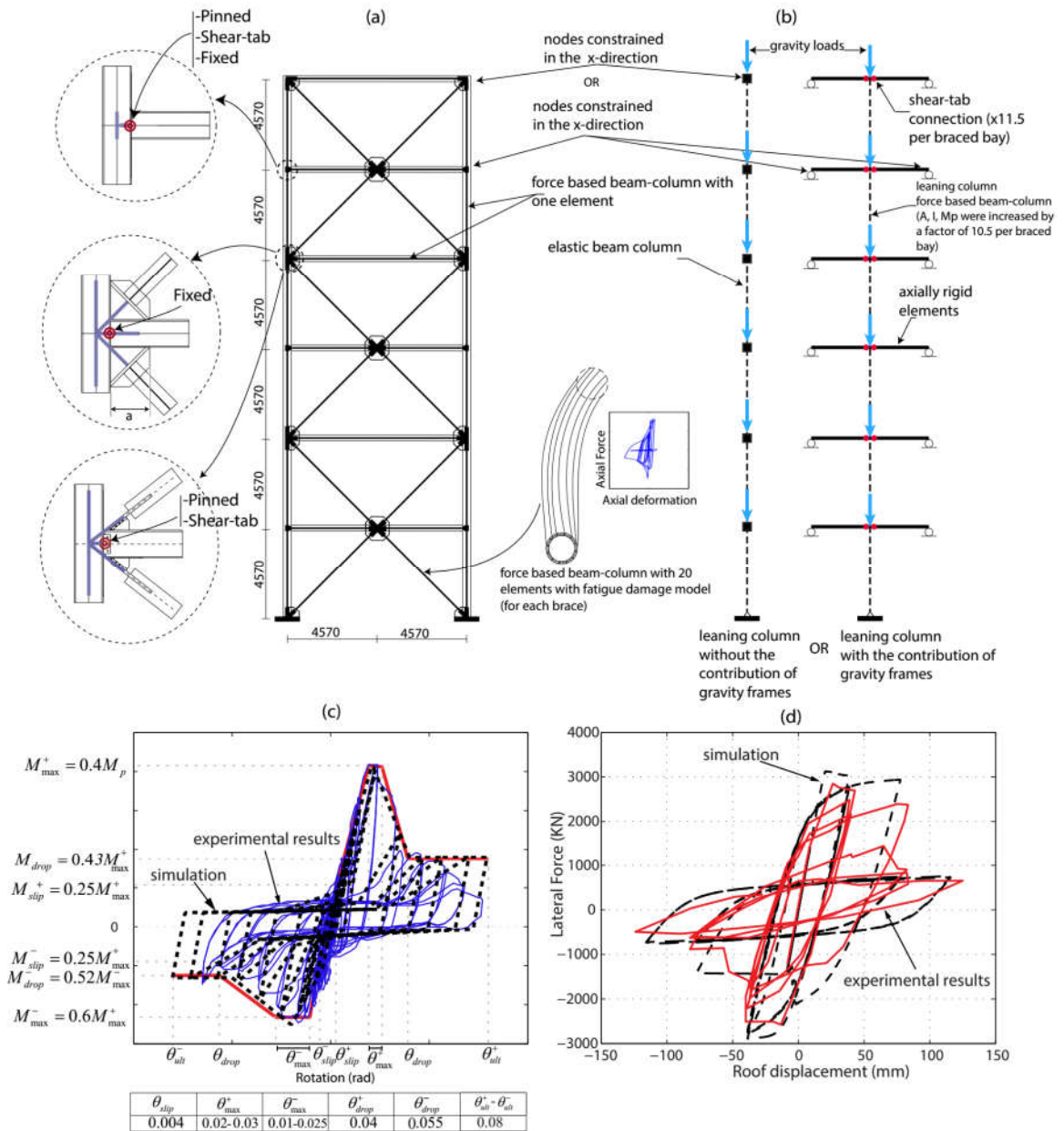


Figure 2.3 a) Schematic of numerical model for six-storey SCBF. b) Leaning column without or with the simulation of lateral load resisting contribution of gravity framing. c) Composite shear-tab connection behaviour (compared to [15]). d) Global hysteretic behaviour of two-storey SCBF (compared to [10])

A non-deteriorating constitutive model material (Steel02) was used for modeling the beams and columns because this was expected to be sufficiently accurate for the beams up to 5% inter-storey drift, which was defined as collapse for this study, as well as for the stocky columns, for which the deterioration of strength and stiffness is not expected to be significant at this drift level [28]. Initial out-of-straightness in the form of a sinusoidal function with an amplitude of $L/500$ [29] was considered, with each brace subdivided into twenty nonlinear beam-column elements. In order to capture fracture due to low-cycle fatigue, the strain history in each individual fiber was tracked according to a rainflow counting procedure [10] and zero stiffness was assigned to any fiber that exceeded the low-cycle fatigue limit recommended by Karamanci and Lignos [30].

A multicomponent connection model consisting of rigid elements, fiber elements, and a nonlinear spring was used to capture the behaviour of the beam-column-gusset plate connections. The gusset plate was modelled using a fiber element with a length equal to twice the gusset plate thickness and with three integration points, and rigid offsets were modelled at the end of the elements, following the recommendations of Hsiao et al. [31]. In columns, these rigid elements extend from the work point to either the physical end of the gusset plate or the physical end of the beam, as shown in Figure 2.3(a). In beams, they extend to 75% of the dimension 'a' (Figure 2.3(a)).

For the nonlinear springs connecting the brace and beam elements to the column, three different assumptions were considered. First, the spring was modelled as a fixed connection as an upper bound on the strength and stiffness that the gusset plate can provide to the connection. Second, omitting the gusset plate from its current position may lead to a shear tab connection between the beam and column, as shown in Figure 2.1(d). Third, as a lower bound on the possible frame contribution and because designers often assume this condition, the spring was modelled as a pin. To simulate the cyclic behaviour of shear-tab

connections including strength and stiffness degradation, the Pinching4 material was employed in OpenSees. The cyclic deterioration parameters were defined as recommended by Elkady and Lignos [32], who calibrated the parameters using the test results of Liu and Astanteh [15] for a shear tab connection with a slab and the proposed moment rotation model in Liu and Astanteh [16]. Figure 2.3(c) compares the hysteresis for a shear tab connection with slab from an experimental study provided in Liu and Astanteh [15] with the hysteresis loops of the shear tab spring model. Where connections were assumed to be fixed, the slab was assumed not to contribute to the response based on the assumption that the connection to the brace would prevent a slab from being attached to the beam where it could interact significantly with the connection. The panel zones were assumed to have adequate strength and stiffness that panel zone deformation could be neglected.

The modelling approach was validated against test results from a full-scale quasi-static cyclic test on two-storey braced frame with HSS braces and tapered gusset plates [10]. All beam-column connections were modelled as fixed. Figure 2.3(d) compares the global hysteretic behaviour of the considered model to the experimental results. The model accurately captures the overall behaviour of the structure and cyclic performance of the frame, and strength and stiffness deterioration of the experimental results is in good agreement with the simulation results. Figure 2.3(d) shows that the peak resistance and the reserve lateral resistance of the model are within 10% and 13% of the experimental results, respectively.

The model contains a leaning column loaded vertically with the tributary seismic load of each floor and constrained to one braced bay node in the horizontal direction. The braced bay beams were verified to have sufficient strength and stiffness that the results were essentially the same as if a rigid diaphragm had been modelled. The P-Delta geometric transformation formulation was used to simulate P- Δ effects. When the gravity framing was to be excluded from the model, elastic beam-column elements were used to model the

leaning column, no lateral stiffness was assigned to these elements, and the mass tributary to the gravity columns was lumped at the column nodes, as shown in Figure 2.3(b). When the lateral load resisting contribution of gravity framing was to be included, one leaning column was used to represent all the gravity columns within the tributary area. In this case, the leaning column was modelled using force-based fiber beam-column elements. Only the gravity columns that are oriented to bend about their strong axis were considered, so the area, moment of inertia and plastic moment capacity of one column were multiplied by a factor of 10.5 for the three- and six-storey archetype buildings, and by a factor of 4.25 for the 12-storey building. The analyses were run with and without shear tab connections in the gravity framing to examine the individual influence of both the gravity columns and gravity framing connections on collapse capacity of SCBFs. When gravity framing connections were included, axially rigid beams with the total flexural stiffness of all gravity beams located within the tributary area on both sides of the leaning column were used to model the gravity connections. To account for all the shear tab connections within the tributary area of the gravity framing, the strength and stiffness of one shear tab connection were increased by a factor of 11.5 for three- and six-storey archetype buildings, and by a factor of 5.25 for the 12-storey building. In all cases, the base of the leaning column was modelled as pinned. Table 2.3 shows the fundamental periods for all considered models. By modelling beam-column connection as fixed (similar to NIST [24] assumptions), the corresponding fundamental periods are $T_1 = 0.58$ s, 1.09 s and 1.93 s for three-, six- and 12-storey buildings, respectively. These periods are within 3% of the periods presented for the same structures in NIST [24]. The fundamental periods indicate that the influence of connection fixity and gravity framing is negligible in the elastic range for the considered buildings because of the large initial stiffness provided by the braces. This implies a negligible variation of the design base shear regardless of the stiffness associated with connections and gravity framing.

Table 2.3 Fundamental periods for models with different modelling assumptions (s)

Building Height	Without Gravity Framing			With Gravity Columns			With Gravity Framing Columns and Connections		
	Pinned	Shear tab	Fixed	Pinned	Shear tab	Fixed	Pinned	Shear tab	Fixed
3 storeys	0.581	0.579	0.576	0.581	0.579	0.576	0.557	0.556	0.553
6 storeys	1.104	1.100	1.087	1.100	1.099	1.080	1.047	1.047	1.046
12 storeys	1.957	1.954	1.930	1.956	1.953	1.930	1.903	1.900	1.897

Tangent stiffness-proportional Rayleigh damping based on 3% of critical damping in the first and third modes was applied using the committed stiffness matrix, as Rayleigh damping using the initial stiffness can overestimate the collapse capacity of SCBFs when it is assigned to the brace elements that exhibit nonlinear behaviour [30]. The eigenvalue analysis was performed and the Rayleigh damping coefficients were recomputed for each integration step during the response history. When the eigenvalues of the first three modes were positive, damping was calculated based on both mass- and stiffness- proportional damping parts of the Rayleigh damping matrix, but when one of the eigenvalues in the first three modes became negative, the stiffness proportional damping part of the Rayleigh damping was omitted to avoid negative damping forces.

2.4 Ground Motion Selection and Scaling

Multiple stripe analysis (MSA) [33] was conducted for the archetype buildings using the set of 44 far-field ground motions that were summarized in FEMA P695 [23]. In this method, all the ground motions are scaled to specific intensity measures (IMs), and nonlinear time history analyses are run for each intensity level. Fragility curves are constructed based on the proportion of ground motions that cause collapse at each IM level using the maximum likelihood statistical approach.

For all considered buildings, seven stripes were considered. For the three- and six-storey buildings, the ground motions were scaled using a multi-period scaling method described

by Hsiao et al. [20]. According to this scaling method, ground motions are scaled to match the target spectrum before and after brace fracture. For those stripes with intensity equal to or lower than the DBE (design basis earthquake), each ground motion was scaled to meet the target spectrum using only the fundamental period based on models without gravity framing (T_1) because brace fracture is not expected at this level. For the three- and six-storey buildings at stripes larger than the DBE, the ground motions were scaled to match the target spectrum at three different periods: the fundamental period (T_1), the period of the structure with one brace removed at the first storey to simulate fracture (T_b) and the period of the structure with both braces removed at the first storey (T_c), as described by Equation 2.1 [20].

$$SF = \frac{Sa_{1,t}}{Sa_{1,g}} w_1 + \frac{Sa_{b,t}}{Sa_{b,g}} w_b + \frac{Sa_{c,t}}{Sa_{c,g}} w_c \quad (2.1)$$

where $Sa_{i,t}$ is the target elastic spectral acceleration value corresponding to each period T_i and $Sa_{i,g}$ is the spectral acceleration value of the ground motion at period T_i , w_i is the weight for each period T_i . The following weights were used for this scaling method: $w_1 = 0.55$, $w_b = 0.35$, $w_c = 0.1$ [20]. For the 12-storey building, the modified scaling approach that was used by Hsiao et al. [24] for a high-rise building (20 storeys) was considered, but did not produce an acceptable match between the mean and target spectra. For that reason, the geometric-mean scaling method was used instead to scale the ground motions over a broad range of periods ($0.2 T_1$ to $1.5 T_1$), following ASCE recommendations [25]. Figure 2.4 shows the 5% damped mean spectra for all considered stripes for all buildings. The mean spectra are very close to the code spectra at the DBE and MCE (maximum considered earthquake) levels at the anchor periods for the three- and six-storey buildings, and at the

first- and second- mode periods for the 12-storey building. All the mean spectra overshoot the target spectra at periods shorter than $T_s = 0.5$ s.

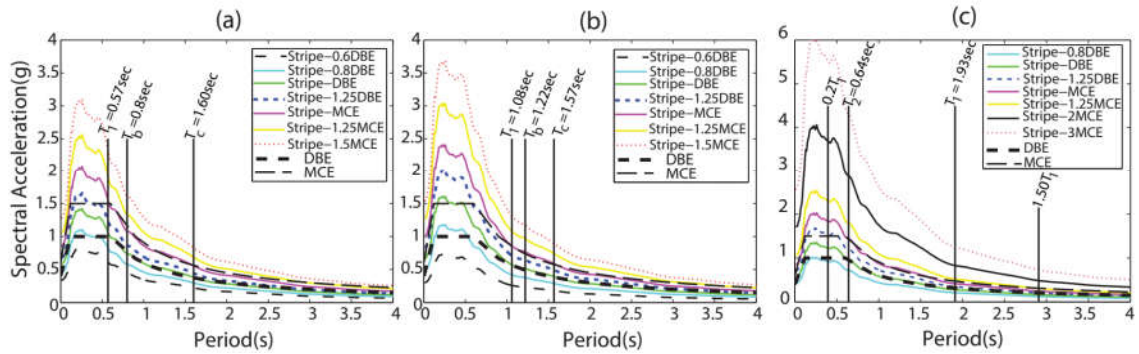


Figure 2.4 Scaled mean 5%-damped spectra for considered stripes, compared with DBE and MCE code-based spectra, for a) 3-storey b) 6-storey c) 12-storey building

2.5 Example Near-Collapse Response of Six-Storey Building

To investigate the influence of the beam-column connection fixity and the gravity framing on the behaviour of the braced frame systems, a representative example of the 6-storey SCBF near collapse is presented first. This section uses the results from component 2 of the Nishi-Akashi Station of the 1995 Kobe record (Table A-4C in FEMA P695 [23]) at an intensity that represents 1.25MCE (Scale Factor=3.8). Structural collapse was defined as a state at which the maximum storey drift reaches 5% [20]. Figure 2.5 shows the inter-storey drift response for the three considered models of the beam-column connections, without and with the contribution of the gravity framing. Figure 2.6 presents the peak inter-storey drift ratios and sequence of damage (beam and column yielding, brace fracture but not yielding) for the same models.

2.5.1 Models without Gravity Framing

The storey drift response histories of the models without gravity framing and with either pinned or shear tab connections are nearly identical, as both develop the same collapse

mechanism. In these two models, at 6.5 s the left brace in the second storey fractures, followed quickly by flexural yielding at the base of the first-storey columns, leading to collapse of the system. This demonstrates that in models with pinned or shear tab connections where the gravity framing is neglected, even a single brace fracture can trigger structural collapse.

Conversely, when the connection condition is modelled as fixed, the same model does not collapse, although the drift demand in the first three storeys still exceeds 2%. The sequence of inelastic events is identified with circled numbers in Figures 2.5(c) and 2.6(c). The frame action participation delays the first brace fracture, and also allows yielding to occur in multiple locations in both beams and columns (steps 4 and 5) before a second brace fractures at 12.0 s. This illustrates how frame action within the braced bay prevents the concentration of inelastic deformation in a single storey, thereby preventing collapse.

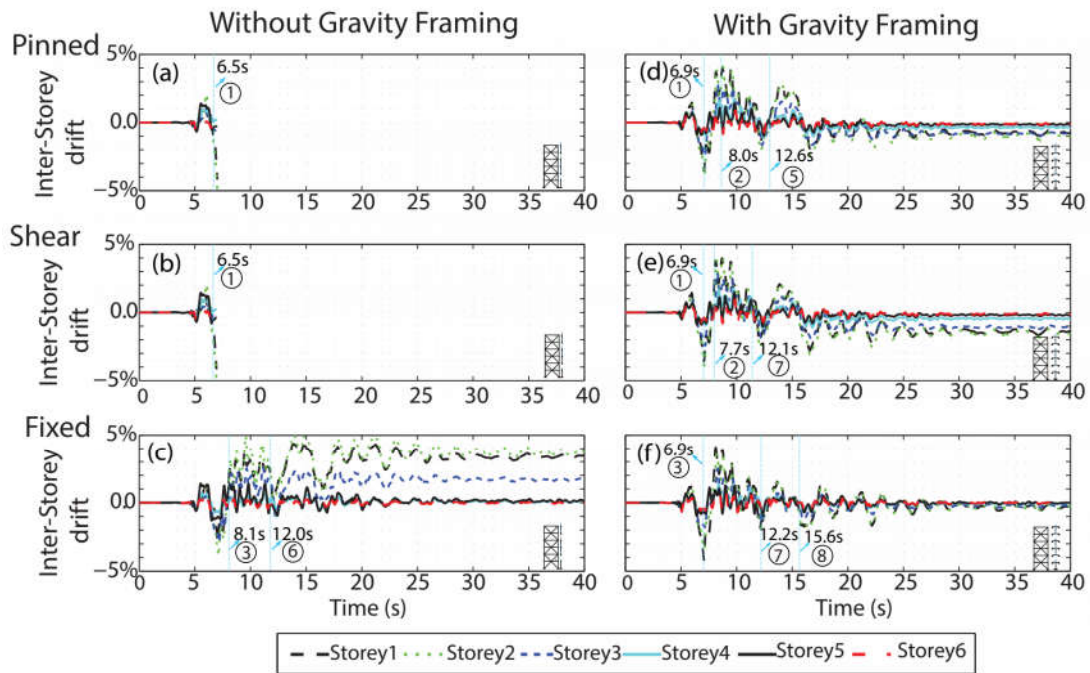


Figure 2.5 Dynamic response of the 6-storey SCBF for the Nishi-Akashi record from the Kobe 1995 ground motion at a scale factor of 3.8 (1.25MCE)

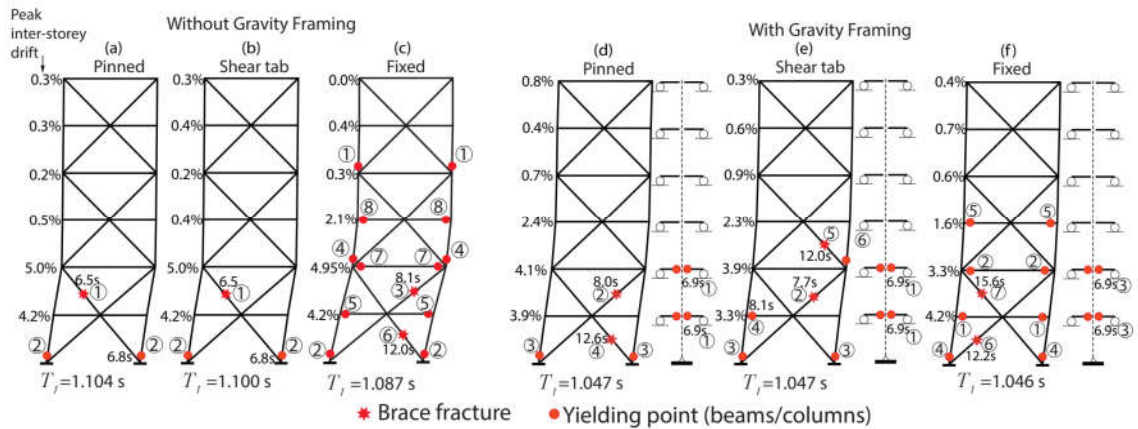


Figure 2.6 Sequence of damage during Nishi-Akashi record from the Kobe 1995 ground motion at a scale factor of 3.8

2.5.2 Models with Gravity Framing

The models described above were also modelled with the additional lateral strength and stiffness of the gravity framing. Figure 2.5 shows that this enhances the distribution of nonlinearity along the height of the building, reducing both the maximum inter-storey drift and the residual drifts. Figure 2.6(d) shows the damage progression for a model with pinned connections when the gravity framing is also modelled. Relative to the case without gravity framing, brace fracture is postponed to the next strong cycle in the other direction (8.0 s). Moreover, after the brace fractures, the gravity framing prevents the collapse that was modelled as occurring immediately after brace fracture when gravity framing was not considered. When the connections in the braced bay are instead modelled as shear tabs, the maximum drift reduces by only 5%. The gravity connections in the first two storeys yield at essentially the same time as in the model with pinned connections, and braces fracture at approximately the same times in both models even if it is not the same brace that fractures second.

Somewhat different results are observed in the model with fixed connections. In this model, yielding occurs at several points in gravity connections and in braced bay elements along the height of the building (steps 1 to 6) before the first fracture happens. This illustrates how fixed connections within the braced bay can further redistribute loads after initial brace buckling or yielding, even beyond the level of redistribution that was seen with gravity framing but pinned or shear tab connections. The residual drifts are also smaller for the model with fixed connections than for the other two models. For instance, the maximum residual drift is 0.95% in the second floor for the model with gravity framing and pinned connections, compared to only 0.37% in the first floor for the model with fixed connections.

2.6 Collapse Risk Assessment

In this section, the FEMA P695 [23] methodology is used to evaluate the collapse capacity of each numerical model. According to this methodology, archetype structures with similar seismic behaviour are assembled into performance groups. Each performance group should consist of at least three archetypes, each designed within a selected range of structural geometry and design parameters so as to reflect the major changes in structural behaviour within the archetype design space. The collapse potential of that archetype is then evaluated for each performance group by comparing the calculated adjusted collapse margin ratio (ACMR) to an acceptable ACMR that was determined according to the uncertainty factors of structural system. The ACMR of a single archetype must be greater than the acceptable collapse margin ratio corresponding to a 20% collapse probability limit ($ACMR_{20\%}$) to pass the trial, and the average value of ACMR for all archetypes in the performance group must also meet a 10% collapse probability limit. The ACMR is computed using the following equation:

$$ACMR = \frac{\hat{S}_{CT}}{S_{MT}} SSF \quad (2.2)$$

where \hat{S}_{CT} is the median collapse intensity computed through nonlinear dynamic analysis, S_{MT} is the MCE ground motion spectral demand, and SSF is the spectral shape factor to account for the frequency content of the ground motion record set. Table 7-3 in FEMA P695 [23] presents the values of $ACMR_{20\%}$ for different values of total system collapse uncertainty (β_{TOT}), which includes the record-to-record uncertainty (β_{RTR}), design requirement robustness (β_{DR}), test data accuracy (β_{TD}) and modelling accuracy (β_{MDL}):

$$\beta_{TOT} = \sqrt{\beta_{RTR}^2 + \beta_{DR}^2 + \beta_{TD}^2 + \beta_{MDL}^2} \quad (2.3)$$

In this study, the record-to-record uncertainty (β_{RIR}) values are determined from the multiple stripe analysis results. As in NIST [24], β_{DR} , β_{TD} and β_{MDL} were all assumed to be equal to 0.2, which represents a quality rating Good (B). The SSF values were determined using Table 7-1 of FEMA P695 [23]. Consider a period based ductility larger than 8 [20], the corresponding SSF factors are 1.33, 1.41 and 1.58 for the three-, six-, and 12-storey models, respectively.

2.6.1 Influence of Connection Fixity on Collapse Risk without Modelling Gravity Framing

Figure 2.7 shows the collapse fragility curves for the considered models without and with the gravity framing modelled. The horizontal axis shows $S_a(T_1)$, the mean spectral acceleration value of the first mode for the ground motion suite, normalized by the MCE ground motion spectral intensity (S_{MT}), so the collapse margin ratio ($CMR = \hat{S}_{CT} / S_{MT}$) can be taken directly from collapse fragility curves as the x-coordinate associated with a 50% probability of collapse. When the contribution of the gravity framing is neglected (Figures 2.7(a-c)), the difference between the median collapse capacities for models with pinned connections and those for models with shear-tab connections is less than 5% for all three buildings. Although increasing the connections' strength and stiffness to be fully fixed does not affect the CMR for the 3-storey building, the median collapse intensity improves by 22% and 30% for 6-storey and 12-storey buildings, respectively. However, the probability of collapse at the MCE level is still unacceptably high (54%) for the 12-storey building, even with this improvement in collapse capacity due to fully fixed connections. This probability of collapse is also much higher than the probability computed in a previous study [24] because of the difference in damping models that were used, as will be discussed in Section 2.6.4.

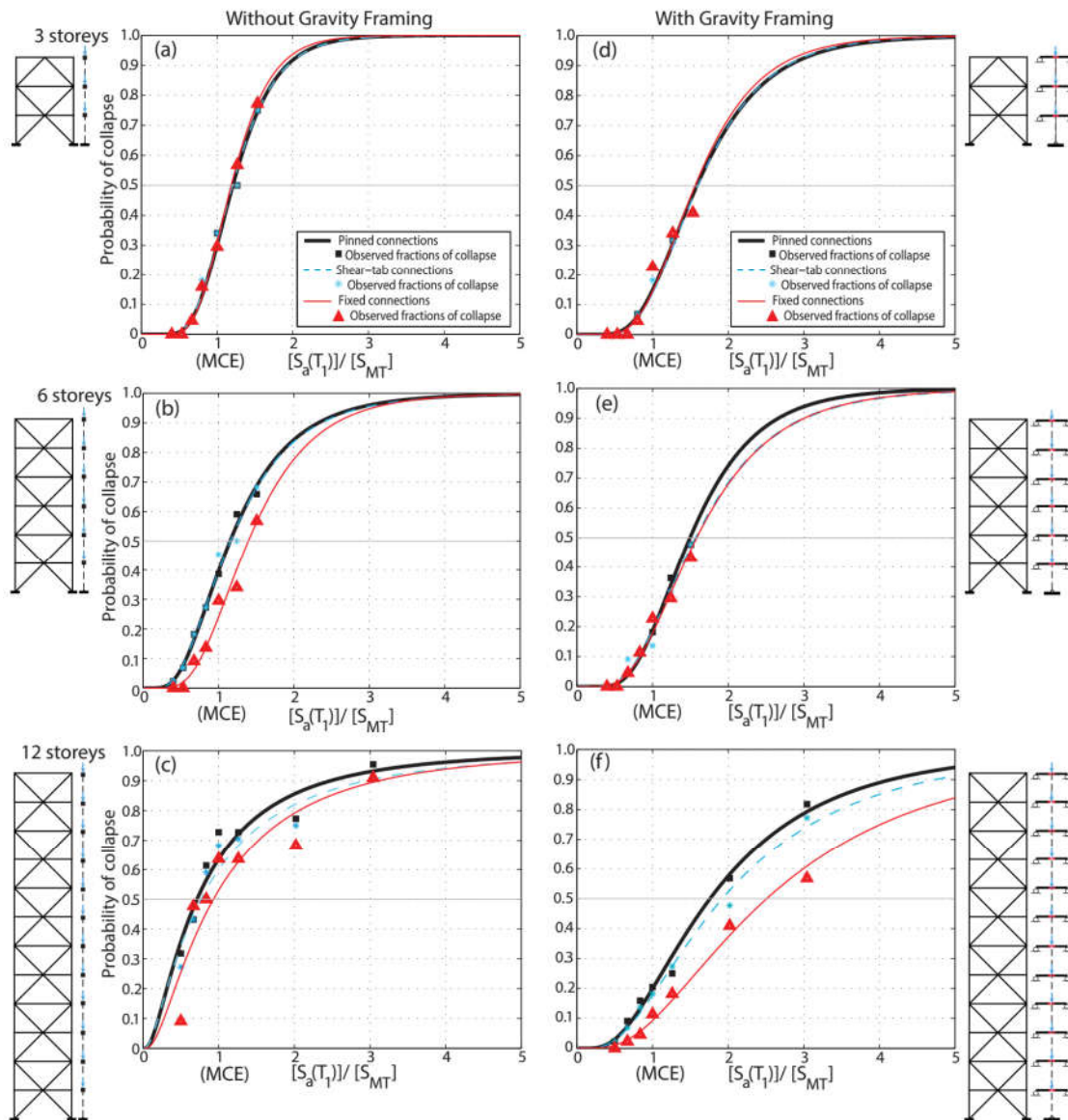


Figure 2.7 Collapse fragility curves for three-, six-, and 12-storey SCBF a)without gravity framing contribution b)with gravity framing contribution

2.6.2 Influence of Gravity Framing on Collapse Risk

The right side of Figure 2.7 presents the collapse fragility curves for models that include the gravity framing (i.e. gravity columns and gravity beam-column connections). Compared to the results for models without gravity framing (left side of Figure 2.7), a clear improvement is seen in the fragility curves for all modelled SCBFs. Regardless of the connection type within the braced bay, the CMR increases from 1.20 to 1.57 for the three-storey building when the gravity framing is considered relative to models without gravity framing. For the six-storey building, the median collapse capacity increases by 11% and 33% for models with fixed connections and shear-tab connections, respectively, when compared to the median collapse capacity of the same frames without modelling the gravity framing. For the 12-storey building, modelling the gravity framing has an even more significant effect on collapse capacity, increasing the CMR by a factor of between 2.5 and 2.7.

Figures 2.7 (d) and (e) indicate that changing the beam-column connections in the braced bay from pinned to fixed has a negligible effect on the median collapse capacity of three- and six-storey buildings when the gravity framing is modelled. This implies that the influence of the flexural reserve capacity of the gravity columns and connections is much more significant than the connections within the braced bay for these buildings. However, there is a significant improvement in collapse capacity with connection fixity in the 12-storey frame, even with gravity framing. For this taller structure, the gravity columns provide less stiffness relative to the braced bay than for the other buildings, and therefore the fixed connections within the braced bay play a greater role in distributing yielding to reduce drift concentration and dissipate energy.

Table 2.4 summarizes the results of the evaluation process for the models without or with the gravity framing contribution. In this table, the calculated ACMR values are compared to acceptable $ACMR_{20\%}$ values in FEMA P695 to evaluate the collapse safety of each

model of its individual archetype building. All models of the three-storey building satisfy the FEMA P695 criterion, and the collapse capacity improves significantly when the gravity framing is included. The 6-storey model performance is unacceptable for the pinned and shear-tab cases when the gravity framing is not modelled. However, assuming fixed connections improves the collapse capacity to be acceptable, and modelling the gravity framing results in an even greater improvement. In the case of the 12-storey building, systems without the gravity framing modelled all have highly unacceptable performance, but modelling the gravity framing greatly enhances their performance to be acceptable.

Finally, when the gravity framing is modelled, the 12-storey SCBF is the least vulnerable to collapse of the three considered buildings, which is consistent with findings from previous earthquakes and from other studies in which low rise SCBFs have been found more vulnerable [34]. Conversely, the results of models without the gravity framing contribution showed that the 12-storey SCBF has the greatest potential for collapse.

2.6.3 Influence of Gravity Columns Alone on Collapse Risk

As discussed in the previous section, the total contribution of gravity framing can improve the collapse capacity of SCBFs significantly. However, this is typically not considered in current design and analysis because of the difficulty of modelling gravity connections and the lack of information about their expected behaviour [35]. A more practical approach for design may be to consider only the portion of gravity framing contribution that comes from continuous gravity columns, which have also been shown to improve collapse capacity [18]. If the gravity columns have sufficient strength and stiffness, they can provide a positive post-yielding stiffness that improves dynamic stability by counteracting P- Δ effects [36].

Table 2.4 Collapse results for all SCBF models

Beam-column connection	Gravity system model	Damping	S _{CT}	S _{MT}	CMR	β	ACMR	Accept ACMR _{20%}	Pass/Fail ratio
3-storey									
Pinned	None	Tangent	1.80g	1.50g	1.20	0.36	1.60	1.52	1.05
Shear-tab	None	Tangent	1.80g	1.50g	1.20	0.37	1.60	1.52	1.05
Fixed	None	Tangent	1.80g	1.50g	1.20	0.34	1.60	1.51	1.06
Fixed	None	Initial	2.00g	1.50g	1.33	0.34	1.78	1.51	1.18
Pinned	Framing	Tangent	2.37g	1.50g	1.58	0.44	2.10	1.6	1.31
Shear-tab	Framing	Tangent	2.37g	1.50g	1.58	0.43	2.10	1.6	1.31
Fixed	Framing	Tangent	2.37g	1.50g	1.58	0.44	2.10	1.6	1.31
Pinned	Column $\alpha \times 0.5$	Tangent	2.01g	1.50g	1.34	0.38	1.78	1.53	1.16
Fixed	Column $\alpha \times 0.5$	Tangent	2.08g	1.50g	1.39	0.39	1.85	1.53	1.21
Pinned	Column $\alpha \times 1.0$	Tangent	1.98g	1.50g	1.32	0.37	1.76	1.53	1.15
Fixed	Column $\alpha \times 1.0$	Tangent	2.12g	1.50g	1.41	0.37	1.87	1.53	1.22
6-storey									
Pinned	None	Tangent	0.97g	0.85g	1.15	0.54	1.61	1.73	0.93
Shear-tab	None	Tangent	0.97g	0.85g	1.15	0.55	1.61	1.73	0.93
Fixed	None	Tangent	1.19g	0.85g	1.40	0.47	1.97	1.63	1.21
Fixed	None	Initial	1.55g	0.85g	1.83	0.58	2.57	1.76	1.46
Pinned	Framing	Tangent	1.22g	0.85g	1.43	0.45	2.02	1.62	1.25
Shear-tab	Framing	Tangent	1.33g	0.85g	1.56	0.50	2.21	1.66	1.33
Fixed	Framing	Tangent	1.34g	0.85g	1.58	0.50	2.22	1.66	1.34
Pinned	Column $\alpha \times 0.5$	Tangent	0.98g	0.85g	1.15	0.49	1.63	1.66	0.98
Fixed	Column $\alpha \times 0.5$	Tangent	1.19g	0.85g	1.40	0.48	1.97	1.63	1.20
Pinned	Column $\alpha \times 1.0$	Tangent	1.19g	0.85g	1.41	0.58	1.99	1.76	1.13
Fixed	Column $\alpha \times 1.0$	Tangent	1.26g	0.85g	1.48	0.58	2.09	1.76	1.19
12-storey									
Pinned	None	Tangent	0.34g	0.47g	0.72	0.97	1.14	2.22	0.51
Shear-tab	None	Tangent	0.36g	0.47g	0.77	0.98	1.22	2.22	0.55
Fixed	None	Tangent	0.44g	0.47g	0.94	0.94	1.49	2.22	0.67
Fixed	None	Initial	1.34g	0.47g	2.85	0.95	4.50	2.22	2.03
Pinned	Framing	Tangent	0.84g	0.47g	1.79	0.67	2.83	1.84	1.54
Shear-tab	Framing	Tangent	0.90g	0.47g	1.91	0.70	3.02	1.88	1.61
Fixed	Framing	Tangent	1.17g	0.47g	2.50	0.69	3.95	1.88	2.10
Pinned	Column $\alpha \times 0.5$	Tangent	0.46g	0.47g	0.98	0.89	1.55	2.22	0.71
Fixed	Column $\alpha \times 0.5$	Tangent	0.66g	0.47g	1.40	0.90	2.21	2.22	1.00
Pinned	Column $\alpha \times 1.0$	Tangent	0.58g	0.47g	1.23	0.66	1.94	1.88	1.04
Fixed	Column $\alpha \times 1.0$	Tangent	0.83g	0.47g	1.76	0.69	2.79	1.91	1.46

The flexural stiffness of gravity columns is mobilized when shear storey drifts become nonuniform after brace buckling and yielding; thus, the relevant flexural stiffness of gravity columns depends on the number and locations of storeys with pronounced brace yielding. As a simplified alternative suitable for routine design, the recommendations proposed in this paper are based on the column stiffness ratio (α), which quantifies the ratio of stiffness between all of the continuous gravity columns and the bracing bent [19]:

$$\alpha = \frac{EI}{kh^3} \quad (2.4)$$

where I is the total moment of inertia provided by all of the continuous gravity columns at a storey level based on their orientations, k is the total lateral stiffness of braced bays at that level based on the axial stiffness of the braces, and h is the height of the storey. For the considered buildings, the values of α are shown in Table 2.2. These values are associated with 10.5 gravity columns per braced bay for the three- and six-storey buildings, and 4.25 gravity columns per braced bay for the 12-storey building, with all columns oriented to bend about their strong axes.

In order to evaluate the importance of gravity column stiffness as part of the overall contribution of the gravity framing to collapse capacity, the analyses described above were repeated considering the contribution of gravity columns without gravity framing connections, and also for models with half the total stiffness of gravity columns (i.e. 0.5α), which corresponds to orienting most gravity columns to bend about their weak axes instead of their strong axes. Figure 2.8 shows the fragility curves for both of these cases. In this figure, the fragility curves from Figures 2.7(a-c) for pinned and fixed connections without modeling the gravity framing are also presented for comparison. Table 2.4 summarizes the results of the evaluation process for the models with the contribution of gravity columns. Sections 2.6.1 and 2.6.2 showed that the difference between models with pinned and shear tab connections was less than a 5% change in the median collapse capacities for all models

with different heights. Therefore, the results in this section are presented only for models with pinned and fixed connections. The CMR values for these cases (for buildings with different heights) are between the CMR values calculated for cases without and with the gravity framing.

The low-rise (three-storey) building is able to pass the FEMA P695 collapse criterion regardless of the beam-column connection fixity, even without considering the gravity framing contribution.

For the mid-rise (six-storey) building, although cases with pinned or shear-tab connections narrowly failed the FEMA P695 criterion when the gravity framing stiffness was artificially reduced, the results when considering full gravity framing connections (Figure 2.7(e)) showed that the beam-column connections within the braced bay have a negligible effect on the collapse fragility. Therefore, it is also recommended that a designer may choose whether to use pinned or fixed connections within the braced bay for mid-rise buildings. This is also consistent with the results presented here with continuous columns and without a modified stiffness ($\alpha \times 1.0$).

For the taller (12-storey) building, no cases satisfied the FEMA P695 collapse criterion without considering the contribution of gravity framing, suggesting that the stiffness of the gravity framing must always be verified regardless of the beam-column fixity within the braced bay. Considering that failure generally initiated in the eleventh storey when the gravity framing was not modelled (as will be shown in Section 2.7), the analyses suggest that α must be verified as greater than 0.015 at every storey when the beam-column connections within the braced bay are pinned, or $\alpha > 0.008$ at every storey when the beam-column connections within the braced bay are fixed. The gravity framing connections are likely to add a beneficial effect, but this is relatively difficult to consider in design and therefore is neglected in these recommendations.

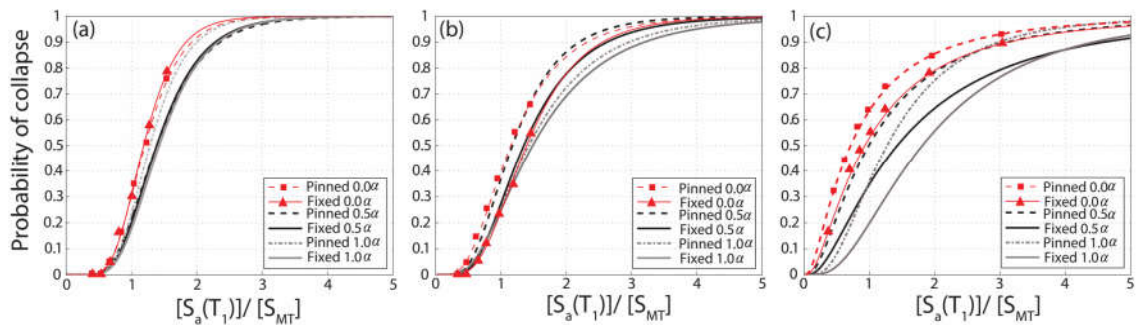


Figure 2.8 Collapse fragility curves for a) three-, b) six-, and c) 12-storey SCBF considering only the contribution of gravity columns

2.6.4 Influence of Damping Model on Collapse Risk

For all of the models discussed above, the tangent stiffness was used to calculate the stiffness-proportional damping component of the Rayleigh damping matrix and the Rayleigh coefficients. To evaluate the significance of this assumption, the analyses described above were repeated for the models with fixed connections when the gravity framing was not modelled, but using the initial stiffness of all structural elements to compute the damping matrix. These assumptions were based on the modelling approach described in NIST [24]. The CMR for the three-storey model increases by 10% for the case with initial stiffness-proportional damping compared to the case with tangent stiffness-proportional damping, and the influence on the results becomes more significant as the building height increases. Figures 2.9(b) and 2.9(c) show that the median collapse capacity increases by 30% and 310% for the six- and 12-storey buildings, respectively. For the 12-storey building, this difference was enough to change the computed ACMR from unacceptable to acceptable. This finding demonstrates the important influence of the inherent damping model on the collapse capacity of SCBFs, and is consistent with previous findings that unrealistic large damping forces can be produced when the Rayleigh damping matrix is computed based on the initial stiffness of CBFs [30].

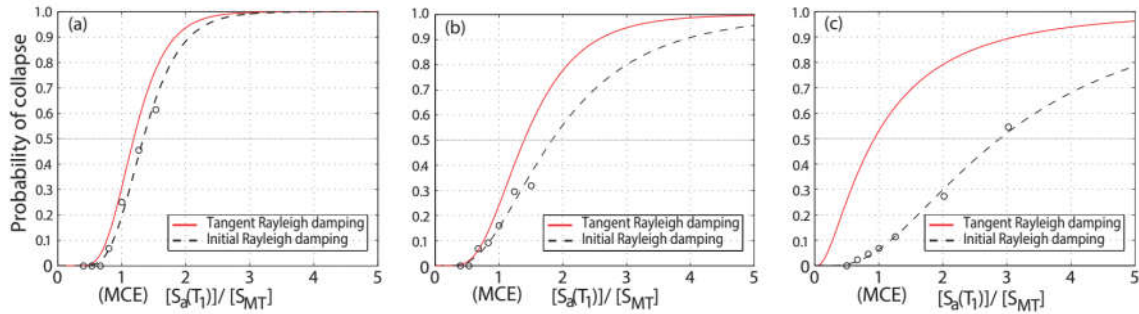


Figure 2.9 Collapse fragility curves for a) three-, b) six-, and c) 12-storey SCBF without gravity framing contribution and fixed connections

2.7 Inter-Storey Drift Response

The distribution of inelastic deformation along the height of the building near collapse has often been identified as a concern for braced frames [37]. This section expands on Section 2.5, which showed an example of how the connection strength and stiffness can change the collapse mechanism of an SCBF, by comparing the median peak inter-storey drift ratios (IDR) of the considered braced frames. Figure 2.10 shows the results for the three and six-storey buildings at MCE, $1.25 \times \text{MCE}$ and $1.5 \times \text{MCE}$, and for the 12-storey building at MCE, $1.25 \times \text{MCE}$ and $2 \times \text{MCE}$. For clarity, the results are shown only for models with the gravity framing neglected and for one model including gravity framing. That model was selected to be the case with shear tab connections in the braced bay because this is expected to be most representative of the response with the new replaceable brace module (Figure 2.1(d)), unless a fixed connection is designed. The median peak IDR is shown in this figure, as well as the limit on the peak inter-storey drifts at the MCE level from ASCE 7-16 [38]. The collapse limit was set as a 5% inter-storey drift ratio, so when an individual storey in a given model reached this limit, the analysis was stopped and the model was considered to have collapsed.

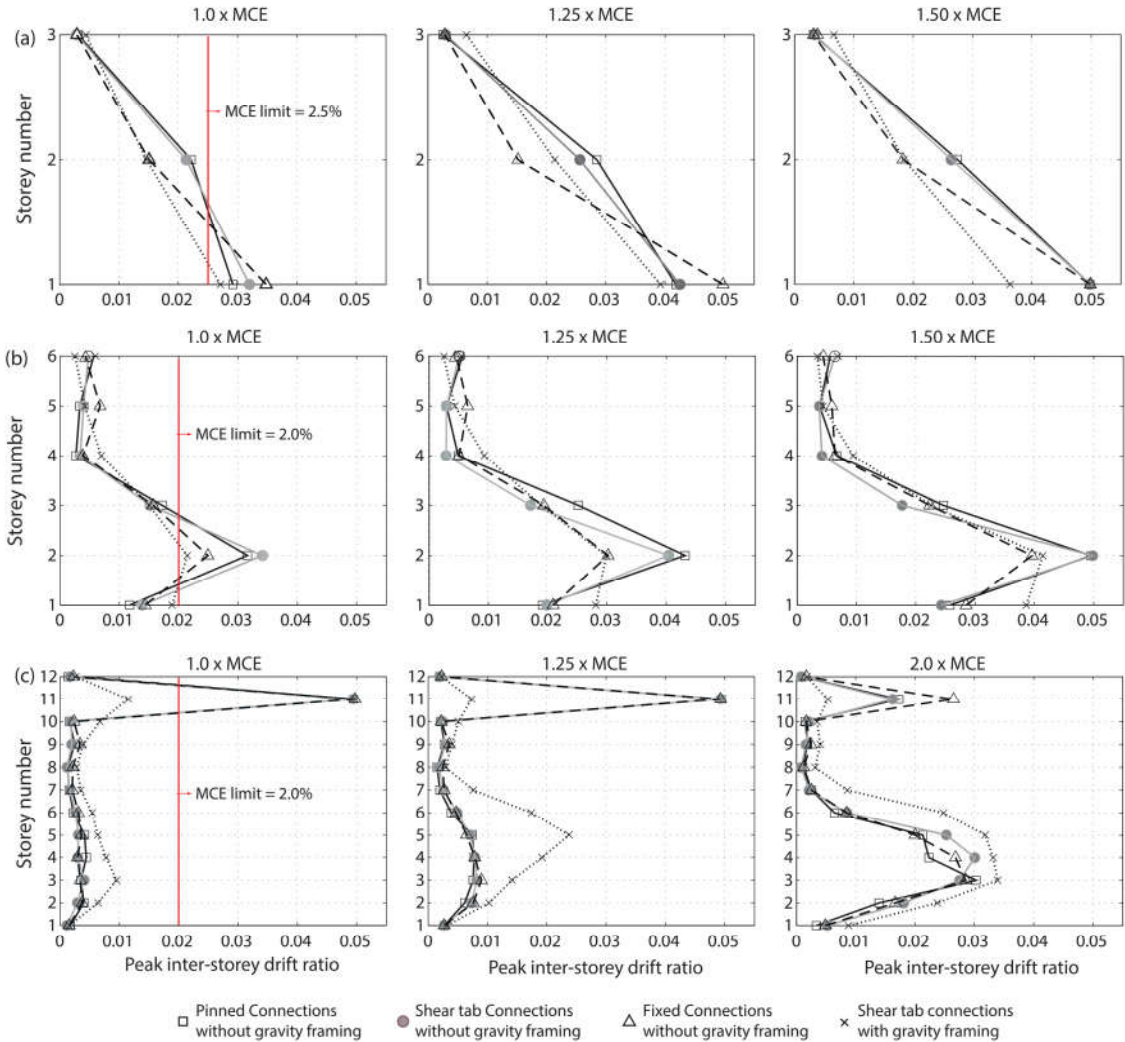


Figure 2.10 Peak inter-storey drift ratios for (a) 3-storey building (b) 6-storey building (c) 12-storey building

For the three-storey model, the median peak IDR at the first storey exceeds the MCE limit, regardless of the connection fixity and the gravity framing modelling. There is only a slight difference between the median peak IDR for models with pinned or shear-tab connections if the gravity framing is not modelled, and assuming fixed connections affects the

distribution of peak IDR over the height, even though it does not affect the collapse capacity (Figure 2.7(a)).

For six-storey buildings, Figure 2.9 shows that the maximum value of median peak IDR occurs in the second floor for all considered models. The median peak IDR response for SCBFs with pinned connections are similar to the median peak IDR response for the models with shear tab connections in models without gravity framing, as was previously seen in the example of Section 5 and in the collapse fragility curves of Figure 2.7(b).

For the 12-storey building, Figure 2.9 shows that changing the connection fixity has only a slight influence on the median peak IDR response, but adding the gravity framing to the model has a substantial effect. The median peak IDR response for the 12-storey SCBFs without the gravity framing contribution shows that large drifts due to brace damage commonly occur at the 11th storey under MCE and 1.25MCE ground motion levels. At twice the MCE level, more than 50% of the ground motions caused collapse (see Figure 2.7(c) and 2.7(f)), but the storey that caused collapse was distributed more uniformly over the height, leading to the median peak IDR being less than 5% at all storeys. When the gravity framing is modelled, the storey that initiates collapse becomes more uniformly distributed.

In order to measure the effects of connection fixity and gravity framing on drift concentration tendency, a drift concentration factor (DCF) was considered, defined as the ratio of maximum storey drift to the maximum roof drift [19]. Values of DCF much greater than unity indicate that drift is not distributed evenly over the building height. DCF index values are shown in Figure 2.11 at the MCE intensity level. Figure 2.11 indicates that the drift concentration severity increases as the building height increases. Figure 2.11(a) shows that providing fixed connections leads to slightly smaller DCF values for the taller frames. The effect of gravity framing on DCF is more significant, especially for the 12-storey frame.

DCF values are also presented for models with only the gravity columns contribution in Figure 2.10(b). DCF values for these systems are comparable to those calculated for models that include the complete gravity framing (Figure 2.11(a)). As expected, increasing the stiffness of continuous gravity columns decreases DCF values.

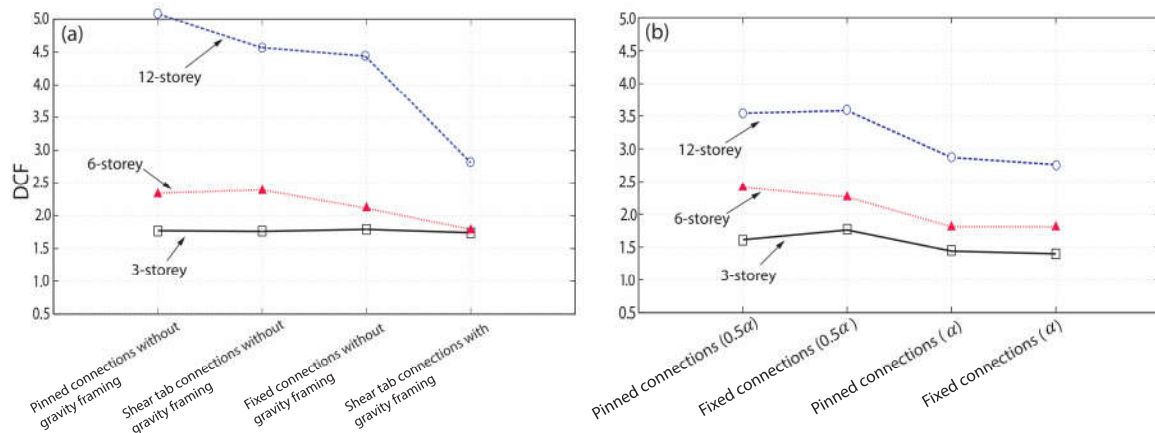


Figure 2.11 DCF index values at MCE level for different models considering a) connection fixity and gravity framing effects b) connection fixity and gravity column effects

2.8 Summary and Design Recommendations

This paper investigated the influence of connection fixity on the collapse capacity of SCBFs, without or with the gravity framing in the numerical model. Three-, six- and twelve-storey SCBF buildings were considered, with three different connection conditions (i.e. pinned, shear tab and fixed) at the beam-column connections. The collapse fragility curves were constructed using multiple stripe analysis. Tangent stiffness proportional Rayleigh damping was used, except that one model for each building was also analyzed using the initial stiffness to compute the damping matrix and Raleigh damping coefficients. The main findings are:

- The difference between models with pinned and shear tab connections was less than a 5% change in the median collapse capacities for all buildings. When the

contribution of the gravity framing was ignored, the connection fixity had essentially no effect on the collapse capacity for the three-storey SCBF, but assuming fixed connections improved the collapse margin ratio by 22% and 33% for six- and 12-storey SCBFs, respectively, relative to a model with pinned connections.

- Modelling gravity framing improved the collapse capacity of the SCBF buildings significantly. Indeed, the influence of gravity framing in the three- and six-storey buildings was so strong that the connection fixity within the braced bay had no influence on the collapse capacity of the system when gravity framing was modelled. For the 12-storey building, modelling the gravity framing increased the collapse margin ratio to be 2.5 times larger on average than for the models without the gravity framing.
- The stiffness matrix used to compute the Rayleigh damping had a significant effect on the collapse margin ratio, particularly in taller buildings. Using the initial stiffness instead of the tangent stiffness increased the collapse margin ratio by 10%, 30% and 310% for three-, six-, and twelve-storey buildings, respectively.
- The modelled connection fixity could also change the plastic failure mechanism near collapse. Assuming fixed connections caused more consistent median inter-storey drift ratios over the height. Modeling gravity framing also changed the plastic mechanism by reducing the peak inter-storey drift ratios, and improving the distribution of nonlinearity along the height of the building.
- For low-rise and mid-rise buildings (up to six storeys), there is no need to provide beam-column fixity within the braced bay because its effect is negligible when compared to that of typical gravity framing. However, for taller buildings (12 storeys), the gravity framing was found to be essential for ensuring an adequate collapse margin ratio, with additional stiffness required when the connections within the braced bay are pinned compared to when they are fixed. A check on

minimum gravity column stiffness of $\alpha > 0.015$ is recommended when the connections within the braced bay are pinned, or $\alpha > 0.008$ when they are designed as fixed.

Based on these findings, gravity framing has a strong influence on the collapse capacity of special concentrically braced frames and it should be considered in collapse modelling of these type of buildings. When sufficient gravity framing is provided to redistribute loads after the onset of brace nonlinearity, as described above, no additional design requirements are needed for the connection fixity within the braced bay.

While the primary objective of this paper was to compare the response of special concentrically braced frames with different degrees of beam-column connection fixity, the results that were based on a 20% probability of collapse for individual archetypes would not be considered acceptable based on a 10% probability of collapse for performance groups. Therefore, they point to a need for further study of the collapse performance of concentrically braced frames, with due consideration of such modelling parameters as gravity framing, inherent damping modeling, panel zone deformations, composite action if present, and beam and column deterioration at drift levels near collapse.

Acknowledgments

The financial support of the Canadian Institute of Steel Construction (CISC) and the National Sciences of Engineering Research Council (NSERC) is gratefully acknowledged.

References

- [1] Astaneh-Asl A. Seismic behaviour and design of gusset plates. Steel TIPS, Structural Steel Educational Council, Moraga, California, December: 1998.
- [2] Lehman DE, Roeder CW, Herman D, Johnson S, Kotulka B. Improved seismic performance of gusset plate connections. J Struct Eng 2008;134:890–901.

- [3] Roeder CW, Lumpkin EJ, Lehman DE. A balanced design procedure for special concentrically braced frame connections. *J Constr Steel Res* 2011;67:1760–72.
- [4] Tsai C-Y, Tsai K-C, Lin C-H, Wei C-Y, Wang K-J, Yu Y-J, et al. Cyclic responses of three 2-storey seismic concentrically braced frames. *Front Arch Civ Eng China* 2010;4:287–301.
- [5] Lumpkin EJ. Enhanced seismic performance of multi-storey special concentrically brace frames using a balanced design procedure. MSc thesis, University of Washington, 2009.
- [6] Stevens D, Wiebe L. Large-scale testing of a replaceable connection for concentrically braced frames. 16th World Conf. Earthq. Eng., Santiago Chile, January 9th to 13th: 2017.
- [7] Yoo JH, Lehman DE, Roeder CW. Influence of connection design parameters on the seismic performance of braced frames. *J Constr Steel Res* 2008;64:607–23.
- [8] Stoakes CD, Fahnestock LA. Cyclic flexural testing of concentrically braced frame beam-column connections. *J Struct Eng* 2011;137:739–47.
- [9] Stoakes CD, Fahnestock LA. Cyclic flexural analysis and behaviour of beam-column connections with gusset plates. *J Constr Steel Res* 2012;72:227–39.
- [10] Uriz P, Mahin SA. Toward earthquake-resistant design of concentrically braced steel-frame structures. UCB/PEER-2008/08, Univ. of California, Berkeley, CA.: 2008.
- [11] Bradley CR, Fahnestock LA, Hines EM, Sizemore JG. Full-scale cyclic testing of low-ductility concentrically braced frames. *J Struct Eng* 2017;143:04017029.
- [12] Sizemore JG, Fahnestock LA, Hines EM, Bradley CR. Parametric Study of Low-Ductility Concentrically Braced Frames under Cyclic Static Loading. *J Struct Eng*

2017;143:04017032.

- [13] Kanyilmaz A. Secondary frame action in concentrically braced frames designed for moderate seismicity: a full scale experimental study. *Bull Earthq Eng* 2016;15:2101–27.
- [14] Malaga-Chuquitaype C, Elghazouli AY. Contribution of secondary systems to the seismic performance of steel framed structures. 14th Eur. Conf. Earthq. Eng., Ohrid, Republic of Macedonia: 2010.
- [15] Liu J, Astaneh-Asl A. Cyclic testing of simple connections including effects of slab. *J Struct Eng* 2000;126:32–9.
- [16] Liu J, Astaneh-Asl A. Moment–rotation parameters for composite shear tab connections. *J Struct Eng* 2004;130:1371–80.
- [17] Green TP, Leon RT, Rassati GA. Bidirectional tests on partially restrained, composite beam-to-column connections. *J Struct Eng* 2004;130:320–7.
- [18] Ji X, Kato M, Wang T, Hitaka T, Nakashima M. Effect of gravity columns on mitigation of drift concentration for braced frames. *J Constr Steel Res* 2009;65:2148–56.
- [19] MacRae GA, Kimura Y, Roeder C. Effect of column stiffness on braced frame seismic behaviour. *J Struct Eng* 2004;130:381–91.
- [20] Hsiao P-C, Lehman DE, Roeder CW. Evaluation of the response modification coefficient and collapse potential of special concentrically braced frames. *Earthq Eng Struct Dyn* 2013;44:657–75.
- [21] Málaga-Chuquitaype C, Elghazouli AY, Enache R. Contribution of secondary frames to the mitigation of collapse in steel buildings subjected to extreme loads. *Struct Infrastruct Eng* 2016;12:45–60.

- [22] Hwang S-H, Lignos D. Effect of modeling assumptions on the earthquake-induced losses and collapse risk of steel-frame buildings with special concentrically braced frames. *J Struct Eng* 2017;143:04017116.
- [23] FEMA P695. Quantification of building seismic performance factors FEMA P695. Federal Emergency Management Agency, Washington, D.C.: 2009.
- [24] NEHRP Consultants Joint Venture. Evaluation of the FEMA P-695 Methodology for Quantification of Building Seismic Performance Factors (NIST GCR 10-917-8). 2010.
- [25] American Society of Civil Engineers (ASCE). Minimum design loads for buildings and other structures (ASCE/SEI 7-05). Reston, Virginia: 2006. doi:10.1061/9780784412916.
- [26] American Institute of Steel Construction. Seismic Provisions for Structural Steel Buildings, ANSI/AISC 341–05. Chicago, IL: 2005.
- [27] McKenna FT. Object-oriented finite element programming: Frameworks for analysis, algorithms and parallel computing. Ph.D. University of California, CA, 1997.
- [28] Newell J, Uang C. Cyclic behaviour of steel columns with combined high axial load and drift demand. Rep. No. SSRP-06/22, Dept. of Structural Engineering, University of California, San Diego: 2006.
- [29] Gunnarsson IR. Numerical performance evaluation of braced frame systems. MSc thesis, University of Washington, 2004.
- [30] Karamanci E, Lignos D. Computational approach for collapse assessment of concentrically braced frames in seismic regions. *J Struct Eng* 2014;140:1–15.
- [31] Hsiao PC, Lehman DE, Roeder CW. Improved analytical model for special

- concentrically braced frames. *J Constr Steel Res* 2012;73:80–94.
- [32] Elkady A, Lignos DG. Effect of gravity framing on the overstrength and collapse capacity of steel frame buildings with perimeter special moment frame. *Earthq Eng Struct Dyn* 2015;44:1289–307.
- [33] Jalayer F. Direct probabilistic seismic analysis: implementing non-linear dynamic assessments. Doctoral dissertation, Stanford University, 2003.
- [34] Chen C-H, Mahin SA. Seismic collapse performance of concentrically steel braced frames. *Proc. Struct. Congr. 19th Anal. Comput. Spec. Conf.*, Orlando, Florida: 2010, p. 1–8.
- [35] Flores F, Charney F, Lopez-Garcia D. The influence of gravity column continuity on the seismic performance of special steel moment frame structures. *J Constr Steel Res* 2016;118:217–30.
- [36] Tremblay R. An inverted V-braced frame system exhibiting bilinear response for seismic stability under long duration subduction earthquakes. *9th Int. Conf. Behav. Steel Struct. Seism. Areas*, Christchurch, New Zealand: 2018.
- [37] Roeder CW, Lehman DE, Clark K, Powell J, Yoo J-H, Tsai K-C, et al. Influence of gusset plate connections and braces on the seismic performance of X-braced frames. *Earthq Eng Struct Dyn* 2011;40:355–74.
- [38] American Society of Civil Engineers (ASCE). *Minimum Design Loads and Associated Criteria for Buildings and Other Structures*. Reston, Virginia: 2017.

3 Seismic Design of Braced Frame Columns with and without Replaceable Brace Modules

Abstract

In special concentrically braced frames (SCBFs), braces are intended to dissipate seismic energy through inelastic buckling and tensile yielding, while the beams and columns should remain elastic according to capacity design. However, past studies have shown that column yielding during seismic events is possible with current design approaches. In this study, nonlinear response history analyses are performed to examine the effects of column design on braced frame seismic performance. Two different connections are considered for joining the braces to the other elements: a typical connection with a gusset plate, and a novel connection in which bolts are used instead of field welding in an effort to confine damage to the replaceable brace modules (RBMs). Three special concentrically braced frames of different heights are modelled. The seismic performance of the structures is discussed in terms of seismic demands on the columns at two intensity levels, as well as collapse capacity. The results show that, when columns are designed considering only the axial force demands from a capacity design procedure, column yielding is frequent, and the columns are not stiff enough to avoid a soft-storey mechanism, leading to an unacceptable collapse capacity. The eccentricity in the beam-column connections with RBMs does not increase the peak column force demand. Modifications are proposed for considering moments in the design procedure to ensure that columns can safely resist the seismically induced axial and flexural demands, so as to pass the collapse capacity criterion of FEMA P695. The improved column design approaches are also shown to reduce the residual drifts, thus facilitating post-earthquake repairs.

Keywords: Seismic design; Concentrically braced frames; Replaceable brace module; Column demand; Collapse fragility

3.1 Introduction

3.1.1 Brace Connection Design

A special concentrically braced frame (SCBF) is capable of providing significant inelastic deformation capacity [1] and is common as the seismic force resisting system for steel buildings in regions of high seismicity in North America. During an earthquake, the braces are intended to dissipate seismic energy through tension yielding, inelastic buckling, and inelastic bending of the braces when they are straightened subsequently. In current practice, a gusset plate is typically used to connect the brace to the frame members (e.g. Figure 3.1(a-b)). An alternative connection detail has recently been developed based on a replaceable brace module (RBM) (Figure 3.1(c-d)) [2,3]. This alternative connection is intended to increase erection speed by using bolts instead of field welding to connect the brace, to avoid cladding damage by making the brace buckle in the in-plane direction, and to reduce the time of post-earthquake repairs by confining all the damage to the RBM. In this connection, the brace module is only connected to the beam, which allows the designer to select beam-column connection types that are simple (e.g. Figure 3.1(c)) or moment resisting (e.g. Figure 3.1(d)). These different connections might place different force demands on the columns, resulting in different collapse capacity.

Traditional gusset plate connections can be designed using the uniform force method (UFM) [4], which has been included in the AISC Manual of Steel Construction since 1992. In the UFM, the work-point of the brace is commonly located at the intersections of centerlines of the beam and the column (Figure 3.1(a-b)), and the welds to the beam and column are designed to satisfy equilibrium such that there is no moment on the column. However, in the proposed alternative connection, the brace module is only connected to the beam, and in simple beam-column connections, the work-point is located at the intersection of the column face and the beam centerline. In this case, the beam-column connection is not designed for a moment, but the eccentricity causes an extra moment on

the column. This eccentricity is equal to half the column depth and is typically smaller than the beam depth, which is the limit on eccentricity in SCBFs as defined in AISC 341-16 [1]. Thus, it is necessary to quantify the axial and flexural demands on columns at different intensity levels and to assess the collapse capacity of the braced frames with different types of beam-column connections. It is also needed to review and enhance the column design provisions as necessary to allow using of the proposed connection in braced frames with different heights.

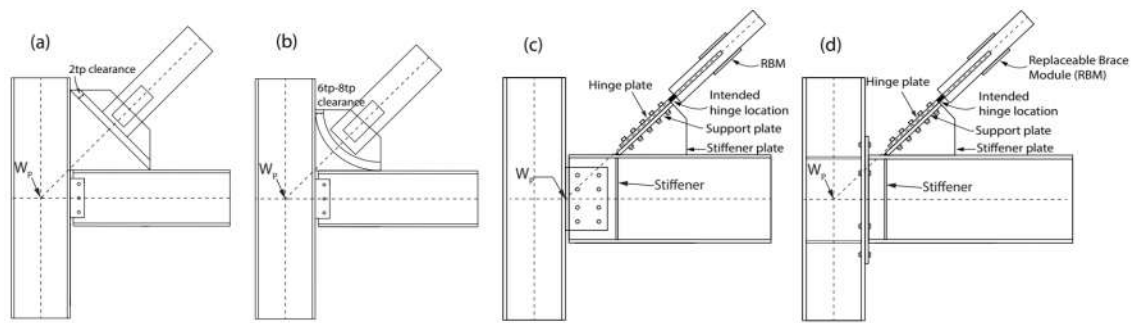


Figure 3.1 Brace to frame elements connection details: Typical gusset plate with a) linear hinge zone, b) elliptical hinge zone; proposed connection with c) single shear tab, and d) bolted unstiffened extended end plate connection

3.1.2 Column Design

An SCBF system is designed to transfer the lateral load from the floor levels to the ground in the linear elastic range primarily via axial forces in braces, beams, and columns. According to AISC 341-16 [1], columns should be designed using the capacity-limited seismic load effect to remain elastic under brace yielding and either buckling or post-buckling forces. Designing for the maximum axial forces from those analyses might be conservative because such high axial forces may never fully develop or be sustained [5]. For that reason, some studies have proposed that the current capacity provisions could be

relaxed [5] and others have suggested new combination rules for computing column axial demand in braced frames to avoid excessive conservatism in design [6]. However, some recent studies have revealed that the collapse capacity for SCBF systems might not be acceptable, even when columns were designed according to current capacity design provisions, when the tangent stiffness matrix is used to calculate the stiffness-proportional damping component of the Rayleigh damping matrix [7,8].

In addition to axial force demands, flexural demand also develops during earthquake loading due to differences in drift angles between adjacent storeys. Depending on the type of beam-column connection, moment frame action and eccentricity between the work-point of the brace and the column centerline can be other sources of flexural demand on columns. In conventional braced frames, the gusset plate increases the flexural strength and stiffness of the beam-column connections [9,10] such that frame action develops that may result in yielding of beam and column members [11]. However, in a frame with RBMs, if a designer chooses to use simple beam-column connections, there will be less moment frame action, which can change the flexural demand on columns. According to AISC 341-16 [1], if the procedure explained above is used to calculate the axial force on columns, the engineer can neglect the flexural demands regardless of beam-column connection fixity. Conversely, in Canada, CSA S16-19 [12] requires an additional bending moment in the plane of the braced bay of $0.2ZF_y$, where Z is the plastic section modulus and F_y is the yield strength of the column section, to be considered in combination with axial loads.

SCBFs are prone to damage concentration in a few weak storeys in strong earthquake events [13,14]. Damage concentration can amplify $P-\Delta$ effects, increasing the storey drift in the softened storey and possibly resulting in large residual displacements. Among different approaches that have been proposed to mitigate this problem, providing continuous columns with sufficient strength and stiffness in both the seismic force resisting system and the gravity framing is one potential strategy [15,16]. In that case, there is a need

to ensure that the flexural capacity of the columns at each storey is enough to redistribute the lateral force demand to the adjacent storeys when braces are in the post-buckling range of response. It has also been reported that considering only the first mode of deformation for designing the columns in mid-rise SCBFs does not necessarily result in the most critical demand [17]. To avoid soft-storey response in SCBFs, a new modified procedure for designing the columns in SCBFs was recently proposed [18]. In the modified procedure, at each storey, it is assumed that the tension brace has fractured and the compression brace has buckled, and the amplified storey shear must be carried by the columns through a mechanism consisting of plastic hinges at the column ends. The seismic response of the considered SCBFs was improved by using this design method, although the quantity of steel needed for the columns increased significantly (e.g. more than doubled in some cases). Thus, additional studies are needed to minimize the material usage while ensuring that the seismic performance of the SCBFs is still acceptable.

3.1.3 Objectives

This article presents a study conducted with the objective of developing improved provisions for designing the columns in SCBFs located in regions of high seismicity. The SCBFs are modelled using two different brace-to-frame connections: 1) conventional connection detailing and 2) the newly proposed connection detail with RBMs. Current provisions included in AISC 341-16 [1] are first considered for designing the reference structures. In the first phase of this study, as the columns are intended to stay elastic during a seismic event following capacity design principles, they are modelled as elastic in order to monitor and compare the peak demands on columns in systems with different connections. Based on the insight gained from this, in the second phase, three alternative methods are considered for determining the moment demand on columns. The seismic response of the SCBFs computed by nonlinear response history analysis (NLRHA) is then examined to assess the potential methods, where the goal is to reduce the storey drift

concentration in order to ensure adequate collapse capacity. The influence of column design on residual drifts is also assessed.

3.2 Design of Reference SCBFs

Three SCBF buildings with a two-storey X configuration, designed for a downtown area of San Francisco, California, are considered in this study. Table 3.1 shows the seismic design parameters. These buildings, which are designed for office occupancy (Risk category II), have a rectangular plan configuration with braced bays located along the perimeter of the building, as shown in Figure 3.2. Each bay of the buildings is 9.14 m wide in both directions, the height of each storey is 4.57 m, and there are no torsional or horizontal irregularities. The seismic weight of each floor and roof is 8800 kN and 6800 kN, respectively. Three different building heights (three, six, and 12 storeys) were designed in accordance with the AISC seismic design provisions [1] for the maximum spectral intensity (D_{max}) associated with the governing seismic design category in compliance with ASCE/SEI 7-16 [19], using the equivalent lateral force (ELF) procedure for the three- and six-storey buildings and the response spectrum analysis (RSA) procedure for the 12-storey building. The braces are circular hollow structural sections (HSS), and their assumed effective length was 70% of the work-point-to-work-point length. The orientation of the columns in the considered frame was such that in-plane bending is about the strong axis, and they are assumed to be fixed at their bases. For the interior gravity columns, a weak-axis orientation is considered, which represents the conservative scenario for contribution to the overall system response. Identical column sections are used for every two consecutive storeys and were selected to ensure that the local slenderness ratios satisfy the limitations for highly ductile members provided by AISC 341-16 [1]. Table 3.2 shows the structural sections used for the considered buildings, and summarizes the geometric properties of the column sections (h/t_w and $b_f/2t_f$ are the web and flange slenderness ratios, respectively) and the slenderness ratio of column members (L_b/r_y). It also contains

the designed demand over capacity axial load ratio, P_r / P_{CL} , where P_r is the axial force demand computed based on the load combinations including the capacity of braces and P_{CL} is the compressive strength calculated using nominal steel properties [20]. During the design, it was tried to keep P_r / P_{CL} as close as possible to one for all storeys.

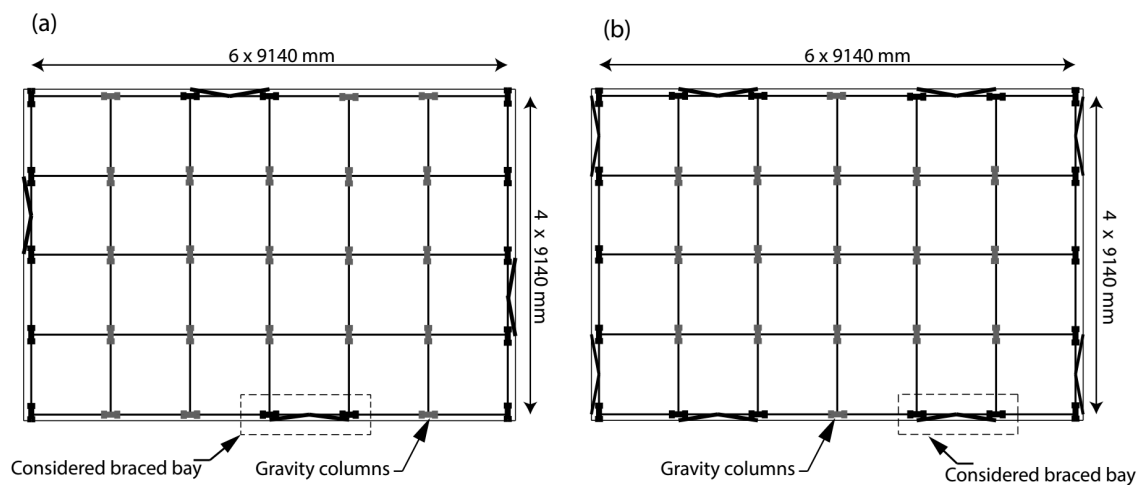


Figure 3.2 Plan configuration of a) three- and six-storey buildings b)12-storey building

Table 3.1 Seismic design parameters

Parameters	Value
Importance factor	1.0
Site class	D (default)
Short period site coefficient (F_a)	1.2
Short period site coefficient (F_v)	1.7
S_{DS}	1.2g
S_{D1}	0.68g

Table 3.2 Section sizes

Storey	Braces	Beams	Columns				
			Section	P_r/P_{CL}	$b_f/2t_f$	h/t_w	L_b/r_y
3-storey							
3	HSS7.5x0.375	W30x173	W12x120	0.05	5.57	13.7	57.5
2	HSS8.75x0.5	W21x111	W12x120	0.79	5.57	13.7	57.5
1	HSS9.625x0.5	W18x65	W12x120	0.85	5.57	13.7	57.5
6-storey							
6	HSS7.5x0.5	W18x97	W14x68	0.83	6.97	27.5	72.5
5	HSS9.625x0.5	W24x131	W14x68	0.93	6.97	27.5	72.5
4	HSS10.75 x0.5	W21x93	W14x176	0.90	5.97	13.7	44.8
3	HSS11.25x0.625	W24x146	W14x176	0.93	5.97	13.7	44.8
2	HSS12.5x0.625	W24x131	W14x342	0.93	3.31	7.41	42.3
1	HSS12.5x0.625	W18x97	W14x342	0.95	3.31	7.41	42.3
12-storey							
12	HSS6.625x0.5	W18x71	W10x68	0.73	6.58	16.70	69.50
11	HSS6.625x0.5	W18x86	W10x68	0.85	6.58	16.70	69.50
10	HSS8.75x0.375	W18x71	W12x136	0.90	4.96	12.30	57.10
9	HSS8.75x0.375	W18x86	W12x136	0.95	4.96	12.30	57.10
8	HSS8.625x0.5	W18x71	W14x90	0.94	5.06	11.60	44.40
7	HSS8.625x0.5	W18x86	W14x90	0.97	5.06	11.60	44.40
6	HSS8.625x0.5	W18x71	W14x311	0.94	3.59	8.09	42.70
5	HSS8.625x0.5	W18x86	W14x311	0.96	3.59	8.09	42.70
4	HSS9.625x0.5	W18x71	W14x398	0.98	2.92	6.44	41.80
3	HSS9.625x0.5	W18x86	W14x398	0.99	2.92	6.44	41.80
2	HSS9.625x0.5	W18x71	W14x550	0.90	2.25	4.79	40.10
1	HSS9.625x0.5	W18x86	W14x550	0.92	2.25	4.79	40.10

3.3 Nonlinear Modelling

The seismic performance of the study frames was evaluated using OpenSees [21]. Figure 3.3 shows a schematic of the models used in the analyses. Force-based fibre beam-column elements were used to model the inelastic behaviour of the beams and columns, each with 5 integration points to account for the distributed plasticity along the length of each element. ASTM A992 grade steel with a nominal yield strength of 345 MPa was considered for beam and column elements. Force-based fibre beam-column elements were also used to capture the cyclic inelastic behaviour of the braces, according to the recommendations of Uriz and Mahin [13]. A uniaxial Giuffre-Menegotto-Pinto steel material (Steel02) with

expected brace yield strength and kinematic and isotropic strain hardening properties was assigned to each fibre. For braces, ASTM A500 Gr-B steel with a nominal yield stress of 317 MPa and over-strength factor (R_y) of 1.4 was considered. Fracture corresponding to low cycle fatigue was also modelled using the relationships recommended by Karamanci and Lignos [8] to define the input parameters of the steel brace model based on the brace geometric and material properties. Braces were modelled using twenty nonlinear beam-column elements with an initial out-of-straightness in the form of a sinusoidal function with an amplitude of $L/1000$. When the actual strength of columns was considered, to trace the global instability of the columns properly, a global out-of-straightness imperfection of $L/1000$ was introduced to the model and eight nonlinear beam-column elements were used for each column [5] with a non-deteriorating material (Steel02) assigned to the fibres. No initial residual stress was included for the columns because its effects on the hysteretic behaviour of the stocky columns, which are used in this study, are negligible [5,22]. Column splices were assumed to be designed as fully rigid and located at 1.7 m above the beam-column connection centerlines.

It has been reported that stocky sections can sustain their flexural strength and stiffness up to drift ratios of 0.07-0.09 rad under high axial load demands [23]. Columns in braced bays experience large axial load fluctuations during a seismic event, but that axial force variation has been found not to cause strength deterioration up to drift ratios of 0.06 for stocky sections [24]. In addition, Elkady and Lignos [25,26] observed that the plastic deformation capacity of steel columns based on a collapse-consistent loading history is twice that of steel columns subjected to a symmetric lateral-loading history. Therefore, although the model used in this study did not capture local web and flange instabilities, this was considered acceptable for the stocky columns that were used in this study up to at least 6% inter-storey drift, which defined collapse for this study.

In the conventional SCBF with typical gusset plate connections, rigid offsets were modelled at the end of the elements, as shown in Figure 3.3(b). In columns, these rigid elements extend from the work point to either the physical end of the gusset plate or the physical end of the beam. In beams, they continue from the work point to the point at 75% of dimension ‘a’ [27]. The gusset plate hinge region was modelled using a fibre beam-column element with a length equal to twice the gusset plate thickness and with three integration points. In this model, it was assumed that the gusset plate could provide sufficient strength and stiffness for the beam-column connection that the beam-column connection could be modelled as fixed. The braces were modelled to buckle in the out-of-plane direction.

Figure 3.3(c) shows details of the numerical model for an SCBF when using the proposed single shear tab connection detail for replaceable brace modules. In this new connection, the in-plane rotation of the brace is accommodated using a clearance distance equal to twice the hinge plate thickness, so the previous modelling procedure for the gusset plates was also used for modelling the hinge plate. Rigid elements were used to represent the physical size and the stiffening effect of the secondary plates and connected the intended hinge location to the centerline of the beam. In this model, because the connection is offset from the column face and the traditional gusset plate does not exist (see Figure 3.1(c)), the beam-column connection was assumed to be pinned. The braces were modelled to buckle in the in-plane direction.

The model contains a leaning column to represent the gravity framing, as indicated in Figure 3.3(a). This leaning column, modelled using force-based beam-column elements, was loaded vertically with the tributary seismic load of each floor, and the mass tributary to the gravity columns was lumped at the leaning column nodes. The gravity system, including gravity columns and beam-column connections with composite action, can improve the collapse capacity of SCBFs [7,28]. The contribution from beam-column

Tangent stiffness-proportional Rayleigh damping based on 3% of critical damping in the first and third modes was applied using the committed stiffness matrix. Tangent stiffness-proportional damping was chosen over initial stiffness-proportional Rayleigh damping because the latter can cause unconservative results in nonlinear time-history analysis [7,8]. During the analyses, eigenvalue analysis was performed at each time step and the Rayleigh damping coefficients were updated. When an eigenvalue became negative, the Rayleigh damping was computed only based on the mass-proportional term to avoid negative damping forces.

3.4 Ground Motion Selection and Scaling

The suite of 44 far-field orthogonal horizontal ground motion components from FEMA P695 [29] was used for the analysis. The target spectrum for selecting and scaling the ground motions is the risk-targeted maximum considered earthquake spectrum (MCE_R) of ASCE/SEI 7-16 [16]. The ground motions were scaled to minimize the sum of the squares of the differences between the target spectrum and the individual records' spectra within the period range of interest, which was taken between $0.2T_l$ and $2T_l$, where T_l is the computed period of the structure for each height. The average spectrum was a little lower than the MCE spectrum. To avoid undershooting the target spectrum beyond the corner period, for each building all the ground motions were further scaled by a common factor such that their average does not fall below 95% of the target spectrum within the period range of interest. As shown in Figure 3.4, while the average 5% damped spectrum was in good agreement with the target spectra over a range of periods of interest of larger than $T_s=0.58$ s, it overshoots the target spectra at smaller periods. After finding the scaling factors for each ground motion, a factor of 2/3 was used to match the average acceleration spectrum to the design earthquake (DBE) level.

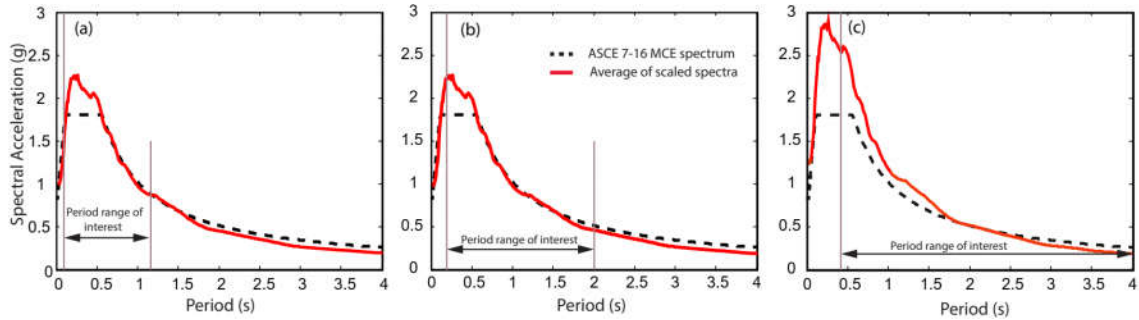


Figure 3.4 Scaling of the selected ground motions for a)three-storey building b)six-storey building c)12-storey building

3.5 Column Demand in SCBFs

3.5.1 Models with Elastic Columns

To find and compare the peak force demands on columns in systems with different connections, the columns were modelled as elastic for the first phase of analysis. The P-M interaction ratio (D/C) was calculated at every time step, and Figures 3.5 to 3.7 show the median and median plus one standard deviation of the maximum P-M interaction ratio during the time-history analyses at DBE and MCE levels of each column segment. These values were obtained from the AISC 360-16 [20] equations:

$$\left\{ \begin{array}{l} \text{When } \frac{P_r}{P_c} \geq 0.2 \rightarrow \frac{D}{C} = \frac{P_r}{P_c} + \frac{8}{9} \left(\frac{M_r}{M_c} \right) \leq 1.0 \\ \text{When } \frac{P_r}{P_c} < 0.2 \rightarrow \frac{D}{C} = \frac{P_r}{2P_c} + \left(\frac{M_r}{M_c} \right) \leq 1.0 \end{array} \right. \quad (3.1)$$

where P_r is the axial load demand at each time step, P_c is the factored available axial strength, M_r is the flexural strength demand at each time step, and M_c is the factored available flexural strength. Figures 3.5 to 3.7 also show the first term (axial force) and

second term (moment) portions of Eq. (3.1) separately at the moment of maximum P-M interaction ratio.

Figure 3.5 shows the results for the three-storey SCBF. As a result of concentration of inelastic deformation in the first storey, the base of the columns experienced high force demands in both the SCBF with RBMs and the SCBF with more conventional gusset plate connections (SCBF with GP). The flexural demand to capacity ratios for the bottom of the first storey columns were about 1.5 at the DBE level. Although the median axial demand was less than 50% of the axial capacity even at the MCE level, the flexural demand reached 2.25 and 2.90 times the flexural capacity for the SCBF with RBMs and the SCBF with GP, respectively, at MCE level. This is because generally the first mode dominates the behaviour of low rise SCBFs, and the seismic demands are the largest at the bottom of the building.

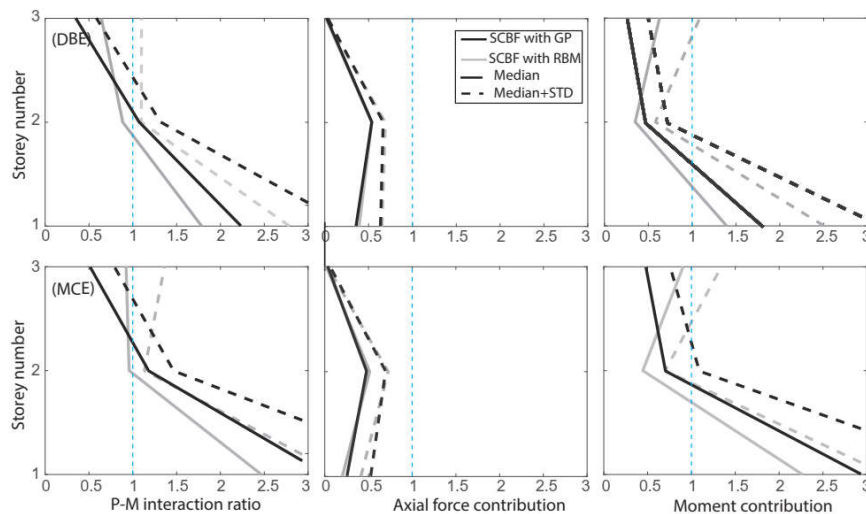


Figure 3.5 Median demand-to-capacity ratios of columns of three-storey SCBF with and without RBM

Figure 3.6 indicates that for the six-storey SCBFs at the DBE intensity level, while the median P-M interaction ratio is smaller than one for columns in the SCBF with RBMs (except at the bottom of the first storey due to the high rotational restraint), it is larger than one for columns located at the fourth and upper levels in SCBF with GP. This is because of the shorter effective brace length and thicker hinge plates in the SCBF with RBMs, which delays brace buckling, and consequently causes fewer variations in drifts resulting in less flexural demand on columns. At the MCE level, all the column segments in the conventional SCBF system experienced median P-M ratios larger than one. This is also the case for all but one level in the SCBF with RBMs. At both considered intensity levels, Figure 3.6 shows that at the moment of maximum P-M interaction ratio, the median and median plus standard deviation of axial force demands are relatively constant at approximately 60%-70% and 80%-100% of the axial resistance of the column, respectively, at both earthquake intensities. However, the flexural demand-to-capacity ratios increase significantly at the MCE level relative to DBE level. This increase is more substantial for the SCBF with RBMs relative to the conventional SCBF, primarily because of the reduced frame contribution to lateral stiffness at higher drift ratios as a result of the assumed pinned beam-column connection. At all levels and at both intensity levels, peak P-M ratios occurred when $P_r / P_c > 0.5$. In this case, ASCE 41 [30] classifies the flexure component as a force controlled action and does not permit any flexural yielding, while some other studies suggest that even at this level of axial demand the columns do possess some ductility in flexure [31]. Regardless, the uneven storey drifts put large flexural moment demands on the columns that exceed their elastic capacities under combined axial loads and moments.

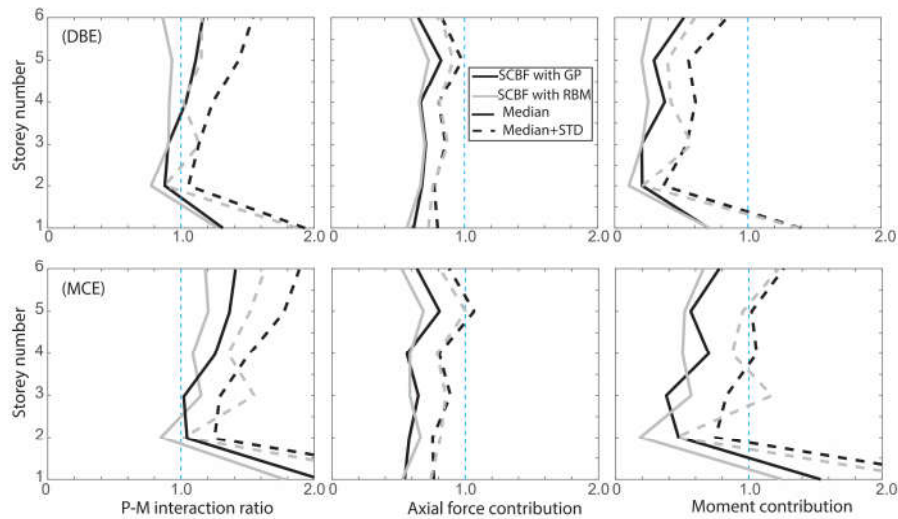


Figure 3.6 Median demand-to-capacity ratios of columns of six-storey SCBF with and without RBM

Figure 3.7 shows the results for the 12-storey SCBFs when their columns were modelled to be elastic. Unlike the six-storey models, the demand on columns was less than their capacity at the DBE and MCE levels for most of the ground motions (except the bottom of the first storey). This is related to the capacity based design procedures, where the columns are designed for a large axial force due to maximum expected compression buckling forces in all braces above the storey under consideration, while simultaneous buckling at all levels is rare in high-rise buildings. However, the median plus standard deviation response of P-M interaction is larger than 90% for most of the storeys at both considered intensity levels, which is not as conservative as expected. The median plus standard deviation curve shows large flexural demand on columns located at the ninth storey and higher for the system with RBMs, induced by the large storey drifts after brace yielding and fracture. This might trigger plastic hinging at both ends of the columns, resulting in a soft-storey response, a behaviour that cannot be predicted in elastic models used for design. This response

suggests that designing the columns based on axial force alone is not an appropriate methodology, especially for columns located at upper levels.

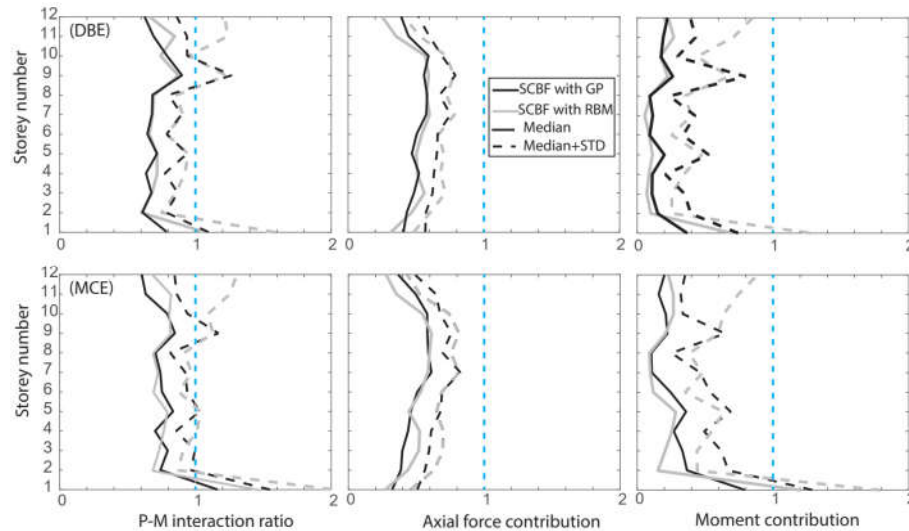


Figure 3.7 Median demand-to-capacity ratios of columns of 12-storey SCBF with and without RBM

The effects of the eccentricity in the SCBFs with RBMs were minimal because the maximum P-M interaction happens at inter-storey drifts larger than 1%, after the braces have buckled, resulting in relatively little flexural demand on columns due to the eccentricity but large flexural demands due to nonuniform drifts. Results showed that at the MCE level, even in these models where the columns were modelled as elastic throughout the analyses, the number of collapses (i.e. the maximum inter-storey drift exceeds 6%) was 13 and 15 for the three-storey, 12 and 14 for the six-storey, and was 16 and 17 for the 12-storey models with conventional connections and with RBMs, respectively. Even without a nonlinear model and a collapse risk analysis, which will be shown later in this paper, the number of collapses implies that larger sections with higher stiffness are needed for the columns to improve the collapse capacity of the system.

3.5.2 Models with Inelastic Columns

In this phase of the study, force-based nonlinear elements were used to model column yielding and buckling. Flexural deteriorations due to local instabilities are not included in the model because they are expected to be significant only at drifts beyond the range of interest. Instead, considering that columns that satisfy the local slenderness limits for highly ductile members as per AISC 341-16 [1] are expected to lose 20% of their flexural strength at about 6% inter-storey drift ratio when subjected to collapse-consistent lateral loading [32], the structure was assumed to have collapsed if the maximum storey drift reached 6%.

In order to reveal the differences in characteristics of seismic response of SCBFs with conventional gusset plate connections (SCBF with GP) and SCBF with RBMs, this section focuses on the peak inter-storey drift ratios (IDR) of the considered frames at the DBE and MCE intensity levels. Figure 3.8(a) shows that for the three-storey SCBF, both frames experienced essentially the same IDR at the DBE level. However, increasing the intensity to the MCE level resulted in higher IDR values in the SCBF with RBMs due to the lower frame contribution. For the six-storey model, the median IDR is better distributed along the height for the SCBFs with RBMs because of their higher compressive strength. For the 12-storey models, as the intensity of the ground motions increases, the drifts tend to concentrate in the lower six storeys, consistent with the findings of Al-Mashaykhi et al. [33]. The median plus standard deviation curves show that SCBFs with RBMs and pinned beam-column connections develop larger inter-storey drifts.

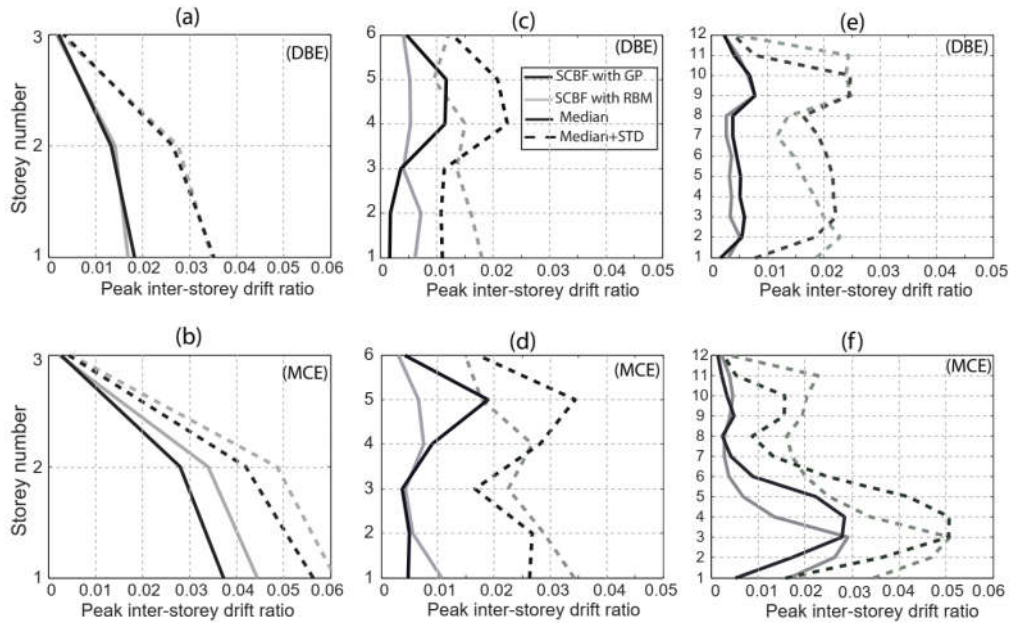


Figure 3.8 Median peak inter-storey drift ratio for: a & b) three-storey, c & d) six-storey, e & f) 12-storey SCBFs

To evaluate the collapse fragility curves, a multiple stripe analysis (MSA) [34] was conducted using stripes at the DBE, MCE and 1.5MCE levels. Following FEMA P695 [29], the adjusted collapse margin ratio (ACMR) was computed using Eq. (3.2), and was then compared to the acceptable collapse margin ratio corresponding to a 10% collapse probability limit ($ACMR_{10\%}$), which is given in Table 7-3 of FEMA P695 for a given total system uncertainty (β).

$$ACMR = \frac{\hat{S}_{CT}}{S_{MT}} SSF \quad (3.2)$$

In Eq. (2), \hat{S}_{CT} is the median collapse intensity, S_{MT} is the MCE ground motion spectral demand, and SSF is the spectral shape factor to account for the frequency content of the ground motion record set. Figure 3.9 shows the resulting fragility curves for the considered

frames. The horizontal axis shows $S_a(T_1)$, the spectral acceleration value of the first mode, normalized by the MCE ground motion spectral intensity (S_{MT}) and multiplied by the SSF factor. Thus, the ACMR value can be taken directly from the collapse fragility curves as the x-coordinate associated with a 50% probability of collapse. Table 3.3 summarizes the results of the evaluation process. In this Table, β_{DR} , β_{TD} , β_{MDL} are the uncertainty values attributed to the robustness of design requirements, the accuracy of test data, the accuracy of the numerical model, respectively and the β_{RIR} is the record-to-record variability of the collapse data. According to Table 3.3, none of the considered SCBFs passes the FEMA P695 collapse criterion. This implies that designing the columns of these example SCBF systems according to current provisions in AISC 341-16 [1], which only consider the axial force demands, does not produce an acceptable collapse capacity regardless of the connection type.

While the collapse fragility curves are generally similar for the SCBFs with conventional connections and with RBMs, for the six-storey SCBF in a model with RBMs the number of collapses at the MCE intensity stripe increases from 13 to 17 because of the reduced frame contribution. For the 12-storey SCBF with RBMs, the number of collapses at the MCE intensity stripe increases by 35% relative to the conventional model. Moreover, 30% of collapses in the SCBF with RBMs originate in upper storeys (i.e. the ninth storey and higher), whereas all of the collapses in the conventional SCBF originate in lower storeys. This observation reveals the critical role of frame action in reducing the higher mode amplifications. The main failure mode that causes collapse is a soft storey due to large storey drift after brace fracture, which places significant bending moments on the columns. Those columns start to yield in flexure even though they do not immediately buckle because the axial force demand remains small ($P_r/P_c < 0.5$) due to limited contribution of the braces in the upper storeys, which have already buckled.

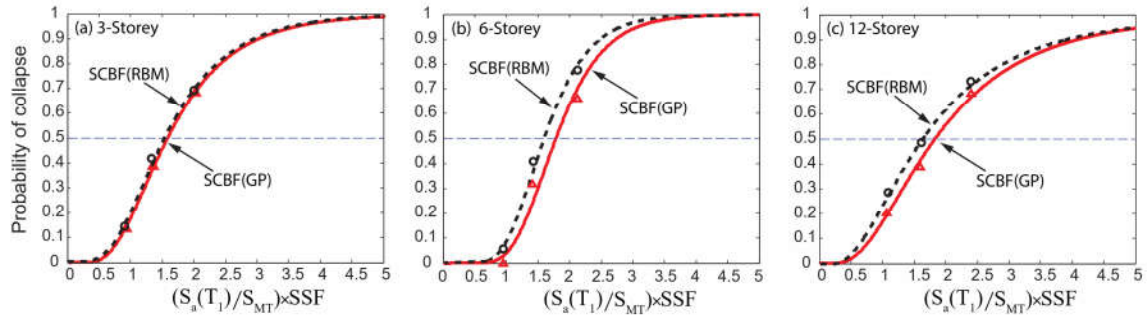


Figure 3.9 Collapse fragility curves a) three-storey b) six-storey c) 12-storey SCBF

Table 3.3 Collapse analysis results for frames designed considering only axial demands

Considered model	$\beta_{DR}, \beta_{TD}, \beta_{MDL}$	β_{RTR}	$SSF \times \hat{S}_{CT}$	S_{MT}	β	ACMR	Acceptable ACMR _{10%}	Pass/Fail ratio
3-storey								
SCBF with GP	0.2	0.45	2.88g	1.80g	0.55	1.60	2.02	0.82
SCBF with RBM	0.2	0.45	2.84g	1.80g	0.55	1.58	2.02	0.78
6-storey								
SCBF with GP	0.2	0.35	1.78g	1.03g	0.50	1.73	1.90	0.91
SCBF with RBM	0.2	0.32	1.66g	1.03g	0.47	1.62	1.84	0.88
12-storey								
SCBF with GP	0.2	0.55	0.63g	0.34g	0.65	1.85	2.30	0.80
SCBF with RBM	0.2	0.55	0.55g	0.34g	0.69	1.62	2.43	0.66

3.6 Alternative Column Design Provisions

In this section, three design procedures are proposed and examined through NLRHA for designing the columns considering both axial force demand and a bending moment demand to ensure that the frame is able to pass the collapse criterion provided by FEMA P695.

In Method 1 (M1), the columns are designed considering the axial force demands according to capacity design, and a moment of $0.2ZF_y$ is added at the column ends, similar to the process required by CSA S16-19 [12] for moderately ductile concentrically braced frames (MD-CBFs). In this methodology, the designed moment demand depends on the column

axial force capacity, because the column sections are first designed for the axial force, and according to those sections, $0.2ZF_y$ values are calculated. However, in SCBFs with more than four storeys, higher mode effects can cause peak inter-storey drift ratios at higher storey levels [33], which results in significant strong axis bending moment demands on columns located at those storeys and adjacent storeys.

In Method 2 (M2), the moment demand is calculated by assuming the braced bay columns at each storey carry 20% of the storey shear design force through a mechanism consisting of hinges at the column ends. Method 2 provides higher moment demands for columns at upper levels in comparison to Method 1. This method is proposed because the columns should be able to transfer the shear to the adjacent storeys after brace yielding and fracture.

In Method 3 (M3), which is intended to be more precise, the location of storeys with high brace buckling potential is predicted based on demand-to-capacity ratio (DCR) analysis [6], and the column moment demand is the calculated assuming that at the predicted storeys the tensile brace has fractured and the compression brace is resisting the post-buckling strength. First, the DCR values at each storey level are computed using Eq. (3.3).

$$DCR_{(i)} = \frac{V_{D(i)}}{V_{cr(i)}} \quad (3.3)$$

where $V_{D(i)}$ is the design shear that was used to design the braces (i.e. results of ELF for three- and six-storey SCBFs and RSA for the 12-storey SCBF) of the i th storey, and $V_{cr(i)}$ is the shear capacity of the i th storey calculated according to Eq. (3.4):

$$V_{cr(i)} = 2(A_{br} F_{cr} \cos \theta)_i \quad (3.4)$$

where A_{br} is the brace section area, F_{cr} is the buckling stress, and θ is the angle of the braces relative to the beam. Based on the analyses discussed in the previous section, it was

observed that more than 80% of collapses originated in storeys with DCR values within 10% of the highest DCR. For that reason, the critical storeys are identified as those with DCR values in that range.

After finding the critical storey, a condition is assumed where the tensile brace has fractured and the compression brace is carrying post-buckling axial capacity (C'_{exp}). As an example, Figure 3.10 shows the moment demands on columns under the assumed condition in the fourth floor based on a linear elastic model in ETABS. In the following equations, $V_{c(i)}$ and $M_{c(i)}$ are the shear force and moment in the braced bay column respectively, and $V_{gc(i)}$ is the shear force in the representative gravity column for storey (i).

For the columns of i th floor to transfer $V_{D(i)} - V_{0.3C_{exp}}$, their shear force is calculated as:

$$2V_{c(i)} + V_{gc(i)} = V_{D(i)} - V_{0.3C_{exp}} \quad (3.5)$$

Based on the results of the initial analyses, the inflection points are assumed to be located as shown in Figure 3.10(b) in floors i and $(i-1)$ allowing the moment demands on the columns to be calculated as:

$$\begin{cases} M_{c(i+1)} = 0 \\ M_{c(i)} = V_{c(i)} \times 0.4h_i \\ M_{c(i-1)} = V_{c(i)} \times 0.6h_i \\ M_{c(i-2)} = 0.25M_{c(i-1)} \end{cases} \quad (3.6)$$

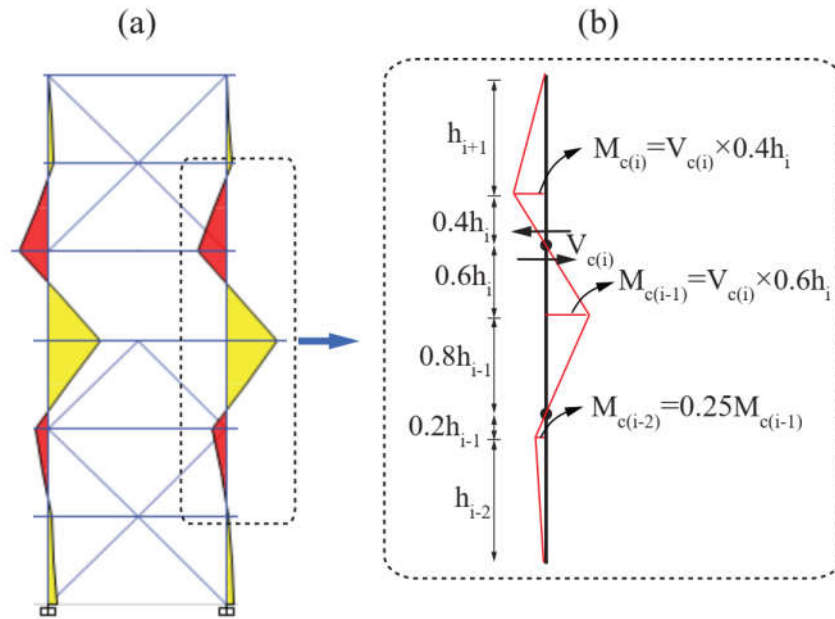


Figure 3.10 Analysis procedure to determine column moment demand a) bending moment diagram on braced bay columns from ETABS, b) Method 3 approximation for finding column moments

Depending on the number of critical storeys, the designer might need to repeat this procedure several times. The columns are then designed for the combination of moment and axial force demand. For the columns with no computed flexural demand, the ratio of the plastic moment capacity relative to adjacent columns is checked to be not less than $2/3$. This is especially important for columns at upper levels because their flexural stiffness and strength are able to influence the shear resistance of the storey after brace buckling, and can cause simultaneous brace buckling in adjacent storeys with weaker columns. If not accounted for in design, this might cause plastic hinging at both ends of the columns and a soft-storey response.

3.7 Application to Example Structures

As an example, Figure 3.11 shows the *DCR* distribution of the three-, six- and 12-storey SCBFs, respectively. This figure also includes the considered range for finding the critical storeys. For the three-storey SCBF, Figure 3.11(a) suggests that drift concentration is most likely in the first storey. For the six-storey SCBF, the first, second, and fourth storeys are located within 10% of the highest DCR and have the highest potential for brace buckling. The primary NLRHA results agree that brace buckling started in these storeys, although columns of the fourth floor in the SCBF with conventional connections at the MCE level affect the shear resistance and transfer the drift concentration to the fifth storey with weaker columns (see Figure 3.8(d)). For the 12-storey SCBF, five storeys are considered as the storeys of high buckling potential. Therefore, Method 3 is applied one, three and five times for finding the moment demands on columns of the three-, six- and 12-storey SCBFs, respectively.

Table 3.4 summarizes the fundamental periods for the original design and the frames designed using all three methods. The influence of different column design methods on the period of the considered buildings is minor because the initial stiffness is provided primarily by the braces. Table 3.5 shows the sections designed for the columns without any flexural demand and with the modified design methods, as well as the demand-to-capacity ratio (D/C from Eq. (3.1)) for the columns of the three-, six- and 12-storey SCBFs. As shown in Table 3.5, using Method 2 and Method 3 results in the same column sections for the three-storey SCBF. This table also includes the material consumption for the braced bay in SCBFs for each design method.

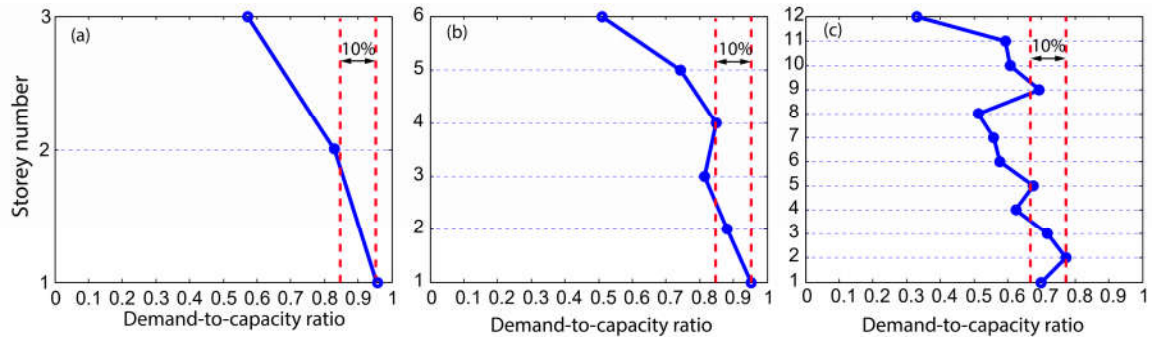


Figure 3.11 Storey shear demand-to-capacity ratio for a) three-storey and b) six-storey and c) 12-storey SCBFs

Table 3.4 Fundamental periods

Building Height	Current Design		Method 1		Method 2		Method 3	
	GP	RBM	GP	RBM	GP	RBM	GP	RBM
Three-storey	0.57 s	0.58 s	0.56	0.57 s	0.54 s	0.55s	0.54 s	0.55 s
Six-storey	0.97 s	1.0 s	0.94	0.95 s	0.92 s	0.94 s	0.90 s	0.91 s
12-storey	1.98 s	2.02 s	1.90 s	1.94 s	1.91 s	1.95 s	1.85 s	1.93 s

3.7.1 Influence of Modified Design Procedures on Collapse Risk of SCBFs

Figure 3.12 shows the collapse fragility curves for the considered models with and without RBMs using the current design (CD) method and the modified design methods. As expected, increasing the column sizes increases collapse capacity. Table 3.6 summarizes the collapse fragility results of the considered SCBFs. For the three-storey SCBF, the use of heavier column sections designed following Method 2 and Method 3 procedures results in passing the collapse criterion, regardless of the connection type. However, considering

an extra moment of $0.2ZF_y$ (Method 1) was not sufficient for either of the systems to pass the criterion.

Table 3.5 Column sections from different design methods

Storey	No flexural demand	D/C	Method 1	D/C	Method 2	D/C	Method 3	D/C
3-storey								
3	W12x120	0.05	W12x136	0.25	W12x210	0.38	W12x210	0.03
2	W12x120	0.79	W12x136	0.91	W12x210	0.96	W12x210	0.76
1	W12x120	0.85	W12x136	0.97	W12x210	1.00	W12x210	0.93
Weight of braced bay	12.0 Ton		12.5 Ton (5% increase)		15.6 Ton (30% increase)		15.6 Ton (30% increase)	
6-storey								
6	W14x68	0.83	W12x87	0.76	W12x136	0.71	W12x136	0.36
5	W14x68	0.93	W12x87	0.82	W12x136	0.92	W12x136	0.99
4	W14x176	0.90	W14x211	0.96	W14x257	0.90	W14x342	0.95
3	W14x176	0.93	W14x211	0.99	W14x257	1.00	W14x342	0.96
2	W14x342	0.93	W14x426	0.97	W14x426	0.99	W14x500	0.98
1	W14x342	0.93	W14x426	0.98	W14x426	1.00	W14x500	0.99
Weight of braced bay	32.9 Ton		37.0 Ton (12% increase)		39.3 Ton (19% increase)		44.0 Ton (33% increase)	
12-storey								
12	W10x68	0.73	W10x77	0.84	W12x96	0.87	W12x152	0.30
11	W10x68	0.85	W10x77	0.94	W12x96	0.94	W12x152	0.33
10	W12x136	0.90	W12x170	0.91	W12x190	0.85	W14x193	0.80
9	W12x136	0.95	W12x170	0.95	W12x190	0.89	W14x193	0.93
8	W14x211	0.94	W14x257	0.96	W14x257	0.96	W14x257	0.99
7	W14x211	0.97	W14x257	0.99	W14x257	0.99	W14x257	1.00
6	W14x311	0.94	W14x370	0.99	W14x370	0.92	W14x370	0.79
5	W14x311	0.96	W14x370	1.00	W14x370	0.94	W14x370	0.81
4	W14x398	0.98	W14x500	0.98	W14x455	0.98	W14x500	0.97
3	W14x398	0.99	W14x500	0.99	W14x455	0.99	W14x500	0.98
2	W14x550	0.90	W14x605	0.99	W14x605	0.90	W14x605	0.99
1	W14x550	0.92	W14x605	1.00	W14x605	0.91	W14x605	1.00
Weight of braced bay	69.5 Ton		78.0 Ton (12% increase)		77.8 Ton (11% increase)		79.9 Ton (15% increase)	

According to Table 3.6, for the six-storey SCBFs, considering an extra $0.2ZF_y$ moment for designing the columns (Method 1) leads to passing the FEMA P695 collapse criterion for SCBF with conventional gusset plate connections (SCBF GP), and the pass/fail ratio is very close to one for the six-storey SCBF with RBMs. Designing the columns using Method 2 results in adequate collapse capacity for both frames. The improvement is

because, according to Method 2, higher moments should be considered for designing columns located at upper floors (see Table 3.5), which results in fewer collapses caused by higher mode effects. Method 3 also leads to acceptable collapse capacities for the considered six-storey SCBFs regardless of the connection type. However, Method 3 requires a higher amount of steel.

For the 12-storey SCBF, Table 3.6 shows that even though all three methods lead to higher collapse capacity, none of the models passes the collapse criterion. This suggests that more redundancy (i.e. secondary behaviour system) is required, which was also seen in an earlier study [7]. For that reason, the analyses were rerun assuming fixed beam-column connections when using RBMs, such as by using the detail shown in Figure 3.1(d). The 12-storey model with fixed beam-column connections and for which columns were designed considering flexural demand using Method 3 provides adequate collapse capacity.

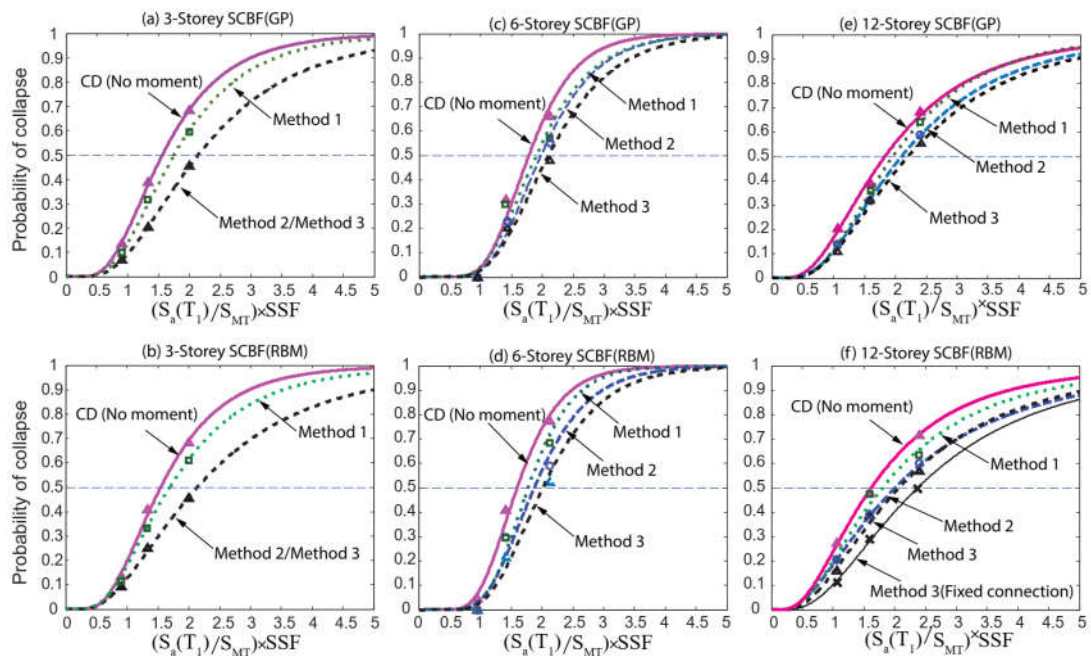


Figure 3.12 Collapse fragility curves for SCBFs with different column sections: a, b) three-storey, c, d) six-storey, and e, f) 12-storey SCBFs

Table 3.6 Collapse analysis results for frames designed considering flexural demands using proposed methods

Considered model	$\beta_{DR}, \beta_{TD}, \beta_{MDL}$	β_{RTR}	$SSF \times \hat{S}_{CT}$	S_{MT}	β	ACMR	Acceptable ACMR _{10%}	Pass/Fail ratio
3-storey								
SCBF GP- M1	0.20	0.46	3.15g	1.80g	0.57	1.75	2.09	0.84
SCBF GP- M2/M3	0.20	0.50	3.96g	1.80g	0.61	2.20	2.17	1.02
SCBF RBM- M1	0.20	0.48	3.06g	1.80g	0.60	1.70	2.16	0.79
SCBF RBM- M2/M3	0.20	0.51	2.84g	1.80g	0.61	2.19	2.17	1.01
6-storey								
SCBF GP- M1	0.20	0.36	1.96g	1.03g	0.49	1.90	1.88	1.01
SCBF GP- M2	0.20	0.35	2.04g	1.03g	0.49	1.98	1.88	1.05
SCBF GP- M3	0.20	0.37	2.16g	1.03g	0.50	2.10	1.90	1.10
SCBF RBM- M1	0.20	0.32	1.82g	1.03g	0.47	1.77	1.84	0.96
SCBF RBM- M2	0.20	0.35	1.93g	1.03g	0.49	1.88	1.88	1.00
SCBF RBM- M3	0.20	0.35	2.08g	1.03g	0.49	2.02	1.88	1.07
12-storey								
SCBF GP- M1	0.20	0.53	0.66g	0.34g	0.62	1.96	2.23	0.88
SCBF GP- M2	0.20	0.57	0.71g	0.34g	0.66	2.10	2.32	0.90
SCBF GP- M3	0.20	0.56	0.73g	0.34g	0.65	2.15	2.30	0.93
SCBF RBM- M1	0.20	0.67	0.61g	0.34g	0.75	1.80	2.61	0.69
SCBF RBM- M2	0.20	0.71	0.68g	0.34g	0.79	2.00	2.77	0.73
SCBF RBM- M3	0.20	0.64	0.70g	0.34g	0.79	2.07	2.53	0.82
SCBF RBM- M3 (Fixed connections)	0.20	0.60	0.78g	0.34g	0.68	2.41	2.38	1.02

3.7.2 Column Strength Utilization

In this section, the column demand-to-capacity ratios based on NLRHA are calculated according to Eq. (3.1) to examine the efficiency of each design method. Figure 13.3 shows the median and median plus standard deviation of the maximum P-M interaction ratios and also the moment contribution at MCE level. For the three-storey SCBF with conventional connections, Figure 3.13(a) and 3.13(b) show that the first mode dominates the behaviour with maximum demands at the bottom of the first storey. However, for the SCBF with RBMs, the upper column segment also experienced high moment demand.

Figure 3.13(c) and 3.13(d) show that for six-storey SCBF designed following Method 2 recommendations, the median column DCR is lower than one at the MCE level for both considered models. The change in column strength and stiffness between fourth and fifth storeys causes high moments in the fifth- and sixth-storey columns. This is because of the large storey drifts that developed in the fourth storey, which induce high moments at the bottom and top of the fifth-storey column. A smaller section was assigned to the fifth and sixth storey columns according to the capacity based design procedure, but because of the splice location, the higher demand to capacity ratios are most significant for the sixth storey columns. DCR values larger than one can occur at the base of the columns because of strain hardening in the columns due to the large plastic deformations, and because of the resistance factors used to calculate the strength values.

Figure 3.13(e) and 3.13(f) show that for the 12-storey models there is only a slight difference between different design methods up to the ninth storey. From the ninth storey to the top of the structure, after using stronger sections, higher mode effects reduced and caused lower D/C values. This effect is more significant in the 12-storey SCBF with RBMs where pinned beam-column connections were considered. After making the connections fixed, the P-M demand ratio reduced by approximately 40% at the top floor relative to the Method 1. Moreover, in the 12-storey model with RBMs and fixed beam-column connections, none of the column sections yielded except at the base.

In general, although using heavier sections (i.e. stiffer elements) results in higher moments, it reduces the axial force ratios, causing the columns to be more ductile in flexure and less vulnerable to instability before large storey drifts.

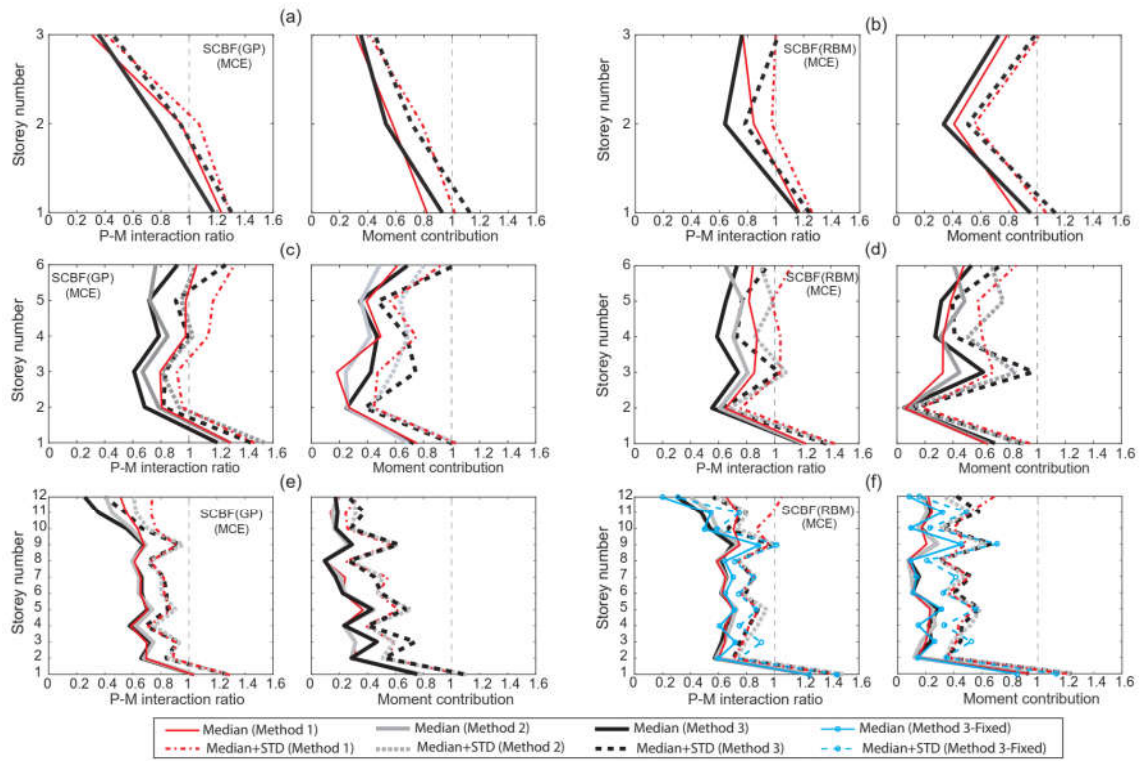


Figure 3.13 Demand-to-capacity ratios of columns of three-, six- and 12-storey SCBF with and without RBMs using modified design methods at MCE

3.7.3 Residual Drifts

One key benefit of SCBFs with RBMs is the intended replaceability of the brace after an earthquake. However, maximum residual inter-storey drift ratio (MRIDR) is important for the assessment of post-earthquake condition of the structure and ease of RBM replacement. Therefore, fragility curves with MRIDR as the engineering demand parameter are constructed for SCBFs with RBMs based on the analyses of Section 3.7.1. Two residual drift demand limits are considered following FEMA P-58 [35]. The first level (DS1) is defined when the MRIDR reaches 0.2%. At this state it is expected that no structural readjustment is required, and the braces can be easily replaced. The second level (DS2)

happens when the MRIDR reaches 0.5%, where both structural and non-structural components are likely to require repair, and the braces can be replaced only after realignment of the structural elements.

Figure 3.14 provides the MRIDR fragility curves for SCBFs with RBMs, where the results do not include the collapsed models. The residual drifts tend to increase as the building height increases. When no flexural demand is considered for designing columns, at DBE level, 60% of the earthquakes cause a residual drift demand higher than 0.2% for three- and six-storey SCBFs, while it is 85% for the 12-storey SCBFs. Accounting for the flexural demands in the design of the columns decreases the residual drifts. For instance, using Method 3 to design the columns results in the probability of exceeding 0.2% MRIDR being 40% and 50% at DBE and MCE levels, respectively, for both three- and six-storey SCBFs. For the 12-storey SCBF, Figure 3.14(e) shows this probability was 63% and 73% at DBE and MCE levels, respectively. On average, the probability of MRIDR exceeding 0.2% reduced by 25% after using Method 3. If a MRIDR of 0.2% represents the limit for replacing RBMs without any repairs, then the average probability of being able to do this when the columns are designed using Method 3 are 52% and 42% at DBE and MCE levels, respectively.

At DBE level, 18%, 22%, and 48% of the earthquakes cause a residual drift demand higher than 0.5% for three-, six- and 12-storey SCBFs, respectively, when columns are designed with no flexural demands. After designing columns based on Method 3, these probabilities reduce to 13%, 5% and 30%, respectively (a reduction of approximately 45% on average), which show a significant probability of 83%, 95% and 70% for replacing the RBMs after straightening the buildings for three-, six- and 12-storey SCBFs, respectively.

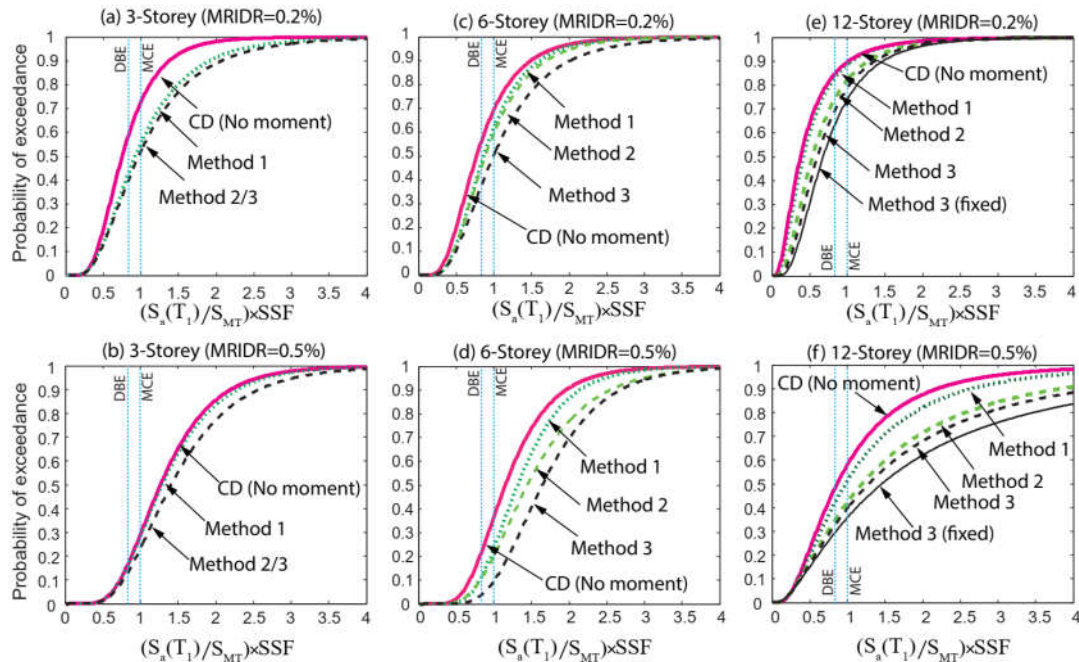


Figure 3.14 Fragility curves for maximum inter-storey residual drift ratios over all storeys for SCBFs with RBMs

3.8 Summary and Design Recommendations

This paper investigated the seismic force demands of columns in SCBFs with conventional braces or with replaceable brace modules. First, the columns were modelled to remain elastic during the analyses to determine their maximum axial and flexural demands. Then, the columns were modelled with nonlinear elements to capture their expected behaviour. Finally, new design recommendations for considering the flexural demand on columns in braced frames were presented and examined. The main findings are:

- Current capacity design approaches lead to frequent column yielding due to combined axial force and bending moment in low- to mid-rise braced frames, but yielding in only a few storeys in high-rise braced frames. Assuming an increasing force demand for columns moving towards the bottom storeys based on the first

mode deformation does not necessarily result in the most critical case, and thus the current design procedure is not as conservative as expected.

- The eccentricity that exists in SCBFs with replaceable brace module beam-column-brace connections, which is less than beam depth, does not increase the demand on columns because the maximum P-M interaction happens at larger inter-storey drifts where the moment contribution is maximum.
- Relative to SCBFs with conventional braces, higher mode effects are more dominant in high-rise SCBFs with replaceable brace modules if pinned beam-column connections are used. This results in a higher probability of collapse at the DBE level, and also high moment demands on columns located in the uppermost storeys. This suggests a need to require fixed beam-column connections for high-rise SCBFs.
- Relative to current design requirements, stronger and stiffer columns are needed to increase the collapse capacity to meet the FEMA P695 collapse criterion.
- Three modified methods were proposed to incorporate the moment demand into the design of columns in SCBFs. The results showed an improvement in the collapse capacity to acceptable levels when using Method 2 and 3, although more frames should be tested before recommending one specific approach.
- Using the modified methods for designing the columns also provides the benefit of reducing residual drifts, leading towards easier structural repairs. The most conservative column design method reduced the probability of exceeding 0.2% residual drift after a DBE-level earthquake from 60%-85% to 40%-63%.

Acknowledgments

The financial support of the Canadian Institute of Steel Construction (CISC) and the National Sciences and Engineering Research Council (NSERC) is gratefully acknowledged.

References

- [1] American Institute of Steel Construction. Seismic Provisions for Structural Steel Buildings, ANSI/AISC 341–16. Chicago, IL: 2016.
- [2] Stevens D, Wiebe L. Experimental testing of a replaceable brace module for seismically designed concentrically braced steel frames. *J Struct Eng* 2019;145..
- [3] Mohsenzadeh V, Wiebe L. Experimental validation of a concentrically braced frame with replaceable brace modules. *J Struct Eng* 2020;Submitted.
- [4] Thornton WA. On the analysis and design of bracing. *Natl. Steel Constr. Conf. Proc.*, Chicago, IL.: American Institute of Steel Construction, Inc.; 1991.
- [5] Lamarche CP, Tremblay R. Seismically induced cyclic buckling of steel columns including residual-stress and strain-rate effects. *J Constr Steel Res* 2011;67:1401–10.
- [6] Cho C, Lee C-H, Kim J-J. Prediction of Column Axial Forces in Inverted V-braced Seismic Steel Frames Considering Brace Buckling. *J Struct Eng* 2011;137:1440–50.
- [7] Mohsenzadeh V, Wiebe L. Effect of beam-column connection fixity and gravity framing on the seismic collapse risk of special concentrically braced frames. *Soil Dyn Earthq Eng* 2018;115:685–97.
- [8] Karamanci E, Lignos D. Computational approach for collapse assessment of concentrically braced frames in seismic regions. *J Struct Eng* 2014;140:1–15.
- [9] Stoakes CD, Fahnestock LA. Cyclic flexural testing of concentrically braced frame beam-column connections. *J Struct Eng* 2011;137:739–47.
- [10] Stoakes CD, Fahnestock LA. Cyclic flexural analysis and behaviour of beam-column connections with gusset plates. *J Constr Steel Res* 2012;72:227–39.
- [11] Lumpkin EJ, Hsiao PC, Roeder CW, Lehman DE, Tsai CY, Wu AC, et al. Investigation of the seismic response of three-storey special concentrically braced frames. *J Constr Steel Res* 2012;77:131–44.

- [12] CSA. Design of steel structures, CAN/CSA S16-19. Canadian Standards Association: Mississauga, ON, Canada. 2019.
- [13] Uriz P, Mahin SA. Toward earthquake-resistant design of concentrically braced steel-frame structures. UCB/PEER-2008/08, Univ. of California, Berkeley, CA.: 2008.
- [14] Rai DC, Goel SC. Seismic evaluation and upgrading of chevron braced frames. *J Constr Steel Res* 2003;59:971–94.
- [15] MacRae GA, Kimura Y, Roeder C. Effect of column stiffness on braced frame seismic behaviour. *J Struct Eng* 2004;130:381–91.
- [16] Ji X, Kato M, Wang T, Hitaka T, Nakashima M. Effect of gravity columns on mitigation of drift concentration for braced frames. *J Constr Steel Res* 2009;65:2148–56.
- [17] Momenzadeh S, Shen J. Seismic demand on columns in special concentrically braced frames. *Eng Struct* 2018;168:93–107.
- [18] Kumar PCA, Anand S, Sahoo DR. Modified seismic design of concentrically braced frames considering flexural demand on columns. *Earthq Eng Struct Dyn* 2017;46:1559–80.
- [19] American Society of Civil Engineers (ASCE). Minimum design loads and associated criteria for buildings and other structures. Reston, Virginia: 2017..
- [20] American Institute of Steel Construction. Specification for structural steel buildings, ANSI/AISC 360-16. Chicago, IL: 2016.
- [21] Pacific Earthquake Engineering Research Centre (PEER). Open System for Earthquake Engineering Simulation v2.4.5 [Computer Software], 2015.
- [22] Elkady A, Lignos D. Dynamic stability of deep slender steel columns as part of special MRFs designed in seismic regions-finite element modeling. 1st Int. Conf. PerformanceBased Life-Cycle Struct. Eng., Hong Kong, China: Faculty of Construction and Environment and the Research Institute for Sustainable Urban Development, Hong Kong Polytechnic Univ.: 2011.

- [23] Newell J, Uang C. Cyclic behaviour of steel columns with combined high axial load and drift demand. Rep. No. SSRP-06/22, Dept. of Structural Engineering, University of California, San Diego: 2006. v
- [24] Zargar S, Medina RA, Miranda E. Cyclic behaviour of deep steel columns subjected to large drifts, rotations, and axial loads. Tenth U.S. Natl. Conf. Earthq. Eng., 2014. doi:10.4231/D3TT4FT5X.
- [25] Elkady A, Lignos DG. Full-scale testing of deep wide-flange steel columns under multiaxial cyclic loading: loading sequence, boundary effects, and lateral stability bracing force demands. *J Struct Eng* 2017;144:1–15.
- [26] Elkady A, Lignos DG. Improved seismic design and nonlinear modeling recommendations for wide-flange steel columns. *J Struct Eng* 2018;144:1–13.
- [27] Hsiao PC, Lehman DE, Roeder CW. Improved analytical model for special concentrically braced frames. *J Constr Steel Res* 2012;73:80–94.
- [28] Hwang S-H, Lignos D. Effect of modeling assumptions on the earthquake-induced losses and collapse risk of steel-frame buildings with special concentrically braced frames. *J Struct Eng* 2017;143:04017116.
- [29] FEMA P695. Quantification of building seismic performance factors FEMA P695. Federal Emergency Management Agency, Washington, D.C.: 2009.
- [30] ASCE. Seismic Evaluation and Retrofit of Existing Buildings, ASCE/SEI 41-17. Reston, VA: American Society of Civil Engineers; 2017.
- [31] Bech D, Tremayne B, Houston J. Proposed Changes to Steel Column Evaluation Criteria for Existing Buildings. Second ATC SEI Conf. Improv. Seism. Perform. Exist. Build. other Struct., San Francisco, CA: American Society of Civil Engineers; 2015.
- [32] Elkady A, Ghimire S, Lignos DG. Fragility curves for wide-flange steel columns and implications for building-specific earthquake-induced loss assessment. *Earthq Spectra* 2018;34:1405–29.

- [33] Al-mashaykhi M, Rajeev P, Wijesundara KK, Hashemi MJ. Displacement profile for displacement based seismic design of concentric braced frames. *J Constr Steel Res* 2019;155:233–48.
- [34] Jalayer F. Direct probabilistic seismic analysis: implementing non-linear dynamic assessments. Doctoral dissertation, Stanford University, 2003.
- [35] FEMA P-58. Seismic performance assessment of buildings - methodology. vol. 1. Washington, DC: 2012.

4 Experimental Investigation of a Concentrically Braced Frame with Replaceable Brace Modules

Abstract

In common practice of designing and building special concentrically braced frames (SCBFs), a gusset plate is used to join the brace to the frame members and is sized such that the brace buckles in the out-of-plane direction. This detailing requires time-consuming field welding, and out-of-plane brace buckling can damage the surrounding partitions and cladding. Moreover, the gusset plate will experience damage when the brace buckles, requiring the plate to be cut out and replaced after the earthquake. To improve this, an alternative connection was recently proposed which was designed to confine all damage to a replaceable brace module (RBM), so as to minimize the time of post-earthquake repairs. Moreover, to improve constructability and repairability, shop-welded/field-bolted connections are used and detailed such that the brace will buckle in the in-plane direction. Previous testing validated this concept only for individual RBMs. To assess the interaction of all the braced frame components, this paper presents the results of an experimental study of 70%-scale one-storey one-bay concentrically braced frame systems with RBMs. Three specimens were tested to examine the response with three different beam-column connection details. For each specimen, a sequence of tests was performed, the first with initial RBMs and the second with replaced RBMs. All the tested systems sustained multiple inelastic cycles with a storey drift range of 3.7% to 4.0% prior to fracture of both braces. The RBMs were replaced easily and provided essentially the same level of performance as the original RBMs. Significant post-fracture strength and stiffness were also observed due to frame action, even without gusset plates at the beam-column intersections.

Keywords: Concentrically braced frames; Replaceable brace module; large-scale experimental testing; Seismic performance

4.1 Introduction

Special Concentrically braced frames (SCBFs) are one of the most common seismic force resisting systems in regions of high seismicity. They possess high initial stiffness and strength that are considered desirable in relatively small and frequent earthquakes. During moderate to severe earthquakes, the braces are expected to dissipate energy through tensile yielding, compressive buckling, and post-buckling behaviour. To ensure that this nonlinearity will occur in the braces, design codes (AISC 2016b; CSA 2014) require the brace connections to be designed to accommodate brace buckling, such as by providing a clearance distance beyond the end of the brace to allow the gusset plate to yield in flexure. The linear clearance distance can lead to large and thick gusset plates, which is not economical, and can cause early brace fracture as a result of inelastic deformation concentration into a shorter length of the brace (Lehman et al. 2008). Moreover, premature toe weld fractures can occur at the gusset plate welds due to opening and closing moments on the connections, which can negatively affect the ductility and energy dissipation of the system (Uriz and Mahin 2008). In addition, significant local yielding has been observed in the beam and column adjacent to the gusset plate as a result of frame action induced by the gusset plate rigidity (Lehman et al. 2008). To reduce these issues, a balanced design procedure has been proposed for designing gusset plates that can be more compact, promoting the ductility of the system and preventing undesirable failure modes (Roeder et al. 2011b).

Conventional brace-to-gusset plate connections allow the brace to buckle in the out-of-plane direction. Full-scale experimental testing has shown that the out-of-plane buckling displacement can be larger than 400 mm before brace fracture (Tsai et al. 2010), which can cause damage to the surrounding partitions or cladding, potentially endangering occupants' lives (Tremblay et al. 1995). To remove that concern, and to avoid toe weld fractures at the gusset plate, a knife plate-to-gusset plate-to-brace connection was detailed and validated

in experimental studies (Lumpkin 2009; Tsai et al. 2013). Results showed that properly sized knife plates performed satisfactorily and accommodated equal or more rotation than the gusset plate connections.

The gusset plate connections described above typically require extensive field welding for joining the brace to the gusset plate, which necessitates special care and is expensive. Moreover, post-earthquake repair or replacement of the gusset plate is likely to be relatively time-consuming because it would require removing the welds. To address all these issues, an alternative connection has been developed (Figure 4.1) to improve the constructability of braced frames by allowing bolts to be used instead of welding on site, to allow the brace to buckle in-plane, and to make the brace unit more easily replaceable by confining all damage to the Replaceable Brace Module (RBM) until brace fracture. An experimental study of the proposed component showed that this new connection will perform satisfactorily in terms of intended hinge location, failure development, drift range before brace fracture, and cumulative energy dissipated (Stevens and Wiebe 2019). However, braced frame behaviour depends on the complete frame system, and in order to assess the performance accurately, the contribution of all frame elements must be considered (Uriz and Mahin 2008). Therefore, large-scale system-level experimental testing is required to examine the ductility and the seismic performance of an SCBF with RBMs.

This paper presents the results of a series of 70%-scale concentrically braced frames with RBMs that was conducted in the Applied Dynamics Laboratory at McMaster University. Frames were tested with three different beam-column connections and their performance together with the RBMs is discussed. The objectives of these tests included evaluating the seismic performance of the SCBF system with RBMs, examining the replaceability of the RBMs and the frame behaviour after replacement, investigating the performance of the

proposed beam-column connections when used with RBMs, and quantifying the contribution of frame action to the overall lateral resistance.

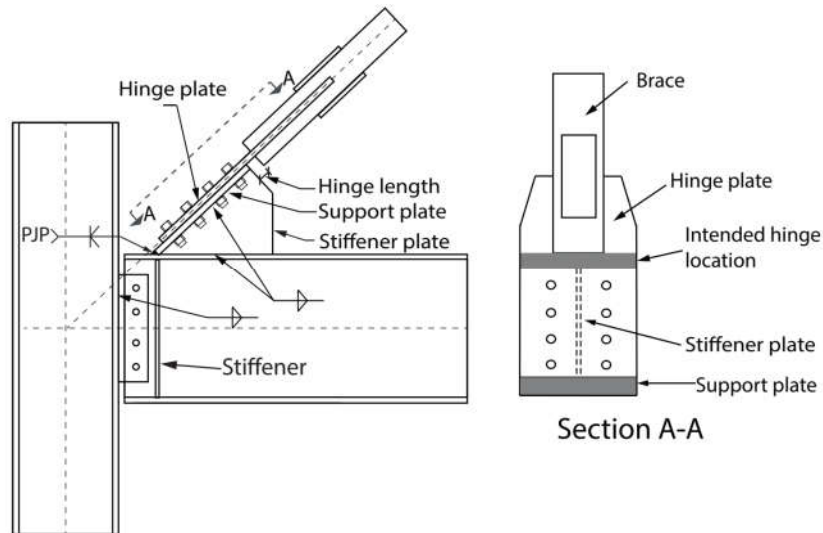


Figure 4.1 Replaceable brace module connection details

4.2 Experimental Program

4.2.1 Reference Structure

Figure 4.2 shows the reference structure for the test and the prototype specimen. The test frames represented a 70%-scale model of a second floor braced bay for a reference structure in Vancouver, British Columbia, which was designed to resist the lateral forces from the equivalent static force procedure following the Canadian code (NRC 2015). The structure was designed according to the provisions of CSA S16-14 (CSA 2014) for moderately ductile concentrically braced frames (MD-CBFs) and was verified to also satisfy the design requirements for special concentrically braced frames (SCBFs) in AISC 341 (AISC 2016b). The design provisions are generally similar, allowing both to be used in regions of high seismicity, with differences that include the response modification factors ($R_{MD}=3.9$,

$R_{SCBF}=6.0$) and the requirement in CSA S16-14 for columns to be designed for a moment of $0.2ZF_y$ at the column ends in the plane of braced frame.

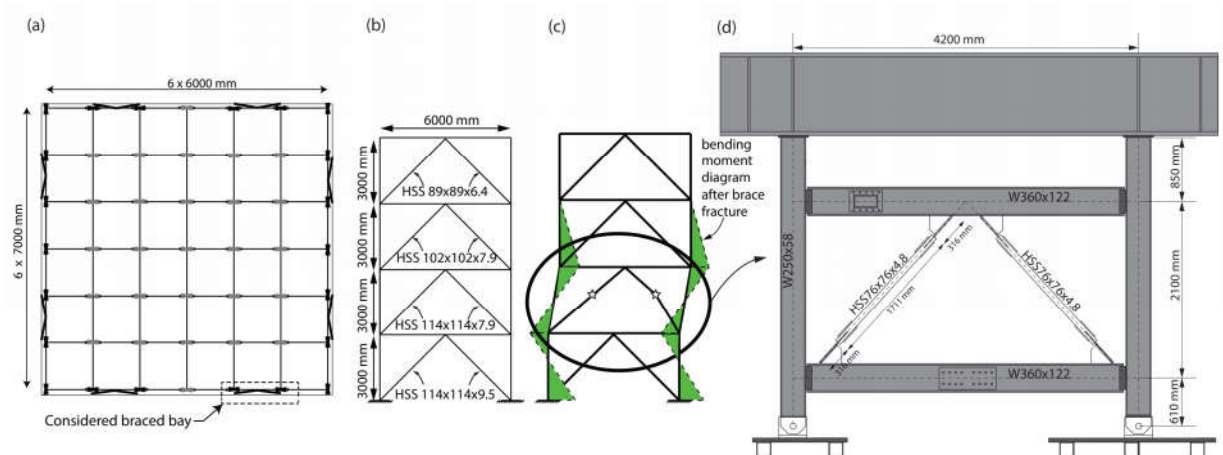


Figure 4.2 Reference building in Vancouver, BC: (a) plan, (b) considered bay, (c) schematic deformed shape and associated column moment diagram, (d) prototype specimen

4.2.2 Test Setup

The setup test was designed to create, as closely as possible, boundary conditions that were representative of those in an actual building, so as to simulate the moment and shear demands on the columns as the frame displaced. To identify these boundary conditions, nonlinear static analysis of a model of the reference structure shown in Figure 4.2(b) was performed in SAP2000 (Computers and Structures 2016) following ASCE-SEI 41-17 (ASCE 2017) recommendations. Lateral load was applied to the model to simulate a large localized inter-storey drift in the second storey, which was chosen because this was the level with the highest demands on the region where the brace connects to the beam. Figure 4.2(c) shows the schematic deformed shape and associated moment diagram of the columns for the considered mechanism. The moment demands on the columns were investigated and boundary conditions were provided to simulate these demands. At the top, the columns were extended and connected to a stiff and strong beam through a very stiff connection. In

order to simulate the effects of the lower storey stiffness, two horizontal struts, which were chosen to provide stiffness similar to that of the lower storey in the design, connected the lower beam to brackets on the strong floor. Pinned connections were used for the columns above midheight of the lower storey, as this was found that to more accurately simulate the inflection point from analysis when the damage concentrated in the second storey. The gravity loads were calculated to provide less than 15% of the expected demand on the columns, and therefore they were not simulated in this experimental study. The composite slab was not considered in this study, but would be expected to amplify the flexural strength and stiffness of the beam.

Figure 4.3 shows the experimental test setup, which contained a reaction frame, a loading frame, and the specimen. The loading frame beams were W460x103 steel sections and were connected to the loading frame columns by plates with slotted holes using the detail proposed by (Eatherton and Hajjar 2010) to accommodate the rotation of the beams relative to the columns under large drifts (see Figure C-8 in Appendix C). The load from the 1000 kN capacity 500 mm stroke actuator was transferred to the upper beam of the specimen through two slip-critical bolted connections to the loading frame beams. The loading frame columns were attached to the strong platform through a pin connection to minimize any unintended contribution to the lateral resistance during the tests. In order to reduce the friction resistance of the connections in the loading frame, the connection surfaces were lubricated with grease.

In order to control the stability of the stiff-strong beam, two out-of-plane restraints were provided using two smaller implement cylinders. Laser displacement transducers were used to measure the out-of-plane displacement and hold the beam at its initial position in that direction.

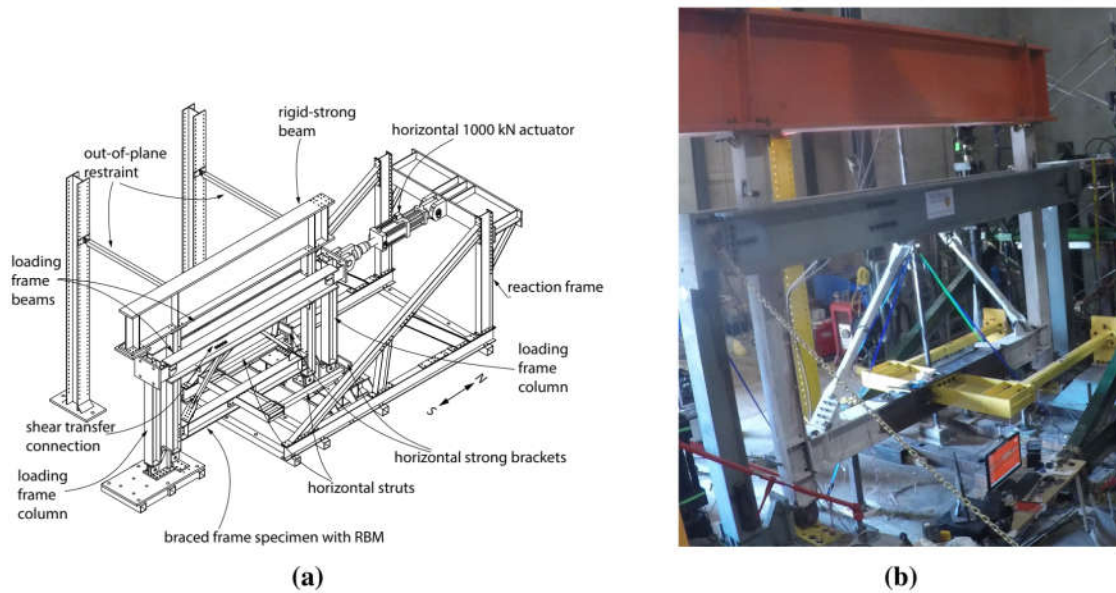


Figure 4.3 Overview of the experimental setup: (a) annotated drawing, (b) photograph

4.2.3 Test Specimens

Testing consisted of three specimens using square HSS tube sections for the bracing members. The braces were 350W G40.20-13/G40.21-13 (CSA 2013) Class C members. The beams and columns were ASTM A992 (ASTM-A992/A992M-11 2015) sections with yield and ultimate strengths of $F_y=360\text{MPa}$ and $F_u=488\text{MPa}$, respectively, according to the mill certificates.

The testing of each specimen consisted of two phases. In the first phase, the frame was subjected to quasi-static cyclic loading up to fracture of one RBM. In the second phase, only the damaged RBMs were replaced, and the behaviour of the frame was investigated under the same loading protocol. After the second phase for each specimen, the setup was partially disassembled to allow the new specimen to be constructed, and the testing process

described above was repeated. Each specimen was built with new elements, except that the same column elements were used in both specimen 2 with EPC and specimen 3 with BUEEPC.

The connection bolts and welds were all designed to resist the full overstrength capacity of the brace. Bolts connecting the brace to the support plate (see Figure 4.1) were pretensioned up to 70% of their ultimate tensile capacity using a torque wrench but were not designed for a calculated slip load. After replacing the brace modules in the second phase test of each specimen, the same bolts were used and pretensioned again. Bolts of the beam-column connections were also designed for strength (see Appendix A for sample calculations), with holes that were 2 mm larger in diameter than the bolts.

The hinge plates were also designed such that all limit state resistances were stronger than the full overstrength capacity of the brace. An additional moment due to the effect of eccentricity between the hinge plate and the support plate was not considered for determining the hinge plate thickness because it had been found unnecessary (Stevens and Wiebe 2019). The support plate and the stiffener plate were designed to have the same thickness as the associated hinge plate. The weld joining the stiffener plate to the beam flange was capacity designed based on the full shear resistance of the stiffener plate. The hinge length, defined as the distance between the end of the support plate and end of the brace (see Figure 4.1) was designed to be twice the hinge plate thickness (Astaneh-Asl et al. 1985).

Table 4.1 summarizes the key parameters of the braces that were tested, including the expected yield strength ($R_y F_y$) that would be used with CSA S16-14 (CSA 2014), local slenderness (b_{el}/t), slenderness ratio (KL/r), and predicted overstrength capacity of the brace in tension (T_u) and compression ($C_u = 1.2C_r$). For computing C_r (compression resistance), the flexural buckling equation from CSA S16-14 was used, based on the length

(L) between the center of hinge zones. To account for the hinge plates providing some restraint that reduced the effective length (KL) of the braces, a theoretical effective buckling length factor was calculated based on a three-hinge mechanism using Eq. 4.1 (Takeuchi and Matusi 2015).

$$K = \frac{1}{1 + M_{ph} / M_{pb}} \quad (4.1)$$

where M_{ph} is the plastic moment capacity of the hinge plate, and M_{pb} is the plastic moment capacity of the brace. Previous results have shown that the effective length factor using Eq. 4.1 was within 12% of the effective length factor derived experimentally (Stevens and Wiebe 2019). Table 4.1 also contains the predicted slip load of the connection, which was calculated based on the formula in CSA S16-14 for bolt slip assuming clean mill scale conditions with a resistance factor (C_s) of one (CSA 2014).

Table 4.1 Details of braces

Specimen	HSS square brace shape	F_y (MPa)	F_u (MPa)	L (mm)	b_{ef}/t	M_{ph} (kN.m)	M_{pb} (kN.m)	K_t	$K_t L/r$	T_u (kN)	C_u (kN)	Slip load (kN)
Specimen 1- with STC & Specimen 2- with EPC	HSS 76x76x4.8	450	514	1775	11.90	3.70	15.48	0.8	49.3	590	536.4	299
Specimen 3- with BUEEP	HSS 76x76x4.8	450	514	1841	11.90	3.70	15.48	0.8	51.1	590	522.9	299

4.2.4 Beam-Column Connection Details

Figure 4.4 shows the three beam-column connection details that were included in the experimental program. The first connection was a single shear tab connection (STC) [Figure 4.4(a)], which was chosen because it is easy to fabricate and erect. The shear tab

was shop-welded to the column and site-bolted to the beam. Short slotted holes were designed for the shear tab plate to permit larger connection rotations before damage. Beam stiffeners were provided where the support plate for the RBM is connected to the beam to prevent web buckling and flange bending. In this connection, the centerline of the brace passed through the center of the beam at the column flange surface. For that reason, the connection was designed to carry only vertical and horizontal forces. It may appear that the columns would need to be designed for an extra moment due to this eccentricity (i.e. equal to half of the column depth). However, this eccentricity does not increase the design demand on the columns because the moment-axial load interaction is maximized at larger drifts, when the moment contribution is maximum because of uneven inter-storey drifts after the braces have buckled and thus contribute much less than their peak force (Mohsenzadeh and Wiebe 2019).

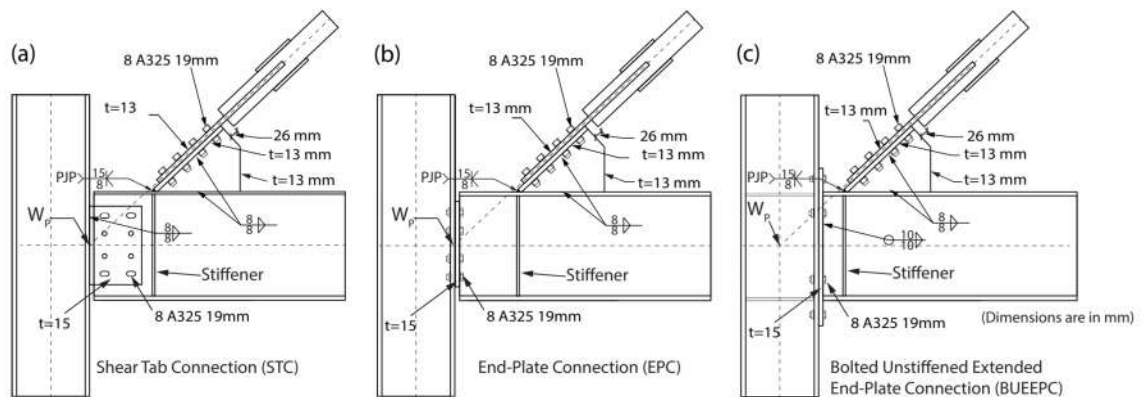


Figure 4.4 Tested connection details: (a) specimen 1 with shear tab connection (STC), (b) specimen 2 with end-plate connection (EPC), and (c) specimen 3 with bolted unstiffened extended end-plate connection (BUEEPC)

The second connection [Figure 4.4(b)] was an end-plate shear connection (EPC), where the end-plate was shop welded to the supported beam and bolted to the column. This type of connection was chosen because of its economy, ease of fabrication, and performance. Like the previous connection, the centerline of the brace passed through the center of the beam at the column flange surface. Therefore, the connection was not designed for a moment.

The third connection detail was a bolted unstiffened extended end-plate moment connection (BUEEPC), shown in Figure 4.4(c). This was selected as an example of a moment-resisting connection, which has been found to be required for taller SCBFs to ensure an adequate margin against collapse (Mohsenzadeh and Wiebe 2018). In this specimen, the work point was at the center of the column. For that reason, there is a moment on the connection, which was considered in designing the connection. The BUEEPC was designed according to AISC 358 (AISC 2016a), except that it was designed to carry the vertical force on the connection and the calculated moment, rather than the plastic moment of the beam. Bolted end-plate connections were made by welding an end-plate to the beam and bolting the end-plate to the column flange. The connection was designed with eight 19 mm (3/4 in) bolts, similar to the STC and EPC connections. In this case, stiffeners were required at the beam flanges to prevent local column web yielding and crippling. The same column elements were used in both EPC and BUEEPC test setups.

Additional details of all connection design calculations are provided in Appendix A.

4.2.5 Loading Protocol and Control

Tests were performed by applying displacement-controlled fully reversed increasing amplitude cyclic loading protocols. The load history followed the ATC-24 testing protocol (ATC 1992), as shown in Figure 4.5, and was based on the predicted inter-storey drift of the frame at the onset of the first buckling (D_y). If no brace fractured by the end of this

protocol, the load history was extended with cycles at $+1D_y$ relative to previous displacement until brace fracture. The applied load was controlled based on the actuator linear variable displacement transducer (LVDT), but the inter-storey drift was used to determine the intended applied displacement, and it was measured using string potentiometers attached to the top and bottom beams, independent of the loading frame. In the second phase of testing Specimens 1 (with STC) and 3 (with BUEEPC), after both braces had fractured, the post-fracture stiffness and resistance of the braced frames were investigated by continuing to apply progressively increasing cycles.

The instrumentation was designed to capture critical aspects of the frame behaviour. The internal load cell in the actuator measured the applied load. Inter-storey drift, axial deformation, and in-plane buckling deflection of braces were measured with string potentiometers. Hinge plate and beam-column connection rotations were measured using LVDTs. In order to establish the internal forces in the elements, sets of strain gauges were attached to all braces, beams and columns. The specimens were whitewashed at the locations where yielding was anticipated.

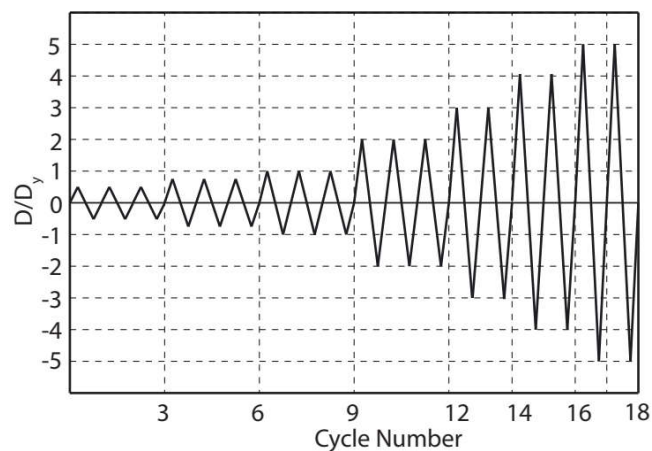


Figure 4.5 Loading protocol

4.3 Experimental Observations

The hysteresis of lateral force versus inter-storey drift ratio for each specimen is plotted in Figure 4.6, where the first column shows the results during the first phase of testing and the second column shows the response of the system during the second phase (i.e. after replacing the damaged brace modules). Displacement is defined as positive when the actuator is pushing the frame (displacement toward the south in Figure 4.3). Because the top and bottom beams were moving during the loading, the actual drifts applied were slightly different from the target values. The shear force is normalized by $2C_r \cos \theta$ of the braces, where θ is the brace angle to the horizontal, because a design engineer would select brace sections such that $2C_r \cos \theta$ is larger than the design horizontal shear force at each level.

In all six tests, specimens sustained multiple inelastic cycles and reached at least the nominal design shear resistance. In all cases, the initial yield mechanism was brace buckling in the in-plane direction, followed by brace tensile yielding and finally brace fracture. Hinges formed in the intended locations in the hinge plates. As the hinge plates were unaffected by the moments associated with the opening and closing of the beam-column connection, no cracks could be detected in the welds between stiffener plate and the beam flange. Moreover, no brace connection failure was seen. The following paragraphs discuss the specific experimental results for each specimen.

4.3.1 Specimen 1 with Single Shear Tab Connections (STC)

Figures 4.6(a) and (b) show the lateral force versus inter-storey drift hysteresis loops for the specimen with the single shear tab connection joining the beams and columns during the first phase and the second phase, respectively. In the first phase, in-plane buckling of the braces was observed visually at about $\pm 0.55\%$ drift (see Figure 4.7a), and hinge plate flexural yielding began due to brace buckling deformation at the same drift. Local cupping

of the braces was first noted at $\pm 1.35\%$ (see Figure 4.7b). The south brace fractured first at the middle of the brace at 1.63% drift when it was in tension (see Figure 4.7c), after which the frame lost 25% of its design shear resistance. The frame was then unloaded before replacing the RBMs. The maximum lateral resistance was 675 kN and -760 kN, and the maximum drift range of the frame prior to south brace fracture was 3.60%.

Figures 4.7(d) and 4.7(e) show that the location of the hinge plate flexural yielding varied according to the end of the brace and direction of buckling. For instance, for the north brace that is shown in Figure 4.7, the yielding area in the bottom hinge plate radiated between the first row of bolts and the end of the brace [Figure 4.7(d)], while the yielding region in the top hinge plate was smaller, developing between the brace end and the support plate [Figure 4.7(e)]. This is typical for all the specimens that were tested in this study, and occurred because the support plates were located at different sides of the brace at the top and bottom. Despite this slightly asymmetrical hinge plate yielding, significant flexural yielding of the hinge plates was noted without any unintended damage. No yielding of the columns or beams could be detected during this phase of testing. Large in-plane deformations of the braces were noticed, with the maximum in-plane displacement observed before brace fracture being 152 mm (8.8% of the brace length), which was within the expected range based on previous studies with more conventional gusset plate connections (Lumpkin 2009).

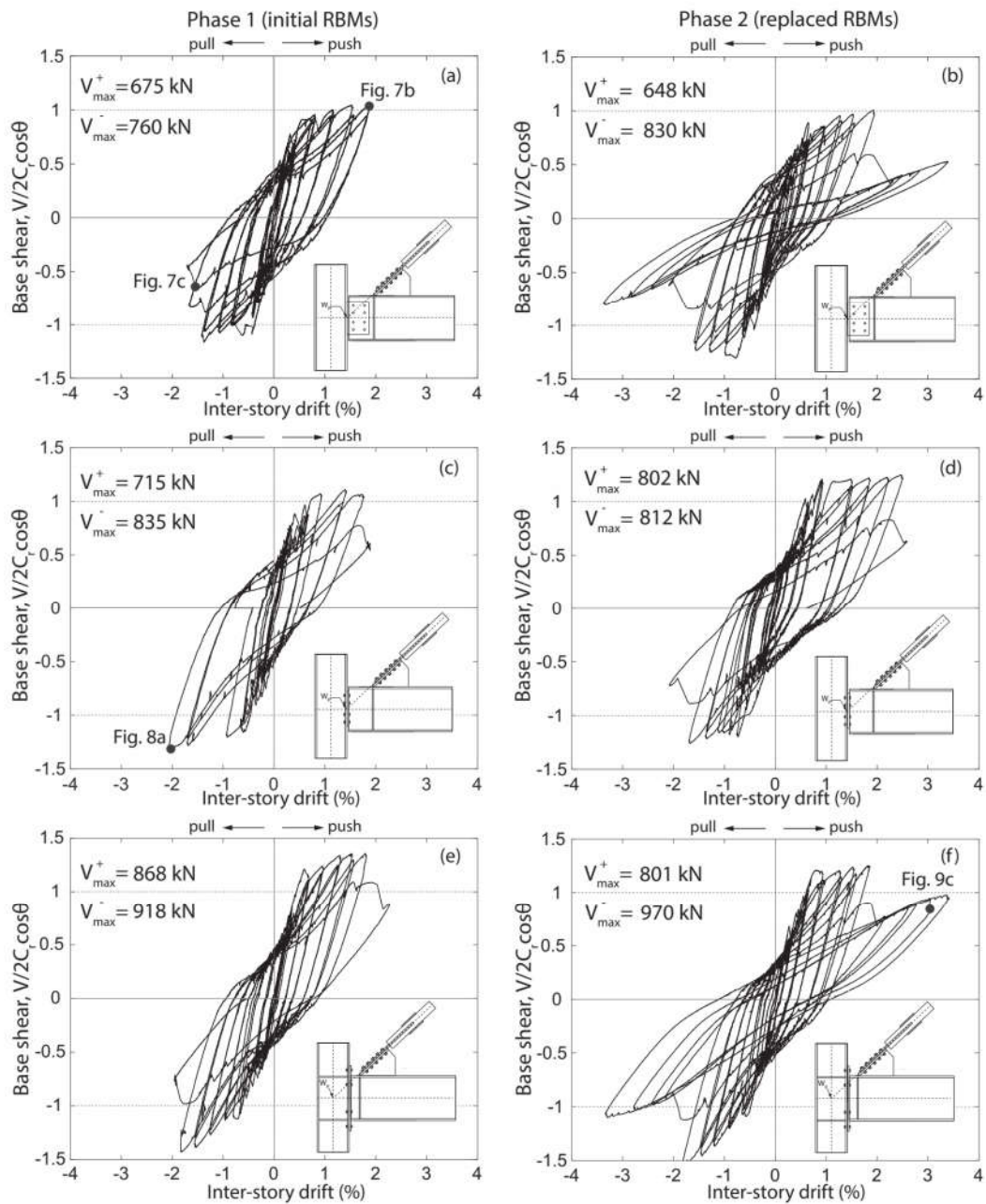


Figure 4.6 Normalized lateral force versus inter-storey drift hysteresis loops: (a) and (b) Specimen 1 (with shear tab connection), (c) and (d) Specimen 2 (with end plate connection), (e) and (f) Specimen 3 (with bolted unstiffened extended end plate connection)

The hysteretic loops were not symmetric as intended; the force required to push the frame to a given drift was smaller than the force needed to pull the frame to the same drift at drift ranges larger than 0.8%. This was because of platform slip under the south column, which caused less bending and thus less shear contribution in the south column when the specimens were pushed. Moreover, the hystereses are not perfectly smooth because of bolt slip in the brace-to-frame connections (i.e. between the hinge plate and the support plate), and also in the connections of the reaction frame. However, given that these connections designed for strength rather than to avoid slip, the response was reasonably smooth.

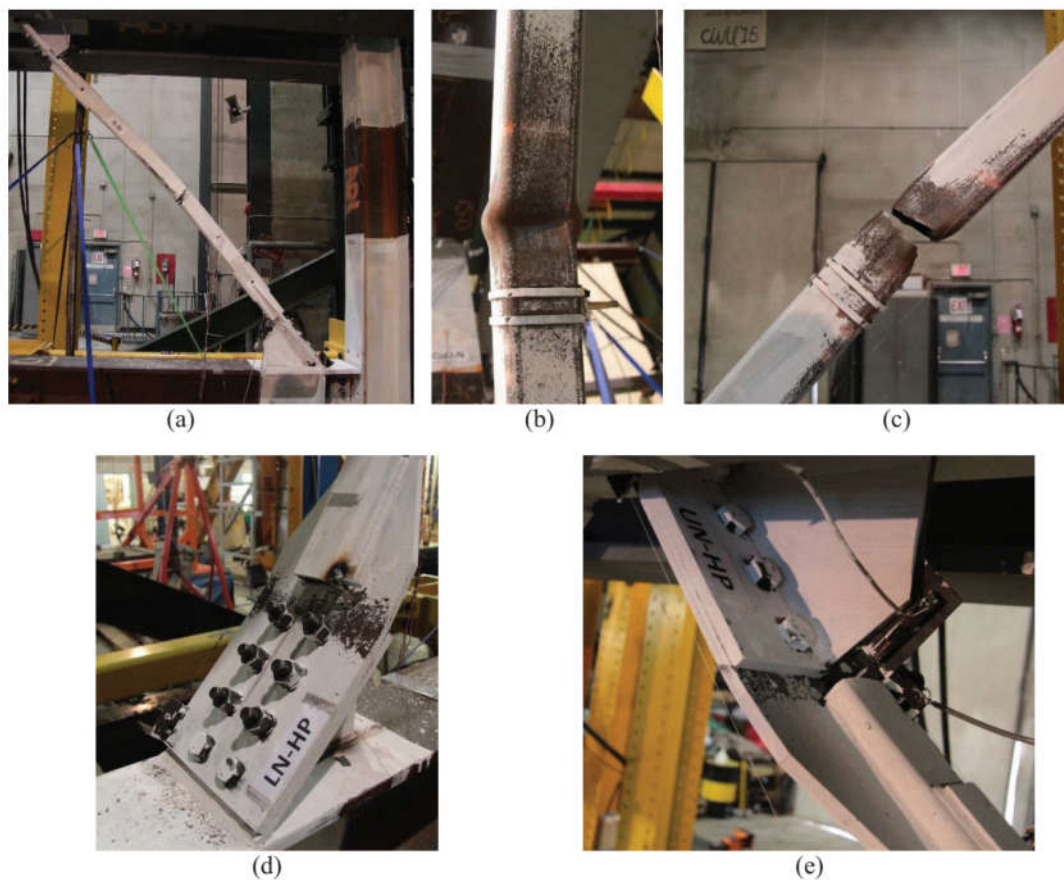


Figure 4.7 Specimen 1 (with STC): (a) initial north brace in-plane buckling; (b) south brace local cupping; (c) south brace fracture; (d) north brace bottom hinge plate; (f) north brace top hinge plate

The residual drift after unloading at the end of the first phase was 0.6%, but the brace modules were removed without difficulty. After straightening the frame, the new brace modules were installed easily, and the second phase of testing was conducted. Figure 4.6(b) shows that the resistance and initial elastic stiffness of the frame were within 9% and 8%, respectively, of what was observed during the first phase. The maximum storey shears before brace fracture were 648 and -830 kN, and the resulting drift range before the second brace fracture was 3.70%. The initiation of brace in-plane buckling and local cupping was at the same cycles as during the first phase, although the north brace buckled in the downward direction. A significant loss of 66% of the frame design shear resistance was measured after the second brace fracture.

After fracture of both braces, loading was continued up to $\pm 3.35\%$ (drift range of 6.7%). Results showed that the frame retained significant lateral resistance, up to 80% of $2C_r \cos \theta$. This corresponds to 98% of $4M_p / L_c$, where M_p is the plastic moment capacity of the column section, and L_c is the distance from center to center of the top and bottom beams. First column yielding occurred at the top of both columns at $\pm 2.80\%$ inter-storey drift. No crack was observed in any welds, and no local inelastic deformation could be identified in the beams in either phase of loading.

4.3.2 Specimen 2 with End Plate Connection (EPC)

Figures 4.6(c) and 4.6(d) show the hysteretic response for the specimen with end plate connections (EPC) during the first and the second phase of testing, respectively. Because of a data acquisition error in the first phase of testing Specimen 2, the data from the second cycle of $3D_y$ and both cycles of $4D_y$ were not recorded, although they were imposed to the specimen.

During testing, in-plane buckling was achieved and brace buckling commenced at about $\pm 0.65\%$ drift. Because of end-plate slip at the lower beam-column connections, brace buckling started with a small delay relative to Specimen 1. Figure 4.8a shows the frame at 2.05% storey drift to the north. After this, when loading in the other direction, the north brace fractured first at +1.75%, and the total drift range prior to this brace fracture was 3.80%. The maximum lateral forces that the system sustained before brace fracture were 715 and -835 kN. The maximum in-plane deflection of the north brace was 149 mm. The response of the frame was ductile and hinge plate yielding developed after brace buckling. When testing beyond brace fracture, minor yielding was noted in both column flanges adjacent to the top and bottom beam-column connections at approximately -2.0% storey drift. While the residual drift at the end of the first phase was 0.5%, the damaged braces were replaced with new ones conveniently, and phase 2 was performed from this point.

In the initial design of the specimens, the column web shear resistance was checked only for the horizontal component of the full overstrength capacity of the brace. However, at the end of the test, modest shear yielding was observed in the web of the columns at the location of the bottom beam-column connections, as shown in Figure 4.8b. This happened because the flexural stiffness of columns was mobilized, increasing the shear demand at those locations. To accommodate this, before starting phase 2, a diagonal stiffener was designed and welded in the panel zone (see Figure 4.8c) to resist the maximum shear that could develop in the column from the frame action, assuming plastic hinges formed at column ends, together with the shear imposed by brace yielding. The continuity plates shown in Figure 4.8c were not required for EPC connections, but were used to prevent local column web yielding when the columns were reused for specimen 3 with BUEEPC.



(a)



(b)



(c)

Figure 4.8 Specimen 2 (with EPC): (a) north brace in-plane buckling; (b) column web yielding in the lower north beam-column connection at the end of the first phase; (c) added a diagonal stiffener

As shown in Figure 4.6d, Specimen 2 with replaced braces reached a higher shear strength than the nominal design strength, and was within 12% of the lateral strength observed in the first phase. The initial elastic stiffness of the frame during this phase was 8% smaller

than in the first phase. The frame was essentially elastic up to $\pm 0.65\%$, and both braces buckled in-plane followed by yielding in the intended locations of hinge plates. The south brace fractured first at -1.70% (total drift range of 4.20%) and the north brace fractured second at $+2.32\%$ (total drift range of 4.03%). This specimen reached similar strength in both directions because it was pushed to larger drifts relative to the drifts to which it was pulled. A loss of 38% of the nominal design shear resistance was observed after the second brace fracture, which is only 57% of what was observed for Specimen 1. Although the frame sustained this significant lateral resistance, the test was stopped to preserve the columns for Specimen 3. Limited column yielding adjacent to the beam-column connections was observed at the end of the test.

4.3.3 Specimen 3 with Bolted Unstiffened Extended End Plate Connection (BUEEPC)

Specimen 3, with bolted unstiffened extended end plate connections (BUEEPC), had similar behaviour in terms of yielding and failure progression to Specimens 1 and 2. However, it experienced higher lateral loads relative to the previous specimens because of its moment resisting connections, as shown in Figure 4.6(e). The frame had a lateral resistance of 868 and -918 kN, which are, on average, 23% and 15% more than Specimens 1 and 2, respectively. The braces began to buckle in-plane at approximately $\pm 0.65\%$ drift. Unlike the first two specimens, in the first phase of testing, loading was continued until both braces fractured. The north brace fractured at the first $+2\%$ drift cycle, and the south brace fractured in the subsequent cycle towards the north at 1.84% . The drift range of the frame prior to north brace fracture was 3.67% , and it was 3.87% before both braces fractured. The maximum in-plane deflection of the brace observed before brace fracture was 150 mm. Minor yielding in the flanges of the columns and minor local yielding of the extended end plates were observed at the end of the test. The residual drift at zero force was 0.49% , but the braces were replaced easily.

The hysteretic behaviour of Specimen 3 after replacing the braces is shown in Figure 4.6(f). The frame developed more than 125% of the design resistance. The frame reached a maximum drift range of 3.77% prior to the second brace fracture, and had a maximum lateral resistance of 801 and -970 kN. The initial elastic stiffness of the frame during this phase was only 2% smaller than what was observed in the first phase. The columns started to yield at the top and bottom of the storey adjacent to the beam-column connections after brace fracture, at $\pm 2.2\%$ drift. Minor whitewash flaking was observed in the panel zones at the same drift range.

Considerable frame reserve capacity was observed after second brace fracture. Large inelastic cycles were applied to the frame up to $\pm 3.3\%$ drift, and significant frame contribution up to the nominal design shear resistance of the frame was observed. Figures 4.9a and 4.9b show the north column flange yielding and the south panel zone at the end of the test, respectively. Significant local yielding of the end plates was noted, and one bolt fractured due to prying action of the south BUEEPC at +3.0% drift, when the frame was pushed to the south direction (see Figure 4.9c). The test was stopped at this point.

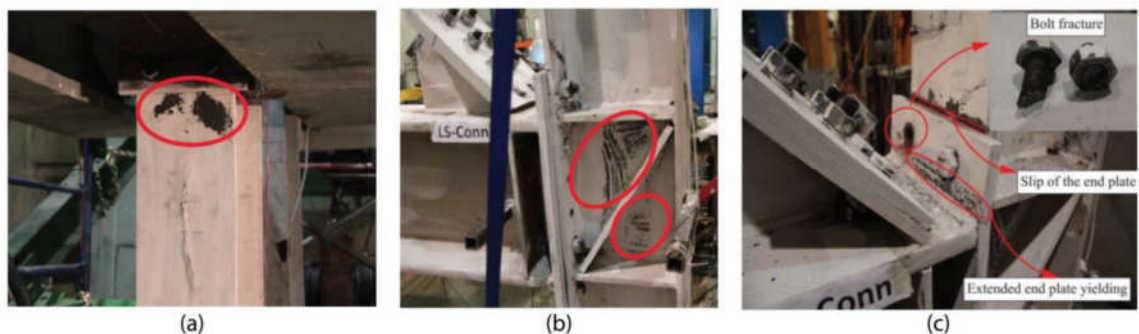


Figure 4.9 Specimen 3 (with BUEEPC) after completion of loading cycles beyond brace fracture: (a) north column yielding; (b) bottom south beam-column connection panel zone; (c) bottom south beam-column connection

4.3.4 General Observations

Table 4.2 summarizes the maximum frame resistance, maximum drifts, elastic stiffness, and stiffness of the frames after both braces fractured. The stiffness of the specimens after brace fracture was calculated as the secant stiffness from the origin to the point with maximum drift. The drift range that was observed for all the specimens in this study is comparable to typical values for SCBFs with more conventional gusset plate connections (Roeder et al. 2011a; Lumpkin et al. 2012), a range that is significantly affected by the brace section compactness (e.g. Han et al. 2007). As shown in Table 4.1, the width-to-thickness ratio of the brace section used was 11.9, compared to 17.6 and 13.5, which are the limits using the nominal yield strength of 350 MPa in CSA S16-14 (CSA 2014) and AISC 341-16 (AISC 2016b), respectively. The elastic stiffnesses of all the specimens in the first phase were within 6% of each other, indicating the minor influence of beam-column connection fixity relative to the large initial stiffness provided by the braces. In each second phase of testing, the system maintained its initial stiffness and strength from the first phase to within 8%. As shown in Table 4.2, 90% and 86% decreases in stiffness were measured in the frame after brace fracture for STC and BUEEPC specimens, respectively.

Table 4.2 Summary of frame behaviour

Parameter	Specimen 1 - with STC		Specimen 2 - with EPC		Specimen 3 - with BUEEPC	
	Phase 1 Initial RBMs	Phase 2 Replaced RBMs	Phase 1 Initial RBMs	Phase 2 Replaced RBMs	Phase 1 Initial RBMs	Phase 2 Replaced RBMs
Failure mode	Brace fracture	Brace fracture	Brace fracture	Brace fracture	Brace fracture	Brace fracture
Predicted base shear at brace buckling, V_{bb} (kN)	644	644	644	644	644	644
Maximum base shear V/V_{bb}	-1.18 / +1.05	-1.28 / +1.01	-1.29 / +1.11	-1.26 / +1.24	-1.42 / +1.34	-1.50 / +1.25
Drift at 1st brace fracture (%)	-1.63 (south brace)	-1.75 (south brace)	+1.75 (north brace)	-1.72 (south brace)	+2.03 (north brace)	+1.90 (north brace)
Drift at 2nd brace fracture (%)	N/A	-1.94 (north brace)	N/A	+2.31 (north brace)	-1.84 (south brace)	-1.87 (south brace)
Maximum drift range (%)	3.60	3.70	3.80	4.03	3.87	3.77
Residual drift (%)	0.60	N/A	0.51	N/A	0.49	N/A
Elastic stiffness (kN/%)	1440	1325	1463	1340	1523	1490
Stiffness after braces fracture (kN/%)	N/A	147	N/A	N/A	N/A	212

4.4 Brace Behaviour

Strain gauge data showed that the storey shear was shared nearly equally between the tension and compression braces at lower levels of drift, and braces yielded in tension and buckled in compression before brace connections reached their strength. Tensile tests of coupons machined from brace material were used to measure the yield ($F_{y,meas}$) and ultimate strengths ($F_{u,meas}$) of the brace material that are summarized in Table 4.3. The maximum compression resistance, C_{max} , of the braces in the tested specimens are compared with the overstrength resistance of the brace in compression predicted by CSA S16-14 (CSA 2014) and AISC 341-16 (AISC 2016b) (C_u and P_{cre} , respectively). The results showed that after accounting for the effect of the hinge plates on the effective length by using Eq. 1, both standards predicted the maximum compression resistance with reasonable

accuracy, with mean experimental to theoretical ratios of 1.11 and 1.12 for CSA S16-14 and AISC 341-16, respectively.

The brace elongation and shortening were measured by string potentiometers that were placed along the length of braces. Results demonstrated that the braces were able to elongate about 0.9% to 1.2%, and sustained 1.8% to 2.5% compressive shortening before brace fracture occurred. These values are in the range of previous observations for the more commonly used connections with out-of-plane buckling braces (Lumpkin 2009).

Table 4.3 lists the first major slip that occurred in the brace connections, neglecting minor localized slips at lower load levels, and compares them with the slip load of the connection predicted per CSA S16-14 (CSA 2014). Neither visible damage nor significant deformation was noted on the bolts after the first phase of testing, so the same bolts were used for the second phase. The actual slip loads were higher than the values obtained from the CSA S16-14 (CSA 2014) by a mean factor of 16%, and were an average of 8% lower in the second phase of testing compared to the first. Bolt slip stopped at larger drifts after the compressive strength of the brace degraded to less than the slip load, as seen in previous component tests (Stevens and Wiebe 2019). During the testing, none of the connections exhibit exactly the same slip load, and consequently no abrupt transition between the non-slip and slip states was observed, even at low drift levels.

Table 4.3 Summary of frame behaviour

Specimen	Phase #	Brace location	$F_{y,max}$ (MPa)	$F_{u,max}$ (MPa)	Peak compression forces (kN)					Slip load (kN)	
					C_{max}	C_u	P_{cre}	C_{max}/C_u	C_{max}/P_{cre}	Actual	Actual/Predicted
Specimen 1	Phase 1	North	415	500	591	506	501	1.16	1.17	341	1.14
		South			558			1.10	1.11	348	1.16
	Phase 2	North	410	491	601	501	496	1.19	1.21	292	0.98
		South			553			1.10	1.11	300	1.00
Specimen 2	Phase 1	North	412	488	492	503	498	0.97	0.98	395	1.32
		South			594			1.18	1.19	401	1.34
	Phase 2	North	410	493	554	501	496	1.10	1.11	422	1.40
		South			N/A*			N/A	N/A	N/A	N/A
Specimen 3	Phase 1	North	411	500	N/A	502	497	N/A	N/A	353	1.18
		South			N/A			N/A	N/A	362	1.21
	Phase 2	North	420	498	540	510	505	1.05	1.06	318	1.06
		South			N/A			N/A	N/A	288	0.96

*N/A: not available.

4.5 Contribution of Frame Action

Column shears were calculated by taking the difference in moments calculated from the strain gauges, which were mounted to the elastic portion of the columns, and dividing by the distance between them. Figure 4.10 shows the portion of the storey shear resisted by the columns, as opposed to the braces, taken at the peaks of each cycle for all the specimens during phases 1 and 2. As expected, the proportion of shear carried by the columns was relatively small (less than 20%) at low drift levels prior to brace buckling. The columns began to carry more shear after brace buckling. Whereas the contribution of columns was less than 45% before brace fracture, the occurrence of one brace fracture resulted in a rapid increase in column shear contribution to 75%-90%. Figure 4.10 illustrates that when the two braces fractured, the columns resisted 90-100% of the storey shear. The remainder was because, although the braces could not resist force in tension after fracture, they still were able to develop some compression load when the two sides of the fractured braces came back into contact.

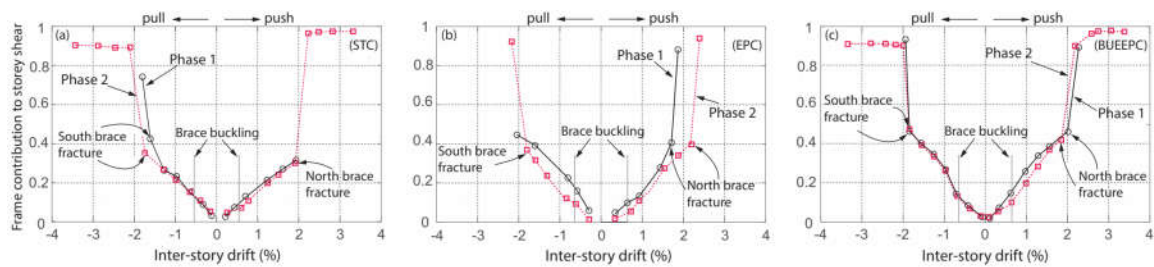


Figure 4.10 Frame contribution to storey shear: (a) Specimen 1 (with STC); (b) Specimen 2 (with EPC); (c) Specimen 3 (with BUEEPC)

4.6 Connection Behaviour

Considering the brace end connections, the LVDT data showed that the maximum rotation varied between 0.12 rad and 0.15 rad for the hinge plates, which is about 75% of the values reported elsewhere for gusset plates at an inter-storey drift range of 3.8% (Lumpkin 2009). Limiting the hinge plate width to the beam flange width to avoid interfering with surrounding elements led to a thicker hinge plate in comparison to a regular gusset plate. For that reason, hinge plates can provide higher rotational stiffness and subsequently smaller rotations at the end of the brace, which necessitates using Eq. 1 for finding the effective length.

For the beam-column connections, the tests were able to simulate the combination of shear, moment and rotation that a connection would experience in an SCBF with RBMs during an earthquake. The behaviour of the proposed beam-column connections was investigated using the connection rotation versus inter-storey drift curves that are shown in Figure 4.11. Only the results of the second phase are shown as higher rotation demands were applied to the connections in that phase. Figure 4.11(a) shows that the shear tab connections encountered rotations larger than 0.032 rad without any reduction in their rotational capability, nor was any local damage observed in the beam flanges and web. Short slotted

bolt holes in the shear tab enabled the connection to experience significant rotation and ductility. Figure 4.12(a) shows the lower south connection at its largest rotation. The end-plate connection (EPC) also provided acceptable performance with a maximum rotation of 0.022 rad. As shown in Figure 4.12(b), no damage was observed in the end plate, the column flange, or the bolts. The connection was likely capable of experiencing higher rotations, but the test was stopped to preserve the columns for the third specimen. In both cases, the lower acceptable rotation capacity of 0.025 rad suggested by Seismic Provisions for Structural Steel Buildings (AISC 2016b) for a simple beam-column connection where a brace connects to the frame elements was likely satisfied.

Unlike what was observed for the two other connection types, the bolted unstiffened extended end-plate connection (BUEEPC) rotation was generally much less than the inter-storey drift, as was intended for this moment-resisting connection. The connection rotation shown in Figure 4.11(c) consists of both the shearing rotation contributed by the panel zone and the gap rotation contributed by the flexural deformation of the end plate and column flange, as well as the extension of the bolts (Shi et al. 2007). After the first cycle to $\pm 3.3\%$ drift, the BUEEPC reached a maximum rotation of 0.022 rad at an inter-storey drift of 3.0% before the first bolt fractured. Figure 4.11(c) shows that the curves are not symmetric for the BUEEPC connections because the lower beam moved much less than the top beam. When the specimen was pushed towards the south, the south connection experienced higher rotation because of the larger contribution of the gap rotation as the extended end-plate separated from the column flange. However, this term is much smaller for the north connection because the end plate and the flange of the column moved towards each other. Beam-column connection failure was expected after brace fracture for this specimen, and it happened at a large drift that is beyond maximum considered earthquake drifts observed in other studies for SCBFs (Mohsenzadeh and Wiebe 2018).

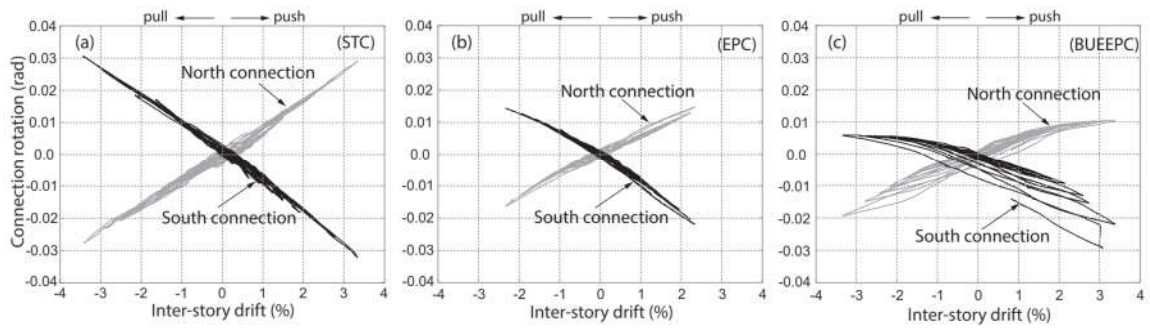


Figure 4.11 Connection rotation vs inter-storey drift: (a) Specimen 1 (with STC); (b) Specimen 2 (with EPC); (c) Specimen 3 (with BUEEPC)

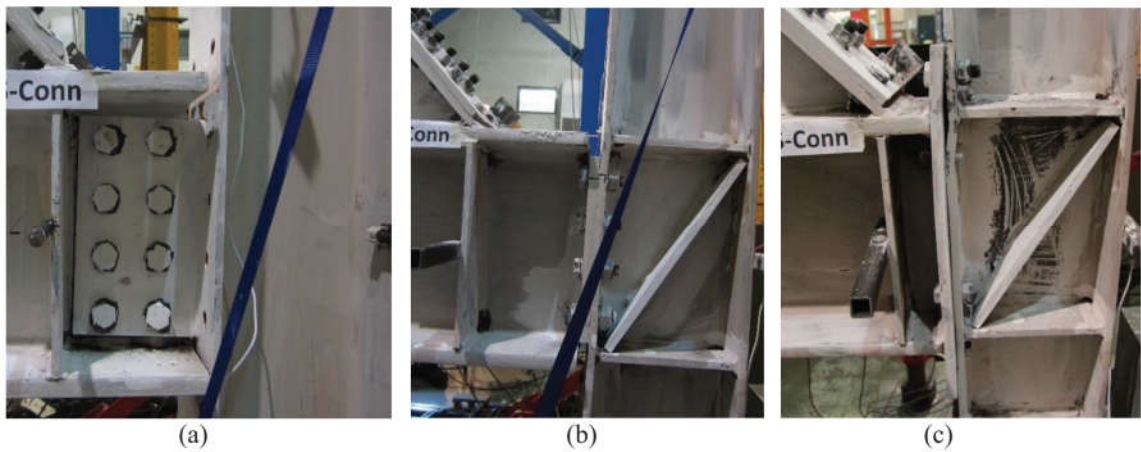


Figure 4.12 (a) STC connection at 0.032 rad rotation; (b) EPC connection at 0.022 rad rotation; (c) BUEEPC connection at 0.02 rad rotation

4.7 Conclusions

This study presented the first large-scale testing of braced frames with Replaceable Brace Modules. The primary objective was to evaluate the overall system-level behaviour of a braced frame with this recently proposed connection detail. Three different beam-column connections were assessed for use in braced frames with RBMs. Two tests were conducted on each specimen, one with initial brace modules and one after replacing damaged brace modules with new ones to examine the brace module replaceability and seismic behaviour of the frame with replaced brace modules. The study found that:

- The tested specimens performed well, with damage confined to the intended locations, and with a storey drift range of 3.7% to 4.0% prior to fracture of both braces. This behaviour is comparable to previous results for special concentrically braced frames with more commonly used gusset plate connections.
- The hinge plates were able to provide sufficient ductility to accommodate large brace in-plane displacements. The drift range of the specimens was largely influenced by the local slenderness of the brace section, rather than hinge plate details.
- All three specimens with replaced brace modules could sustain their initial stiffness and strength after successive load reversals. A maximum reduction of 8% in strength and stiffness was observed for the specimens with replaced brace modules compared to the specimens with the initial brace modules.
- After both braces fractured, the lateral strength and stiffness of the system diminished significantly. However, considerable lateral strength of 80% and 100% of the storey design shear was developed for specimens with shear tab connections and extended end plate connections, respectively, through frame action.
- The single shear tab connection (STC) provided a stable response and experienced a large rotation of 0.032 rad without any local damage, weld fracture, or reduction in resistance. The eccentricity that existed in this connection did not cause any unpredictable behaviour. This connection is a good option should designers wish for

connections in low- and mid-rise braced frames with RBMs for the advantages of rotation capacity, easy fabrication and erection, and economy.

- The end plate shear connection (EPC) showed an acceptable performance with a maximum rotation of 0.022 rad, with no local damage. However, because it is stiffer than the shear tab connection, it can cause higher shear demand on the column, potentially necessitating column strengthening. For that reason, if a simple beam-column connection is desired, the EPC is likely less preferable than the STC.
- The bolted unstiffened extended end plate connection (BUEEPC) could accommodate a large inter-storey drift of 3.3% prior to fracture of a bolt. This connection had the benefit of increasing the redundancy of the braced frame and provided considerable reserve capacity up to the nominal design shear of the storey. This connection is desirable for a designer seeking for more reserve capacity in braced frames with RBMs.

In summary, based on the current work, the recently proposed connection for joining the brace to the beam, accompanied by the tested beam-column connections, offers easier initial installation and post-earthquake repair, while providing similar seismic performance to more traditional solutions.

Acknowledgments

The authors appreciate the work of the summer research interns Berg Ellemers and Anirban Kundu (Mitacs Globalink Research Intern) and the help of the technical staff (Kent Wheeler and Paul Heerema) at the Applied Dynamics Laboratory. Funding for this project has been provided by the Canadian Institute of Steel Construction (CISC) and the National Sciences and Engineering Research Council (NSERC). The wide flange sections were donated by Salit Steel and the HSS sections were donated by Atlas Tube. Fabrication services were provided by Walters Inc. Their support is gratefully acknowledged.

References

- AISC (2016a). *Prequalified connections for special and intermediate steel moment frames for seismic applications*. ANSI/AISC 358, Chicago, Illinois.
- AISC (2016b). *Seismic provisions for structural steel buildings*. ANSI/AISC 341, Chicago, Illinois: AISC.
- ASCE (2017). *Seismic rehabilitation of existing buildings*. ASCE/SEI 41-17, Richmond, Virginia.
- Astaneh-Asl, A., Goel, S., and Hanson., R. (1985). “Cyclic out-of-plane buckling of double-angle bracing.” *J. Struct. Eng.*, ASCE, 111(5), 1135–1153.
- ASTM-A992/A992M-11 (2015). *Standard specification for structural steel shapes*. ASTM International, West Conshohocken, Pennsylvania.
- ATC (1992). *Guidelines for cyclic seismic testing of components of steel structures*. ATC 24, Redwood City, CA: ATC.
- Computers and Structures (2016). *Structural Analysis Program, SAP-2000NL Version 16.0.0: Integrated Finite Element Analysis and Design of Structures*. Berkeley, Calif.
- CSA (2013). *General requirements for rolled or welded structural quality steel/structural quality steel*. G40.20-13/G40.21-13, Mississauga, ON, Canada: CSA.
- CSA (2014). *Limit states design of steel structures*. CAN/CSA S16-14. Canadian Standards Association, Toronto, ON, Canada: CSA.
- Eatherton, M. R. and Hajjar, J. F. (2010). “Large-scale cyclic and hybrid simulation testing and development of a controlled rocking steel building system with replaceable fuses.” *Report No. NSEL-025*, Newmark Structural Engineering Laboratory, Urbana IL, United States.

Han, S. W., Kim, W. T., and Foutch, D. A. (2007). “Seismic behaviour of HSS bracing members according to width-thickness ratio under symmetric cyclic loading.” *J. Struct. Eng.*, ASCE, 133(2), 264–273.

Lehman, D. E., Roeder, C. W., Herman, D., Johnson, S., and Kotulka, B. (2008). “Improved seismic performance of gusset plate connections.” *J. Struct. Eng.*, 134(6), 890–901.

Lumpkin, E. J. (2009). “Enhanced seismic performance of multi-storey special concentrically brace frames using a balanced design procedure.” M.S. thesis, University of Washington, University of Washington.

Lumpkin, E. J., Hsiao, P. C., Roeder, C. W., Lehman, D. E., Tsai, C. Y., Wu, A. C., Wei, C. Y., and Tsai, K. C. (2012). “Investigation of the seismic response of three-storey special concentrically braced frames.” *J. Constr. Steel Res.*, 77, 131–144.

Mohsenzadeh, V. and Wiebe, L. (2018). “Effect of beam-column connection fixity and gravity framing on the seismic collapse risk of special concentrically braced frames.” *Soil Dyn. Earthq. Eng.*, 115, 685–697.

Mohsenzadeh, V. and Wiebe, L. (2019). “Seismic design of columns in concentrically braced frames with replaceable brace modules.” *Proc., 12th Canadian Conference on Earthquake Engineering.*, Quebec, QC.

NRC (2015). *National building code of Canada 2015*. NBCC-15, Ottawa, ON, Canada: NRCC.

Roeder, C. W., Lehman, D. E., Clark, K., Powell, J., Yoo, J. H., Tsai, K. C., Lin, C. H., and Wei, C. Y. (2011a). “Influence of gusset plate connections and braces on the seismic performance of X-braced frames.” *Earthq. Eng. Struct. Dyn.*, 40(4), 355–374.

Roeder, C. W., Lumpkin, E. J., and Lehman, D. E. (2011b). “A balanced design procedure for special concentrically braced frame connections.” *J. Constr. Steel Res.*, 67(11), 1760–1772.

Shi, Y., Shi, G., and Wang, Y. (2007). “Experimental and theoretical analysis of the moment–rotation behaviour of stiffened extended end-plate connections.” *J. Constr. Steel Res.*, 63(9), 1279–1293.

Stevens, D. and Wiebe, L. (2019). “Experimental testing of a replaceable brace module for seismically designed concentrically braced steel frames.” *J. Struct. Eng.*, 145(4), 04019012.

Takeuchi, T. and Matsui, R. (2015). “Cumulative Deformation Capacity of Braces Under Various Cyclic Loading Histories.” *J. Struct. Constr. Eng. (Transactions AIJ)*, 77(677), 1131–1140.

Tremblay, R., Filiatrault, A., Timler, P., and Bruneau, M. (1995). “Performance of steel structures during the 1994 Northridge earthquake.” *Can. J. Civ. Eng.*, 22(2), 338–360.

Tsai, C. Y., Tsai, K. C., Lin, C. H., Wei, C. Y., Wang, K. J., Yu, Y. J., and Wu, A. C. (2010). “Cyclic responses of three 2-storey seismic concentrically braced frames.” *Front. Arch. Civ. Eng. China*, 4(3), 287–301.

Tsai, C. Y., Tsai, K. C., Lin, P. C., Ao, W. H., Roeder, C. W., Mahin, S. A., Lin, C. H., Yu, Y. J., Wang, K. J., Wu, A. C., Chen, J. C., and Lin, T. H. (2013). “Seismic design and hybrid tests of a full-scale three-storey concentrically braced frame using in-plane buckling braces.” *Earthq. Spectra*, 29(3), 1043–1067.

Uriz, P. and Mahin, S. A. (2008). “Toward earthquake-resistant design of concentrically braced steel-frame structures.” *Report No. UCB/PEER-2008/08*, University of California, Berkeley

5 Conclusion and Recommendations

This final chapter summarizes the important findings of this work and recommends some areas for further research on special concentrically braced frames (SCBFs) with replaceable brace modules (RBMs).

5.1 Summary

Concentrically braced frames with replaceable brace modules have the potential of improving the constructability of braced frames, mitigating the structural damage during earthquakes, and minimizing the time of post-earthquake repairs. To fill the gaps between the component-level performance of RBMs and system-level behaviour of SCBFs with RBMs, this thesis focused on the overall system-level seismic performance of SCBFs with RBMs in three steps. Firstly, the effects of beam-column connection fixity on the behaviour of three SCBFs were investigated to determine what level of fixity, if any, is required to ensure adequate collapse capacity of an SCBF. Secondly, the effects of column design parameters on braced frame seismic performance were investigated, where two different brace-to-frame connections were considered: 1) conventional gusset plate connection and 2) the newly proposed connection detail with RBMs. Detailed numerical modelling was undertaken to develop improved provisions for designing columns in SCBFs. Finally, a large-scale experimental program was conducted to evaluate the seismic performance of braced frames with initial and replaced RBMs where realistic boundary conditions were provided. Three different beam-column connections that can be used in SCBFs with RBMs were designed and tested. The findings of the work presented in this thesis and potential areas of future research of this new system are outlined in the following sections.

5.2 Conclusions

5.2.1 Effects of Beam-Column Connections Fixity and Gravity Framing on Collapse Capacity of Special Concentrically Braced Frames

Structural engineers usually design Special Concentrically Braced Frames (SCBF) neglecting the rotational stiffness and strength of beam-to-column connections in an SCBF as well as the contribution of the gravity load resisting structure to the total stiffness and strength of the structure. Sometimes, the stiffness and strength of beam-to-column connections and gravity load resisting system are neglected also in research studies. It was investigated if and how much these two aspects may affect the collapse capacity of SCBFs. Extensive nonlinear time history analyses were conducted and the following conclusions were made:

- If the stiffness and strength provided by the gravity resisting system are neglected, the type of beam-to-column connections in an SCBF has some effect on the collapse capacity that generally improves as stiffness and strength of the connection increases. The improvement was negligible for the three-storey frame, while it was appreciable for the six- and twelve-storey frames.
- Modelling the shear-tab connections and columns of the gravity resisting system significantly improves the performance of the SCBF and makes it almost independent of the type of beam-to-column connections in the braced bay.
- The damping model can significantly affect the computed collapse capacity of SCBFs. Using the initial stiffness instead of tangent stiffness to compute the Rayleigh damping increased the collapse margin ratio by 10%, 30% and 310% for three-, six-, and twelve-storey buildings, respectively.

5.2.2 Seismic Design of Braced Frame Columns

In SCBFs, braces are intended to dissipate energy through inelastic buckling and tensile yielding, whereas the beams and columns should remain elastic according to the capacity design concept. The seismic force demands on columns in SCBFs with conventional braces or with replaceable brace modules were investigated. New design recommendations for considering the flexural demand on columns in braced frames were presented and examined. The collapse fragility curves were constructed after considering the new recommendations for designing the columns. The main findings are:

- Assuming an increasing force demand for columns moving towards the bottom storeys based on the first mode deformation does not necessarily result in the most critical case, and thus the current design procedure is not as conservative as expected.
- Relative to current design requirements, stronger and stiffer columns are needed to increase the collapse capacity to meet the FEMA P695 collapse criterion.
- Three modified methods were proposed to incorporate the moment demand into the design of columns in SCBFs. The results showed an improvement in the collapse capacity to acceptable levels when using Methods 2 and 3, although more frames should be tested before recommending one specific approach.
- The effects of the eccentricity in the SCBFs with RBMs were minimal because the maximum P-M interaction happens at inter-storey drifts larger than 1%, after the braces have buckled, resulting in relatively little flexural demand on columns due to the eccentricity but large flexural demands due to nonuniform drifts.
- Using the modified methods for designing the columns also provides the benefit of reducing residual drifts, leading towards easier structural repairs.

5.2.3 Large-Scale Experimental Testing of a Concentrically Braced Frame with Replaceable Brace Modules

Large-scale experimental testing of three SCBFs with RBMs was performed at the Applied Dynamics Laboratory at McMaster University. Two tests were conducted on each specimen, one with initial brace modules and one after replacing damaged brace modules. Three different beam-column connections were designed (considering erection time and fabrication costs), and their performance together with the RBM was discussed. The study found that:

- In all of the specimens, damage was generally confined to the intended locations until brace fracture and the storey drift was comparable to previous results for SCBFs with more commonly used gusset plate connections.
- All three specimens with replaced brace modules could sustain their initial stiffness and strength after successive load reversals.
- After both braces fractured, considerable lateral strength was developed through frame action.
- The single shear tab connection provided a stable response and experienced a large rotation of 0.032 rad without any local damage, weld fracture, or reduction in resistance.
- The end plate connection showed an acceptable performance with a maximum rotation of 0.022 rad, with no local damage.
- The bolted unstiffened extended end plate connection could accommodate a large inter-storey drift of 3.3% prior to fracture of a bolt.
- Based on this study, the recently proposed connection for joining the brace to the beam, accompanied by the tested beam-column connections, offers easier initial

installation and post-earthquake repair, while providing similar seismic performance to more traditional solutions.

5.3 Recommendations for Further Research

Despite the comprehensive nature of the work presented in this thesis, several aspects of SCBFs with RBMs still require future study. Potential areas for further research identified through the completion of this work are:

- Test a multi-level SCBF specimen with RBMs with two-storey X-braced configuration, and with varying brace sizes along the height. This specimen should be loaded from each storey and employ a cyclic or pseudo-dynamic loading protocol. This test would allow for the investigation of the performance of beam-column connections and RBMs where two braces are also connected.
- A full parametric study is desirable using a finite element model to better optimize the design of details when using RBMs. Potential variables for such a study include different brace shapes, fillet weld sizes of the support and stiffener plates, larger hinge lengths, fillet weld size of the shear tab plate to the column, shear tab plate thickness, weld size of the extended end plate connection, and the diagonal stiffener in the panel zone.
- Details should be proposed for the new connection where it joins to the beam such that the concrete slab does not prevent replacing the RBMs after an earthquake.
- Larger bolt holes in the support plates can improve the replaceability of the RBMs. However, additional research is necessary to ensure that larger holes cannot negatively affect the performance of the system.
- Further development of the design procedure would be desirable to promote a desirable hierarchy of damage and fracture while maximizing drift capacity and energy dissipation, with reference to the Balance Design Procedure [1].

- Building structures with CBFs have a reserve of stiffness and strength in the beam-column connections of the CBF and of the gravity resisting system that can improve their performance with respect to that predicted by the bare CBF model. More research should be conducted to propose a design procedure that takes into account the beneficial influence of the real stiffness and strength of beam-column connections. This procedure would make the design of CBF systems more efficient.
- Further research is required to determine how the relative demand to capacity ratios (D/C) in braces along the height of building should be distributed such that optimal performance from each storey is achieved.
- The new alternative connection can be extended to buckling restrained braced frames (BRBFs), referring also to earlier work by Berman and Bruneau [2]. Related experimental and analytical works are needed for BRBFs.
- The new connection can be used to rehabilitate existing steel/concrete moment resisting frames. Additional research into the rehabilitation of existing structures is required to advance the seismic performance evaluation and rehabilitation of these systems with the new connection.
- The loading protocol that was used in this study was quasi-static, which is able to capture the nonlinear cyclic behaviour of the specimens. However, the actual seismic event is dynamic and time-varying which may cause different local and global response. Future research could investigate these effects.

References

- [1] Roeder CW, Lumpkin EJ, Lehman DE. A balanced design procedure for special concentrically braced frame connections. *J Constr Steel Res* 2011;67:1760–72.
- [2] Berman JW, Bruneau M. Cyclic Testing of a Buckling Restrained Braced Frame with Unconstrained Gusset Connections. *J Struct Eng* 2009;135:1499–510.

Appendix A New Connection Design Examples

This appendix contains the example calculations that were used for designing the specimen. These calculations demonstrate how similar connections can be designed within the framework of the current design codes. In these calculations the Canadian standard CSA S16-14 is the primary reference, but AISC design provisions are used in some cases. Equations are from S16-14 unless otherwise noted.

A.1 Material Properties

From the 11th edition CISC *Handbook of Steel Construction* (CISC, 2014) Table 6-3, the material property of the elements are as follows:

Beams and columns: ASTM A992 ($F_y = 345 \text{ MPa}$, $F_u = 450 \text{ MPa}$)

Braces: G40.21 350W ($F_y = 350 \text{ MPa}$, $F_u = 450 \text{ MPa}$)

Plates: G40.21 300W ($F_y = 300 \text{ MPa}$, $F_u = 440 \text{ MPa}$)

A.2 Brace Overstrength Resistance and Predicted Yield Drift

From CISC *Handbook of Steel Construction* (CISC, 2014) page 6-109, the geometric properties are as follows:

HSS76×76×4.8

$A = 1310 \text{ mm}^2$, $I_x = 1.08 \text{ e}6 \text{ mm}^4$, $S_x = 28.5 \text{ e}3 \text{ mm}^3$, $Z_x = 34.4 \text{ e}3 \text{ mm}^3$

$$\frac{b}{t} = 11.9 < 0.65 \sqrt{\frac{E}{R_y F_y}} = 0.65 \sqrt{\frac{2 \text{ e}5}{1.4 \times 350}} = 13.13 \quad (\text{AISC})$$

$$\frac{b}{t} = 11.9 < \frac{330}{\sqrt{F_{ye}}} = \frac{330}{\sqrt{460}} = 15.4 \quad (\text{CSA} - 27.5.3.2(i))$$

$$T_u = A_g R_y F_y = 1310 \times 1.4 \times 350 = 642 \text{ kN} \quad (27.5.3.4)$$

A factor of $C_p = 1.1$ was also considered to account for strain hardening and other factors that might affect the brace's overstrength capacity. This is not required by the code, however it was considered here to provide an additional margin to ensure that the capacity of the actuator in the laboratory would not be exceeded.

$$T_u = C_p A_g R_y F_y = 1.1 \times 1310 \times 1.4 \times 350 = 706 \text{ kN}$$

The compressive capacity was calculated using Equation 4.1 of this thesis to determine the effective length factor:

$$L = 1775 \text{ mm}, M_{ph} = 350 \times 250 \times \frac{13^2}{4} = 3.70 \text{ KN.m}, M_{pb} = 34.4e3 \times 450 = 15.48 \text{ kN.m}$$

$$K_t = \frac{1}{1 + \left(\frac{M_{ph}}{M_{pb}}\right)} = \frac{1}{1 + \left(\frac{3.70}{15.48}\right)} = 0.80$$

$$\frac{K_t l}{r} = \frac{0.80 \times 1775}{28.8} = 49.3$$

$$F_e = \frac{\pi^2 E}{(49.3^2)} = 812 \text{ MPa} \quad (13.3.1)$$

$$\lambda = \sqrt{\frac{R_y F_y}{F_e}} = \sqrt{\frac{450}{812}} = 0.74 \quad (13.3.1)$$

$$C_r = 1310 \times 1.4 \times 350 \times (1 + 0.74^{2 \times 1.34})^{-1/1.34} = 487.4 \text{ kN} \quad (13.3.1)$$

$$\rightarrow C_u = 1.2 \times 487.4 = 585 \text{ kN}$$

The associated displacements were then calculated as:

$$\Delta_{y^-} = \frac{P^- L}{AE} = \frac{585e3 \times 1775}{1310 \times 2e5} = 3.96 \text{ mm}$$

$$\Delta_{y^+} = \frac{P^+ L}{AE} = \frac{642e3 \times 1710}{1310 \times 2e5} = 4.2 \text{ mm}$$

This resulted in the predicted force-displacement response shown below:

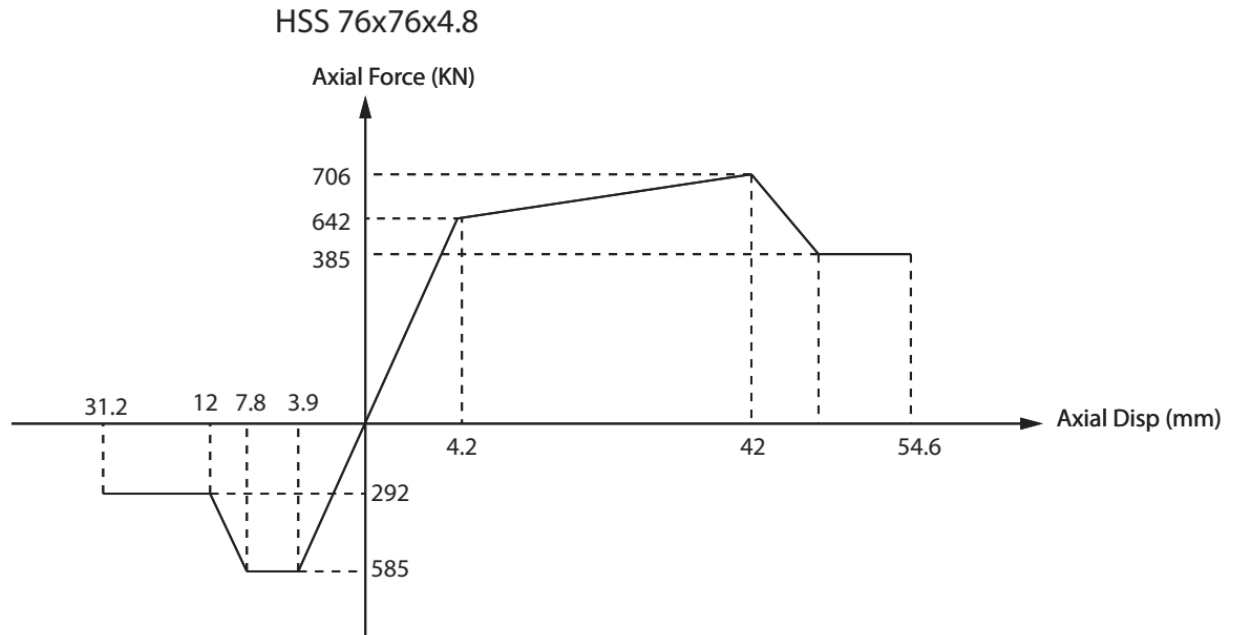


Figure A-1 Axial Force-deformation relation for used braces

The following calculations were used to determine the associated yield drift of the frame:

$$\theta = \tan^{-1}\left(\frac{2284}{2094}\right) = 47.5^\circ$$

$$\Delta(\text{top beam}) = 1.48\delta(\text{brace disp})$$

First point :

$$\delta_1 = 3.9 \text{ mm} \quad \Delta_1 = 3.9 \times 1.48 = 5.8 \text{ mm}$$

$$\text{Lower storey stiffness} = 300 \frac{kN}{mm}$$

$$\text{Base shear at } \Delta_y = 490 \times 2 \times \cos(47) = 665 \text{ kN}$$

Top storey displacement at this moment :

$$\Delta_y = 5.8 \text{ mm} + \frac{665}{300} = 8.02 \text{ mm}$$

$$D_y = \frac{8.02}{2100} = 0.38\%$$

The brace and connection forces under the associated peak tension and compression forces are shown in Figure A-2.

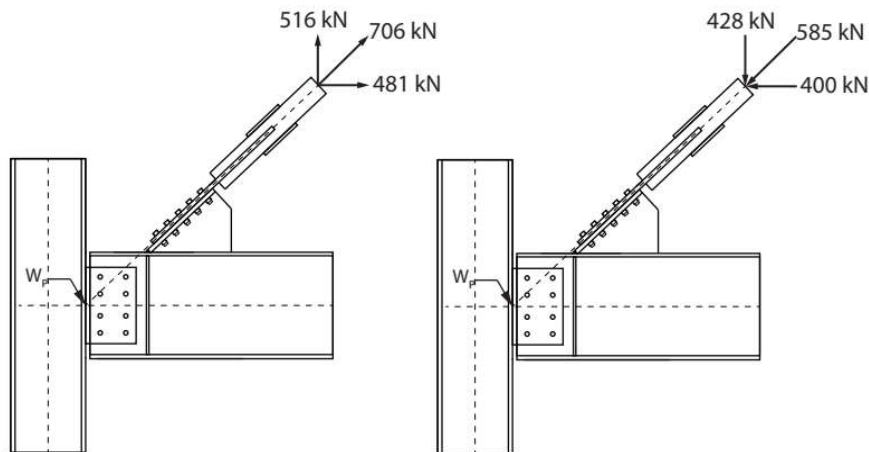


Figure A-2 Applied forces in tension and compression

A.3 Hinge Plate Design

A.3.1 Hinge Plate Dimensions

The hinge plate width was chosen to be less than the beam flange width to prevent interference with non-structural elements.

Hinge plate width = $245\text{ mm} < (b_{f(\text{beam})} = 256\text{ mm})$

A.3.2 Design of Bolts between Hinge Plate and Support Plate

Strength per A325 3/4" bolt in single shear bearing with threads excluded:

$$V_r = 0.6\phi_b A_b F_u$$

$$V_r = 0.6 \times 0.8 \times 285 \times 825 = 112.8\text{ kN}$$

The number of bolts required is:

$$n_b \geq \frac{T_u}{V_r}$$

$$n_b \geq \frac{706}{112.8} = 6.25$$

Therefore, use 8 3/4" A325 bolts.

Minimum bolt spacing is: $2.7 \times \frac{3}{4} \times 25.4 = 51.5\text{ mm}$

Using 4 rows of bolts with minimum spacing of 70 mm, the connection dimensions are shown in Figure A-3.

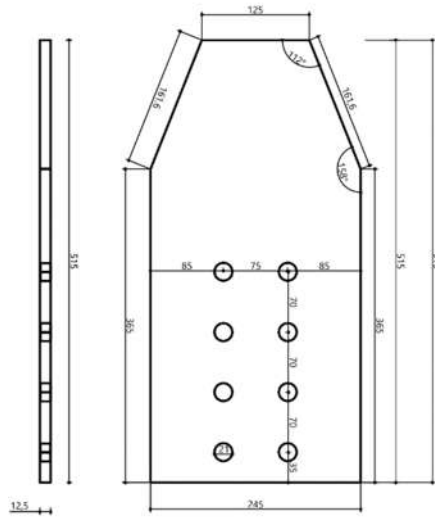


Figure A-3 Hinge plate detail

Checking for the reduced bolt shear strength due to the length of splice plate:

$$L \leq 760 \text{ mm} \quad (13.12.1.2)$$

$$210 \text{ mm} \leq 760 \text{ mm}$$

Therefore no reduction in bolt strength is required.

A.3.3 Hinge and Support Plate Thickness

To prevent gross yield of the hinge plate:

$$A_g \geq \frac{T_u}{\phi F_y} \quad (13.2(a)(i))$$

$$t_h \times 245 \geq \frac{706e3}{0.9 \times 300} \rightarrow t_h \geq 10.7 \text{ mm}$$

To prevent net section fracture along the first line of bolts:

$$A_{ne} \geq \frac{T_u}{\phi_u F_u} \quad (13.2(a)(iii))$$

$$t_h \times (245 - 2 \times 21) \geq \frac{706e3}{0.75 \times 440} \rightarrow t_h \geq 10.5 \text{ mm}$$

To prevent the three critical modes of block shear shown in Figure A-4:

$$\phi_u \left[U_t A_n F_u + 0.6 A_{gv} \frac{F_y + F_u}{2} \right] \geq T_u \quad (13.2(a)(ii))$$

Case 1:

$$A_n = (2 \times 85 - 21) \times t_h = 149 t_h \text{ mm}^2$$

$$A_{gv} = 2 \times 245 \times t_h = 490 t_h \text{ mm}^2$$

$$t_h \geq \frac{706e3}{0.75 \left[1 \times 149 \times 440 + 0.6 \times 490 \times \frac{300 + 440}{2} \right]} = 5.4 \text{ mm}$$

Case 2:

$$A_n = (75 - 21) \times t_h = 54 t_h \text{ mm}^2$$

$$A_{gv} = 2 \times 245 \times t_h = 490 t_h \text{ mm}^2$$

$$t_h \geq \frac{706e3}{0.75 \left[1 \times 54 \times 440 + 0.6 \times 490 \times \frac{300 + 440}{2} \right]} = 7.1 \text{ mm}$$

Case 3:

$$A_n = 0$$

$$A_{gv} = 4 \times 245 \times t_h = 980 t_h \text{ mm}^2$$

$$t_h \geq \frac{706e3}{0.75 \left[1 \times 0 \times 440 + 0.6 \times 980 \times \frac{300 + 440}{2} \right]} = 4.3 \text{ mm}$$

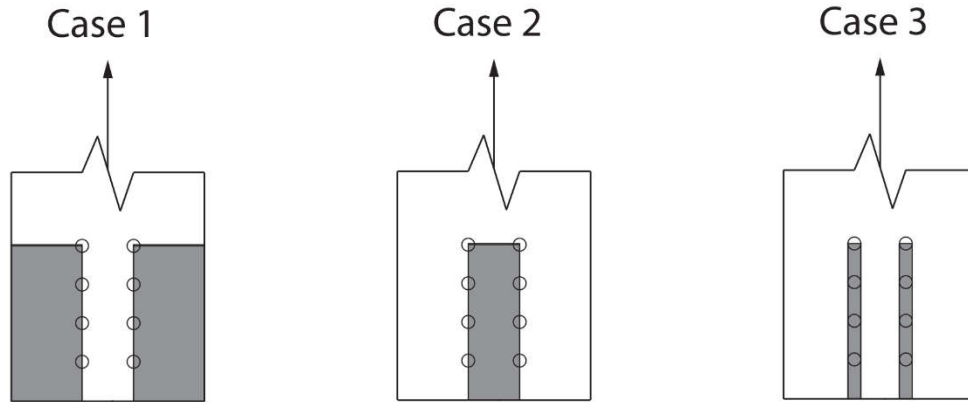


Figure A-4 Block shear failure modes

The most critical condition of gross yield is satisfied by using 12.7 mm (0.5 in) plate.

To check the bolt bearing:

$$B_r = 3\phi_{br}ndtF_u \quad (13.12.1.2(a))$$

$$B_r = 3 \times 0.8 \times 8 \times 19 \times 12.7 \times 440 = 2038 \text{ kN}$$

A.3.4 Hinge Plate Buckling

Between the brace end and the first row of bolts:

$$L = 35 + 25 = 60 \text{ mm}$$

$$\frac{KL}{r} = \frac{1.2 \times 60}{\frac{t_h}{\sqrt{12}}} = \frac{1.2 \times 60}{\frac{12.5}{\sqrt{12}}} = 20$$

Since KL/r is smaller than 25, yielding controls as per AISC Specification J4.4(a).

A.3.5 Hinge Plate to Brace Weld

Using an 8 mm (single pass) E49xx fillet weld, the strength per mm of weld is:

$$V_r = 0.67 \phi_w A_w X_u (1 + 0.5 \sin^{1.5} \theta) M_w$$

$$V_r = 0.67 \times 0.67 \times \frac{8}{\sqrt{2}} \times 1 \times 490 \times (1 + 0) \times 1 = 1244 \text{ N / mm} = 1.24 \text{ kN / mm}$$

$$l_w = \frac{706e3}{4 \times 1.24e3} = 142 \text{ mm}$$

A weld length of 200 mm for the hinge plate to brace was selected.

A.3.6 Brace Slot Cover Plates

Brace net section:

$$A_n = A_g - 2 \times (12.5 + 2.5) \times 4.8 = 1166 \text{ mm}^2$$

$$\bar{x} = \frac{B^2 + 2BH}{4(B + H)} \quad (\text{AISC – Table D3.1})$$

For a square HSS where B=H:

$$\bar{x} = \frac{3H}{8} = \frac{3 \times 76}{8} = 28.5$$

$$A_{ne} = \left(1 - \frac{\bar{x}}{l_w}\right) A_n = \left(1 - \frac{28.5}{200}\right) \times 1310 = 1123.3 \text{ mm}^2$$

Brace net section tensile resistance:

$$T_r = \phi_u A_{ne} F_u = 0.75 \times 1123 \times 450 = 379 \text{ kN}$$

The resistance can be increased per S16-14 clause 27.5.4.2.

$$T_r = 379 \times \frac{R_y}{\phi} = 379 \frac{1.2}{0.9} = 505 \text{ kN}$$

The remaining net section tension resistance that must be resisted by cover plates is:

$$T_r = 706 \text{ kN} - 505 \text{ kN} = 201 \text{ kN}$$

The cover plates will be 50 mm wide to allow clearance for welds on the HSS wall. Try a 10 mm thick plate:

$$T_r = 2(\text{cover plates}) \times \phi_u \left(1 - \frac{\bar{x}}{l_w}\right) A_n F_u$$

$$T_r = 2 \times 0.75 \times 0.75 \times \left(1 - \frac{38}{200}\right) (50)(10)(440) = 200 \text{ kN}$$

Therefore, 50x10 mm cover plates are sufficient for net section resistance.

Cover plate to brace welds:

$$T_u = A_c R_y F_y = 50 \times 10 \times 1.1 \times 300 = 165 \text{ kN}$$

Using 5 mm E49xx fillet welds on each side:

$$l_w \geq \frac{165 \text{ kN}}{2 \times 0.682} = 121 \text{ mm}$$

$$l_w = 150 \text{ mm}$$

A.3.7 Support and Stiffener Plates

Since the support plate will be under similar loading conditions to the hinge plate, the 245 mm wide and 12.7 mm thick plate will pass all the same tension and bolt checks at the hinge plate. The stiffener plate was also selected to have the same 12.7 mm thickness. The weld joining the stiffener plate to the beam flange was capacity designed based on the full shear resistance of the stiffener plate.

$$T = 0.66 F_y \times A_{\text{stiffener plate}}$$

$$T = 0.66 \times 300 \times 254 \times 12.5 = 628.6 \text{ kN}$$

Using an 8 mm (single pass) E49xx fillet weld, the strength per mm of weld is:

$$V_r = 0.67 \phi_w A_w X_u (1 + 0.5 \sin^{1.5} \theta) M_w$$

$$V_r = 0.67 \times 0.67 \times \frac{8}{\sqrt{2}} \times 1 \times 490 \times (1 + 0) \times 1 = 1244 \text{ N / mm} = 1.24 \text{ kN / mm}$$

$$V_r = 1.24 \text{ kN / mm} \times 254 \text{ mm} \times 2 = 630 \text{ kN}$$

A.3.8 Bearing Strength of the Beam

In this section, web crippling, web yielding and flange local bending are checked.

- Web crippling:

$$B_r = 0.6 \phi_{be} w^2 \sqrt{F_y E} \quad (14.3.2(b)(ii))$$

$$B_r = 0.6 \times 0.75 \times 13^2 \sqrt{345 \times 2e5} = 630 \text{ kN} \geq 428 \text{ kN} \rightarrow \text{OK}$$

- Web yielding

The web yielding strength of the beam is calculated using an end loaded case and a bearing area equal to the normal width of the main support plate.

$$B_r = \phi_{be} w (N + 4t) F_y$$

$$B_r = 0.75 \times 13 \times (12.5 \cos 47.5 + 4 \times 21.7) \times 345 = 320 \text{ kN} \leq 516 \text{ kN} \rightarrow \text{Not OK}$$

Therefore, bearing stiffeners are required.

$$T - B_r = 516 - 320 = 196 \text{ kN}$$

For a stiffener width of 100 mm on each side of the web, the minimum area of each bearing stiffener is:

$$T - B_r \leq \phi A_b F_y$$

$$A_b \geq \frac{196e3}{0.9 \times 300} = 725 \text{ mm}^2$$

$$A_b = 2ct_s = 2 \times 100t_s \rightarrow t_s = \frac{725}{200} = 3.6 \text{ mm}$$

Use 10 mm thickness plates to satisfy clause 14.4.2

$$\frac{b}{t} = \frac{100}{10} \leq \frac{200}{\sqrt{300}} = 11.5 \rightarrow OK$$

Bearing stiffener weld:

If we use a 5 mm fillet weld:

$$l_w \geq \frac{196}{4 \times 0.682} = 72 \text{ mm}$$

However, it is recommended that the stiffeners should extend at least 2/3 the depth of the beam to allow more uniform force transfer to the beam web and beam-column connection region. Therefore, the recommended bearing stiffener length is 320 mm.

Note: These stiffeners might not be required because some load goes through the stiffener plate.

- Flange local bending (AISC360-16 (J10-1))

$$R_n = \frac{1}{2} \times 6.25 F_{yf} t_{yf}^2 = 0.5 \times 6.25 \times 345 \times 21.7^2 = 507.7 \text{ kN} \leq 516 \text{ kN}$$

A pair of transverse stiffeners shall be used as they were designed for web yielding limit state.

A.4 Beam-Column Connections

In this section, three beam-column connection details are detailed: single shear tab connection, end-plate connection and bolted unstiffened extended end-plate connection. Figure A-5 shows the connection details.

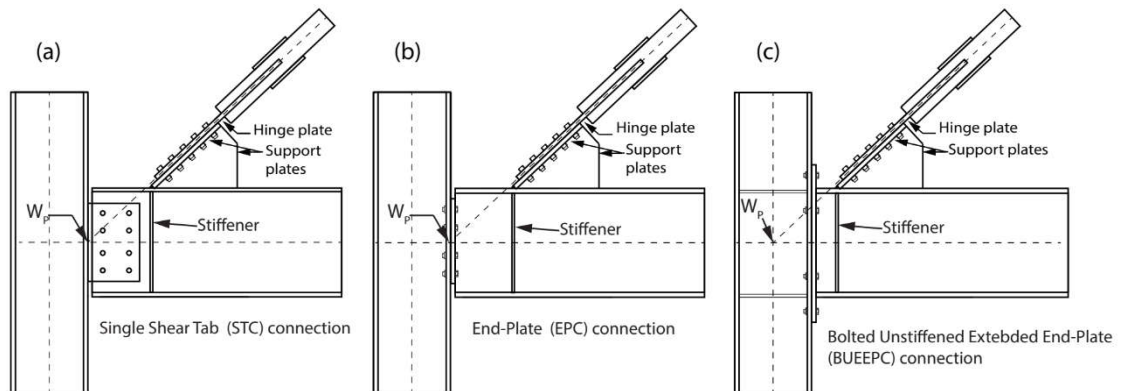


Figure A-5 Proposed connection details

A.4.1 Single Shear Tab Connection

A single shear tab beam connection will be used to connect the beam to the column. The shear tab will be shop-welded to the column and site-bolted to the beam. As shown in Figure A-5(a), the centerline of the brace passed through the center of the beam at the column flange surface. For that reason, the connection is designed to carry only vertical and horizontal forces. In Figure A-6, 80 kN is assumed to be a result of ELF procedure for finding lateral loads applying at the connection location.

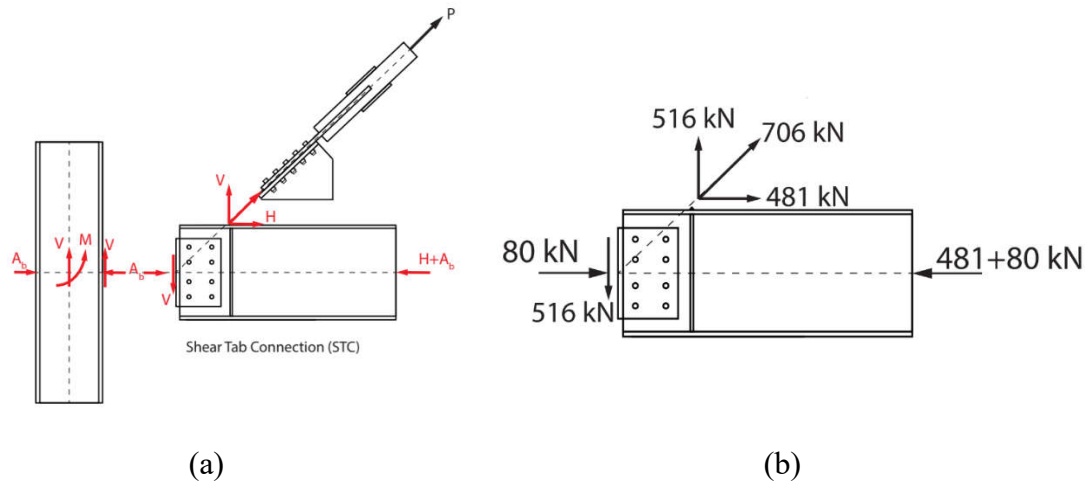
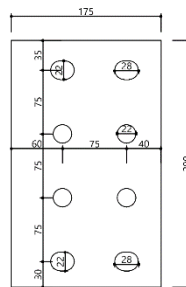


Figure A-6 Connection free body diagram

The following plate detail is used for the shear tab, including short slotted holes at the top and bottom bolt lines to permit some rotation:



- Shear tab to column weld design: Based on mechanics

$$f_H = \frac{80kN}{2 \times 290 mm} = 0.14 \frac{kN}{mm}$$

$$f_v = \frac{516kN}{2 \times 290 mm} = 0.90 \frac{kN}{mm}$$

$$f_r = \sqrt{0.14^2 + 0.90^2} = 0.91 \frac{kN}{mm}$$

Use 8mm E49xx fillet weld.

- Shear tab thickness (based on shear stress distribution over a rectangular section):

$$f_v = \frac{3}{2} \times \frac{516000}{(290)t} \leq 0.66 F_y$$

$$t \geq \frac{3}{2} \times \frac{516000}{290 \times 198} = 13.5 \text{ mm}$$

Use 5/8 in (15.9 mm) plates.

- Shear tab bolts design

Both shear force and torsion effects should be considered. Based on mechanics:

$$V = 516 \text{ kN}$$

$$T = Ve = 516 \times (60 + 75 / 2) = 50.3 \text{ kN.m}$$

$$J = 4 \times 285 \times (37.5^2 + 112.5^2) + 8 \times 285 \times 37.5^2 = 19.2e6 \text{ mm}^4$$

$$f_{vy} = \frac{V}{nA_b} + \frac{Tx}{J} = \frac{516e3}{8 \times 285} + \frac{50.3e6 \times 37.5}{19.2e6} = 226.3 + 98.2 = 324.5 \text{ N / mm}^2$$

$$f_{vx} = \frac{H}{nA_b} + \frac{Ty}{J} = \frac{80e3}{8 \times 285} + \frac{50.3e6 \times 112.5}{19.2e6} = 325 \text{ N / mm}^2$$

$$f_v = \sqrt{f_{vx}^2 + f_{vy}^2} = 420 \text{ N / mm}^2 \approx \text{factored shear stress of bolts} = \frac{113 \text{ kN}}{285} = 400 \text{ N / mm}^2$$

- Shear tab weld design to the beam

This weld is designed using Table 3-28 CSA S16-14.

$$D = \frac{P}{CL}$$

$$k = \frac{160}{290} = 0.55$$

$$\text{Table 3-28 (bottom line)} \rightarrow x = 0.144$$

$$aL + xL = 180 \text{ mm}, L = 290 \text{ mm}$$

$$290a + 0.144(290) = 180 \rightarrow a = 0.48$$

for $a = 0.48$ and $k = 0.55 \rightarrow C = 0.25$

$$D = \frac{516}{0.25 \times 290} = 7.1 \text{ mm} \rightarrow \text{USE } D = 8 \text{ mm}$$

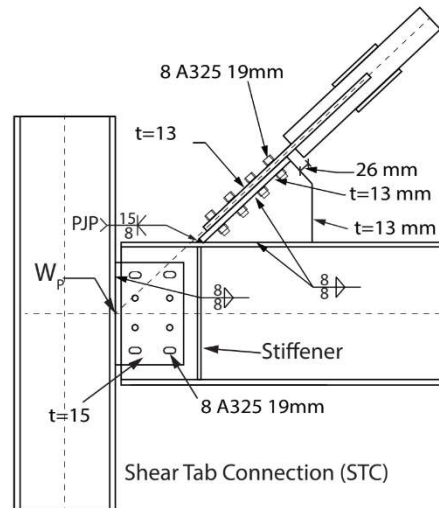


Figure A-7 Shear tab connection details

A.4.2 End Plate Connection

An end-plate beam-column connection will be used to connect the beam to the column. The end plate will be shop-welded to the beam and site-bolted to the column. As shown in Figure A-5(b), the centerline of the brace passed through the center of the beam at the column flange surface. For that reason, the connection is designed to carry only vertical and horizontal forces.

- End plate bolts design:

Both shear force and torsion effects should be considered. Based on mechanics:

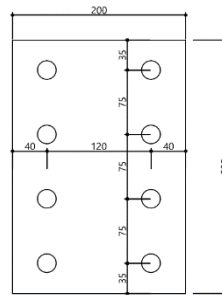
$$V = 516 \text{ kN}$$

$$H = 80 \text{ kN}$$

$$f_{vy} = \frac{V}{nA_b} = \frac{516e3}{8 \times 285} = 226.3 \text{ N / mm}^2$$

$$f_{vx} = \frac{H}{nA_b} = \frac{80e3}{8 \times 285} = 35.1 \text{ N / mm}^2$$

$$f_v = \sqrt{f_{vx}^2 + f_{vy}^2} = 230 \text{ N / mm}^2 \leq \text{factored shear stress of bolts} = \frac{79 \text{ kN}}{285} = 277 \text{ N / mm}^2$$



- End plate to column weld design: Based on mechanics

$$f_H = \frac{80 \text{ kN}}{2 \times 295 \text{ mm}} = 0.14 \frac{\text{kN}}{\text{mm}}$$

$$f_v = \frac{516 \text{ kN}}{2 \times 295 \text{ mm}} = 0.90 \frac{\text{kN}}{\text{mm}}$$

$$f_r = \sqrt{0.14^2 + 0.90^2} = 0.91 \frac{\text{kN}}{\text{mm}}$$

Use 8mm E49xx fillet weld.

- End Plate Thickness

According to Table 3-39 a minimum required end-plate thickness is 6.9mm. To facilitate the fabrication, a plate of 15 mm is used (similar to single shear tab connection).

- Minimum required web thickness of supported beam (Table 3-39)

$$12.1 \times \frac{516}{684} = 9.12 \text{ mm} \leq 13 \text{ mm OK}$$

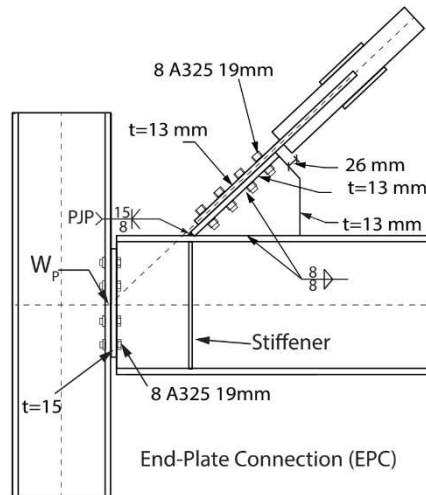


Figure A-8 End plate connection details

A.4.3 Bolted Unstiffened Extended End Plate Connection

In this connection, the centroid of the brace, beam, and column all pass through the center of the connection in the column. For that reason, there is a moment on the connection itself due to the different horizontal and vertical distances from the center of the beam and the location of the brace force. An extended end-plate connection is designed to carry the moment and the vertical force on the connection. Bolted end-plate connections are made by welding the beam to an end-plate and bolting the end-plate to the column flange. The connection is designed with eight 3/4-in bolts (similar to RCBF-EP specimen) when threads are excluded. In this case, stiffeners on the web of the column are required at the points of concentrated loads (at the locations of beam flanges).

Figure A-9 shows the free body diagram and of this connection and associated forces.

$$M = 481 \times 0.1815 - 516 \times .045 = 64 \text{ kN.m}$$

Plastic moment capacity of the beam is $M_p = R_y Z F_y = 2270 \times 10^3 \times 345 = 782 \text{ kN.m}$

Since connections which transmit a negligible moment ($< 0.2M_p$) are classified as simple connections, this connection is designed to be able to transmit $0.2M_p = 156.4 \text{ kN.m}$. Although the connection is not being designed for the full capacity of the beam, Chapter 6 of AISC 358-16 (Prequalified Connections for Special and Intermediate Steel Moment Frames for Seismic Applications) is used for designing the connection.

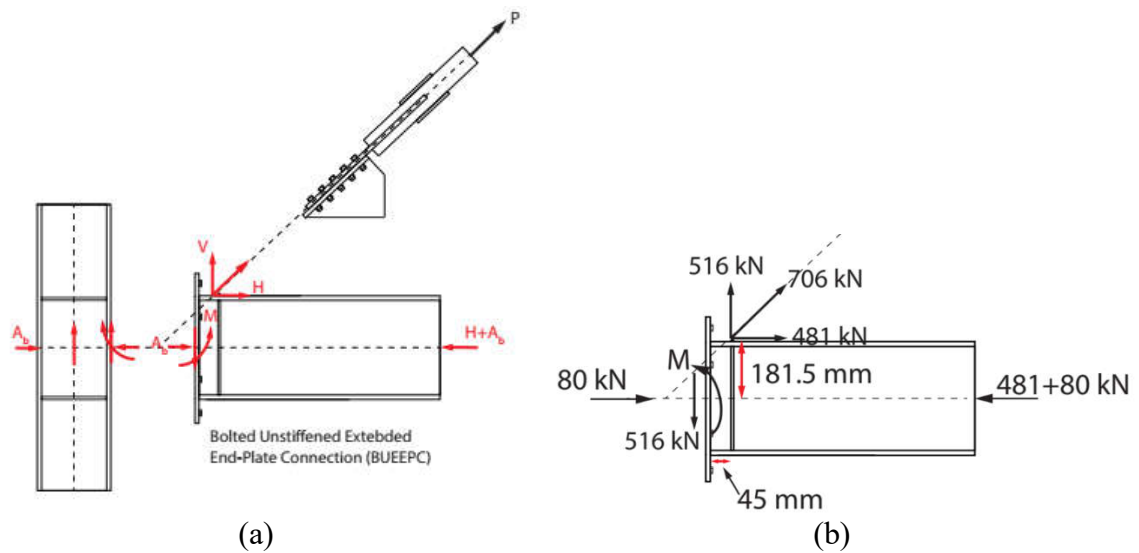
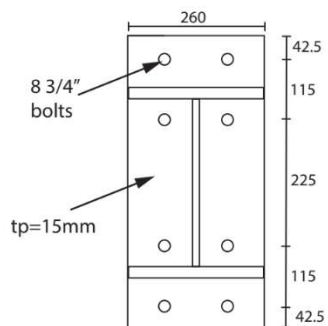


Figure A-9 Bolted Unstiffened End plate connection free body diagram

If the following plate detail is used for the extended end plate:



Two limit states should be checked based on bolts resistance and plate thickness.

- Bolt resistance limit state (equation 6.8-4, AISC 358-16)

$$M_f = 2T_r \times (h_o + h_1)$$

However, bolts are carrying both tension and shear.

Clause 13.12.1.4 (CSA S16)

$$\left(\frac{V_f}{V_r}\right)^2 + \left(\frac{T_f}{T_r}\right)^2 \leq 1$$

$$V_f = \frac{516}{8} = 64.5 \text{ kN}$$

$$\left(\frac{64.5}{113}\right)^2 + \left(\frac{T_f}{T_r}\right)^2 \leq 1 \rightarrow \left(\frac{T_f}{T_r}\right)^2 \leq 1 - 0.33 \rightarrow T_f = 0.82T_r = 115.6 \text{ kN}$$

$$M_{f1} = 2T_r \times (h_o + h_1) = 2 \times 115.6 \times (290 + 405) = 160.7 \text{ kN.m}$$

- End-plate thickness limit state (equation 6.8-5, AISC 358-16)

$$M_f = \frac{\phi F_{yp} \times Y_p \times t_p^2}{1.11}$$

$$Y_p = \frac{b_p}{2} \left[h_1 \left(\frac{1}{p_{fi}} + \frac{1}{s} \right) + h_0 \left(\frac{1}{p_{fo}} \right) - \frac{1}{2} \right] + \frac{2}{g} [h_1 (p_{fi} + s)]$$

where, $p_{fo} = 45 \text{ mm}$, $p_{fi} = 46 \text{ mm}$

$$s = \frac{1}{2} \sqrt{b_p g} = \frac{1}{2} \sqrt{260 \times 120} = 88.3 \text{ mm}$$

$$Y_p = \frac{260}{2} \left[280 \left(\frac{1}{46} + \frac{1}{88.3} \right) + 395 \left(\frac{1}{45} \right) - \frac{1}{2} \right] + \frac{2}{120} [290(46 + 88.3)] = 2928.8$$

$$M_{f2} = \frac{\phi F_{yp} \times Y_p \times t_p^2}{1.11} = \frac{0.9 \times 300 \times 2928.8 \times 15^2}{1.11} = 160.3 \text{ kN.m}$$

$$M_f = \min(M_{f1}, M_{f2}) = 160.3 \text{ kN.m} > 0.2 M_p$$

- Check shear yielding of the extended portion of the four-bolt extended unstiffened end-plate

$$\frac{F_{fu}}{2} \leq \phi_d (0.6) F_{yp} b_p t_p$$

$$F_{fu} = \frac{M_f}{d - t_{bf}} = \frac{160.7 \times 10^6}{363 - 21.7} = 470.8 \text{ kN}$$

$$\frac{470.8}{2} \leq 0.9 \times 0.6 \times 300 \times 260 \times 15 = 631.8 \text{ kN OK}$$

- Check shear rupture of the extended portion unstiffened end-plate

$$\frac{F_{fu}}{2} \leq \phi (0.6) F_{up} A_n$$

$$A_n = t_p [b_p - 2(d_b + 3)] = 15 \times [260 - 2 \times (22)] = 3240 \text{ mm}^2$$

$$\frac{470.8}{2} \leq 0.75 \times 0.6 \times 440 \times 3240 = 641.5 \text{ kN OK}$$

- Check bolt-bearing/tear-out failure of the end-plate and column flange:

End – plate

$$V_u \leq \phi R_n = \phi n_i r_{ni} + \phi n_o r_{no}$$

$$r_{ni} = 1.2 \times 31.5 \times 15 \times 440 = 249.5 \text{ kN} < 2.4 \times 19 \times 15 \times 440 = 300.9 \text{ kN}$$

$$r_{no} = 1.2 \times 93 \times 15 \times 440 = 736.5 \text{ kN} > 2.4 \times 19 \times 15 \times 440 = 300.9 \text{ kN}$$

$$516 \text{ kN} \leq 0.75 \times 2 \times (249.5 + 300.9) = 825.6 \text{ kN}$$

column flange

$$V_u \leq \phi R_n = \phi n_i r_{ni} + \phi n_o r_{no}$$

$$r_{ni} = 2.4 \times 19 \times 13.5 \times 440 = 270.9 \text{ kN}$$

$$r_{no} = 1.2 \times 93 \times 13.5 \times 440 = 663 \text{ kN} > 2.4 \times 19 \times 13.5 \times 440 = 270.9 \text{ kN}$$

$$516 \text{ kN} \leq 0.75 \times 2 \times (270.9 + 270.9) = 812.7 \text{ kN}$$

- Check the column flange for flexural yielding

$$t_{cf} \geq \sqrt{\frac{1.11M_f}{\phi F_{yc} Y_c}} \text{ (From Table 6.5)}$$

$$Y_c = \frac{b_{cf}}{2} \left[h_1 \left(\frac{1}{s} \right) + h_0 \left(\frac{1}{s} \right) \right] + \frac{2}{g} \left[h_1 \left(s + \frac{3c}{4} \right) + h_0 \left(s + \frac{c}{4} \right) + \frac{c^2}{2} \right] + \frac{g}{2}$$

$$S = \frac{1}{2} \sqrt{b_{cf} g} = \frac{1}{2} \sqrt{203 \times 120} = 78$$

$$Y_c = \frac{203}{2} \left[280 \left(\frac{1}{78} \right) + 395 \left(\frac{1}{78} \right) \right] + \frac{2}{120} \left[280 \left(78 + \frac{3 \times 115}{4} \right) + 395 \left(78 + \frac{115}{4} \right) + \frac{115^2}{2} \right] + \frac{120}{2}$$

$$Y_c = 878.36 + 1579.5 + 60 = 2517.8$$

$$t_{cf} \geq \sqrt{\frac{1.11 \times 160.3 \times 10^6}{0.9 \times 345 \times 2517.8}} = 15 \text{ mm}$$

Column flange thickness is 13.5 mm. So we need to provide continuity plates.

- Determine the required stiffener force

Column flange flexural design strength is

$$\phi_d M_{cf} = \phi_d F_{yc} Y_c t_{cf}^2 = 0.9 \times 345 \times 2517.8 \times 13.5^2 = 142.5 \text{ kN.m}$$

$$\phi_d R_n = \frac{\phi_d M_{cf}}{(d - t_{bf})} = \frac{142.5 \text{ kN.m}}{363 - 21.7} = 417.5 \text{ kN}$$

Check the column web yielding strength of the unstiffened column web at the beam flanges

$$F_{fu} \leq \phi_d R_n$$

$$R_n = C_t (6k_c + t_{bf} + 2t_p) F_{yc} t_{cw} = 1 \times (6 \times 34 + 21.7 + 2 \times 15) \times 345 \times 8 = 705.7 \text{ kN}$$

$$470.8 \text{ kN} \leq 0.9 \times 705.7 = 635.1 \text{ kN}$$

Check the unstiffened column web buckling strength at the beam compression flange.

$$F_{fu} \leq \phi_d R_n$$

$$R_n = \frac{24t_{cw}^3 \sqrt{EF_{yc}}}{h} = \frac{24 \times 8^3 \times \sqrt{2e5 \times 345}}{363 - 2 \times 34} = 346 \text{ kN}$$

$$470.8 \geq 0.9 \times 346 = 311.4 \text{ kN} \quad \text{NOT OK}$$

Check the unstiffened column web crippling strength.

$$F_{fu} \leq \phi R_n, \phi = 0.75$$

$$R_n = 0.8t_{cw}^2 \left[1 + 3 \left(\frac{N}{d_c} \right) \left(\frac{t_{cw}}{t_{cf}} \right)^{1.5} \right] \sqrt{\frac{EF_{yc} t_{cf}}{t_{cw}}}$$

$$N = 203 + 2 \times 15 = 233$$

$$R_n = 0.8 \times 8^2 \times \left[1 + 3 \left(\frac{233}{252} \right) \left(\frac{8}{13.5} \right)^{1.5} \right] \sqrt{\frac{2e5 \times 345 \times 13.5}{8}} = 0.8 \times 64 \times 2.265 \times 10790 = 1251 \text{ kN}$$

$$470.8 \text{ kN} \leq 0.75 \times 1251 = 938 \text{ kN} \quad \text{OK}$$

So the required strength for stiffener plates is:

$$F_{su} = F_{fu} - \min(\phi R) = 470 - 311.4 = 158.6 \text{ kN}$$

To satisfy clause 14.4.2 I use: 2Plate 225×90×12.5

- Panel zone check

$$V_R = 0.66F_y A_w = 0.66 \times 345 \times 8 \times 252 = 459 \text{ kN}$$

$$0.9V_R = 413 \text{ kN} \leq 470.8 \text{ kN}$$

Therefore a doubler plate is required. However, results of the testing showed that we need to design the panel zone for the shear force due to column bending in addition to the 470.8 kN from the beam (F_{fu}).

$$V = V_{column} + F_{fu}$$

$$V = \frac{2M_p}{2.1} + F_{fu} = \frac{2 \times 292}{2.1} + 470.8 = 748.9 \text{ kN}$$

$$V_{stiffener} = 748.9 - 413 = 335.9 \text{ kN}$$

Using diagonal reinforcement on one side:

$$0.9 \times 0.6 A_{st} \times 300 \times \cos 56 \geq 335.9 \text{ kN}$$

$$A_{st} \geq 3698 \text{ mm}^2 \rightarrow t_{st} \geq \frac{3698}{400} = 9.2 \text{ mm}$$

USE Plate 400 × 10

Weld size required for the end reaction:

The end reaction is resisted by the weld between the flange and the end-plate:

If 10 mm weld is used, according to Table 3-24b:

$$516 \text{ kN} \leq 2 \times 1.56 \times (363 - 2 \times 34) = 920 \text{ kN} \rightarrow OK$$

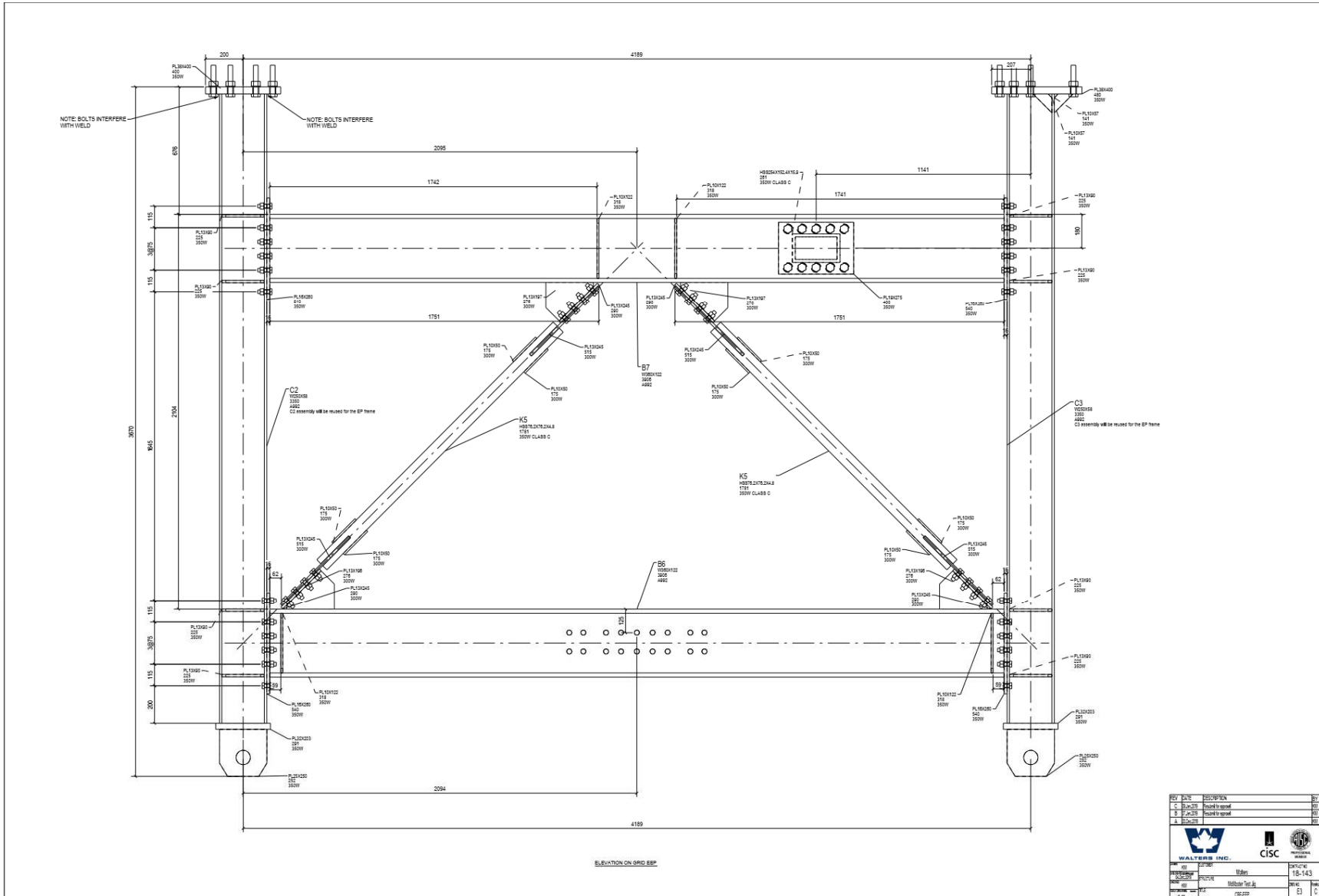
For connecting the beam flange to end-plate 10 mm fillet weld is used:

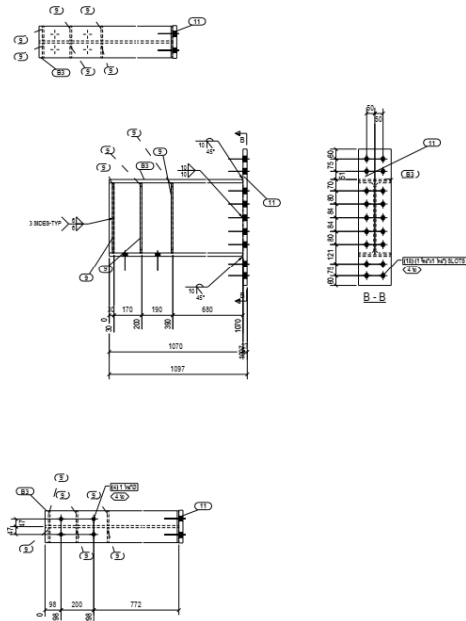
$$F_{fu} = 470.8 \leq (2 \times 257 - 13) \times 2.33 = 1167 \text{ kN}$$

Figure A-10 shows the detail of the connection.

Appendix B SCBF with RBMs Subassembly Shop Drawings

This appendix includes the shop drawings for the concentrically braced frame with replaceable brace modules from the experimental program discussed in Chapter 4.



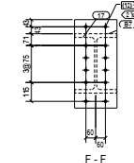
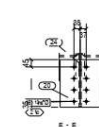
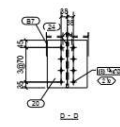
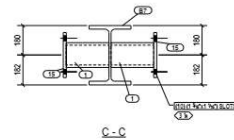
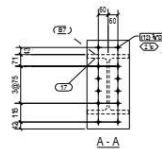
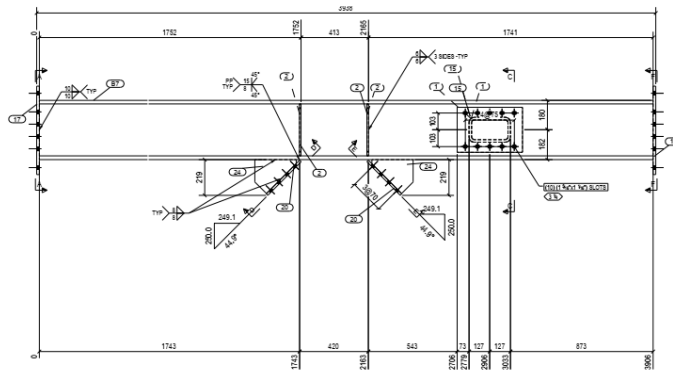
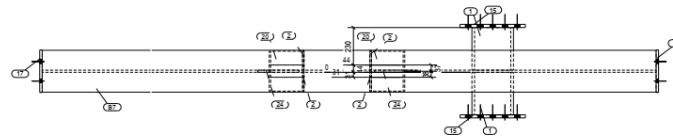


NOTE: NO OVERWELDING

MATERIAL LIST FOR ONE ASSEMBLY										ALL DATA FOR QUANTITIES TO BE DETERMINED				
QTY	MARK	DESCRIPTION	GRADE	LENGTH	REMARKS	MARK	ASB #	PROSP	PROSP	PROSP	PROSP	PROSP	PROSP	PROSP
1	B3	WALDOX	50	1070	TOP CHORD			11.1	1					
2	B3	WALDOX	50	1097	TOP CHORD			11.1	1					
3	B3	WALDOX	50	1070	TOP CHORD			11.1	1					
4	B3	WALDOX	50	1097	TOP CHORD			11.1	1					
5	B3	WALDOX	50	1070	TOP CHORD			11.1	1					
6	B3	WALDOX	50	1097	TOP CHORD			11.1	1					
7	B3	WALDOX	50	1070	TOP CHORD			11.1	1					
8	B3	WALDOX	50	1097	TOP CHORD			11.1	1					
9	B3	WALDOX	50	1070	TOP CHORD			11.1	1					
10	B3	WALDOX	50	1097	TOP CHORD			11.1	1					
11	B3	WALDOX	50	1070	TOP CHORD			11.1	1					
12	B3	WALDOX	50	1097	TOP CHORD			11.1	1					
13	B3	WALDOX	50	1070	TOP CHORD			11.1	1					
14	B3	WALDOX	50	1097	TOP CHORD			11.1	1					
15	B3	WALDOX	50	1070	TOP CHORD			11.1	1					
16	B3	WALDOX	50	1097	TOP CHORD			11.1	1					
17	B3	WALDOX	50	1070	TOP CHORD			11.1	1					
18	B3	WALDOX	50	1097	TOP CHORD			11.1	1					
19	B3	WALDOX	50	1070	TOP CHORD			11.1	1					
20	B3	WALDOX	50	1097	TOP CHORD			11.1	1					
21	B3	WALDOX	50	1070	TOP CHORD			11.1	1					
22	B3	WALDOX	50	1097	TOP CHORD			11.1	1					
23	B3	WALDOX	50	1070	TOP CHORD			11.1	1					
24	B3	WALDOX	50	1097	TOP CHORD			11.1	1					
25	B3	WALDOX	50	1070	TOP CHORD			11.1	1					
26	B3	WALDOX	50	1097	TOP CHORD			11.1	1					
27	B3	WALDOX	50	1070	TOP CHORD			11.1	1					
28	B3	WALDOX	50	1097	TOP CHORD			11.1	1					
29	B3	WALDOX	50	1070	TOP CHORD			11.1	1					
30	B3	WALDOX	50	1097	TOP CHORD			11.1	1					
31	B3	WALDOX	50	1070	TOP CHORD			11.1	1					
32	B3	WALDOX	50	1097	TOP CHORD			11.1	1					
33	B3	WALDOX	50	1070	TOP CHORD			11.1	1					
34	B3	WALDOX	50	1097	TOP CHORD			11.1	1					
35	B3	WALDOX	50	1070	TOP CHORD			11.1	1					
36	B3	WALDOX	50	1097	TOP CHORD			11.1	1					
37	B3	WALDOX	50	1070	TOP CHORD			11.1	1					
38	B3	WALDOX	50	1097	TOP CHORD			11.1	1					
39	B3	WALDOX	50	1070	TOP CHORD			11.1	1					
40	B3	WALDOX	50	1097	TOP CHORD			11.1	1					
41	B3	WALDOX	50	1070	TOP CHORD			11.1	1					
42	B3	WALDOX	50	1097	TOP CHORD			11.1	1					
43	B3	WALDOX	50	1070	TOP CHORD			11.1	1					
44	B3	WALDOX	50	1097	TOP CHORD			11.1	1					
45	B3	WALDOX	50	1070	TOP CHORD			11.1	1					
46	B3	WALDOX	50	1097	TOP CHORD			11.1	1					
47	B3	WALDOX	50	1070	TOP CHORD			11.1	1					
48	B3	WALDOX	50	1097	TOP CHORD			11.1	1					
49	B3	WALDOX	50	1070	TOP CHORD			11.1	1					
50	B3	WALDOX	50	1097	TOP CHORD			11.1	1					
51	B3	WALDOX	50	1070	TOP CHORD			11.1	1					
52	B3	WALDOX	50	1097	TOP CHORD			11.1	1					
53	B3	WALDOX	50	1070	TOP CHORD			11.1	1					
54	B3	WALDOX	50	1097	TOP CHORD			11.1	1					
55	B3	WALDOX	50	1070	TOP CHORD			11.1	1					
56	B3	WALDOX	50	1097	TOP CHORD			11.1	1					
57	B3	WALDOX	50	1070	TOP CHORD			11.1	1					
58	B3	WALDOX	50	1097	TOP CHORD			11.1	1					
59	B3	WALDOX	50	1070	TOP CHORD			11.1	1					
60	B3	WALDOX	50	1097	TOP CHORD			11.1	1					
61	B3	WALDOX	50	1070	TOP CHORD			11.1	1					
62	B3	WALDOX	50	1097	TOP CHORD			11.1	1					
63	B3	WALDOX	50	1070	TOP CHORD			11.1	1					
64	B3	WALDOX	50	1097	TOP CHORD			11.1	1					
65	B3	WALDOX	50	1070	TOP CHORD			11.1	1					
66	B3	WALDOX	50	1097	TOP CHORD			11.1	1					
67	B3	WALDOX	50	1070	TOP CHORD			11.1	1					
68	B3	WALDOX	50	1097	TOP CHORD			11.1	1					
69	B3	WALDOX	50	1070	TOP CHORD			11.1	1					
70	B3	WALDOX	50	1097	TOP CHORD			11.1	1					
71	B3	WALDOX	50	1070	TOP CHORD			11.1	1					
72	B3	WALDOX	50	1097	TOP CHORD			11.1	1					
73	B3	WALDOX	50	1070	TOP CHORD			11.1	1					
74	B3	WALDOX	50	1097	TOP CHORD			11.1	1					
75	B3	WALDOX	50	1070	TOP CHORD			11.1	1					
76	B3	WALDOX	50	1097	TOP CHORD			11.1	1					
77	B3	WALDOX	50	1070	TOP CHORD			11.1	1					
78	B3	WALDOX	50	1097	TOP CHORD			11.1	1					
79	B3	WALDOX	50	1070	TOP CHORD			11.1	1					
80	B3	WALDOX	50	1097	TOP CHORD			11.1	1					
81	B3	WALDOX	50	1070	TOP CHORD			11.1	1					
82	B3	WALDOX	50	1097	TOP CHORD			11.1	1					
83	B3	WALDOX	50	1070	TOP CHORD			11.1	1					
84	B3	WALDOX	50	1097	TOP CHORD			11.1	1					
85	B3	WALDOX	50	1070	TOP CHORD			11.1	1					
86	B3	WALDOX	50	1097	TOP CHORD			11.1	1					
87	B3	WALDOX	50	1070	TOP CHORD			11.1	1					
88	B3	WALDOX	50	1097	TOP CHORD			11.1	1					
89	B3	WALDOX	50	1070	TOP CHORD			11.1	1					
90	B3	WALDOX	50	1097	TOP CHORD			11.1	1					
91	B3	WALDOX	50	1070	TOP CHORD			11.1	1					
92	B3	WALDOX	50	1097	TOP CHORD			11.1	1					
93	B3	WALDOX	50	1070	TOP CHORD			11.1	1					
94	B3	WALDOX	50	1097	TOP CHORD			11.1	1					
95	B3	WALDOX	50	1070	TOP CHORD			11.1	1					
96	B3	WALDOX	50	1097	TOP CHORD			11.1	1					
97	B3	WALDOX	50	1070	TOP CHORD			11.1	1					
98	B3	WALDOX	50	1097	TOP CHORD			11.1	1					
99	B3	WALDOX	50	1070	TOP CHORD			11.1	1					
100	B3	WALDOX	50	1097	TOP CHORD			11.1	1					



18-143



NOTE: NO OVERWELDING

Profile: W360x122 Height = 362 Width = 267 Web #1 = 12.7 Flange #1 = 22.2

MATERIAL LIST FOR ONE ASSEMBLY		RT	TOTAL REQUIRED	1	QTY	UNIT	REMARKS
QTY	MARK	DESCRIPTION	GRADE	LENGTH	REMARKS		
0	SP	W360x122	SLC	362	Donated by S&B or RT		
1		PL 3/8x12x16	SLC	211			
2		PL 1/8x122	SLC	218			
15		PL 1/8x212	SLC	400			
17		PL 1/8x262	SLC	540			
20		PL 1/8x242	SLC	560			
2		PL 1/8x12x17	SLC	234			

ALL BOLTS SHOWN TIGHT UNLESS OTHERWISE NOTED

Refer to RLS S&B CAMBER

WALTERS INC. CISC

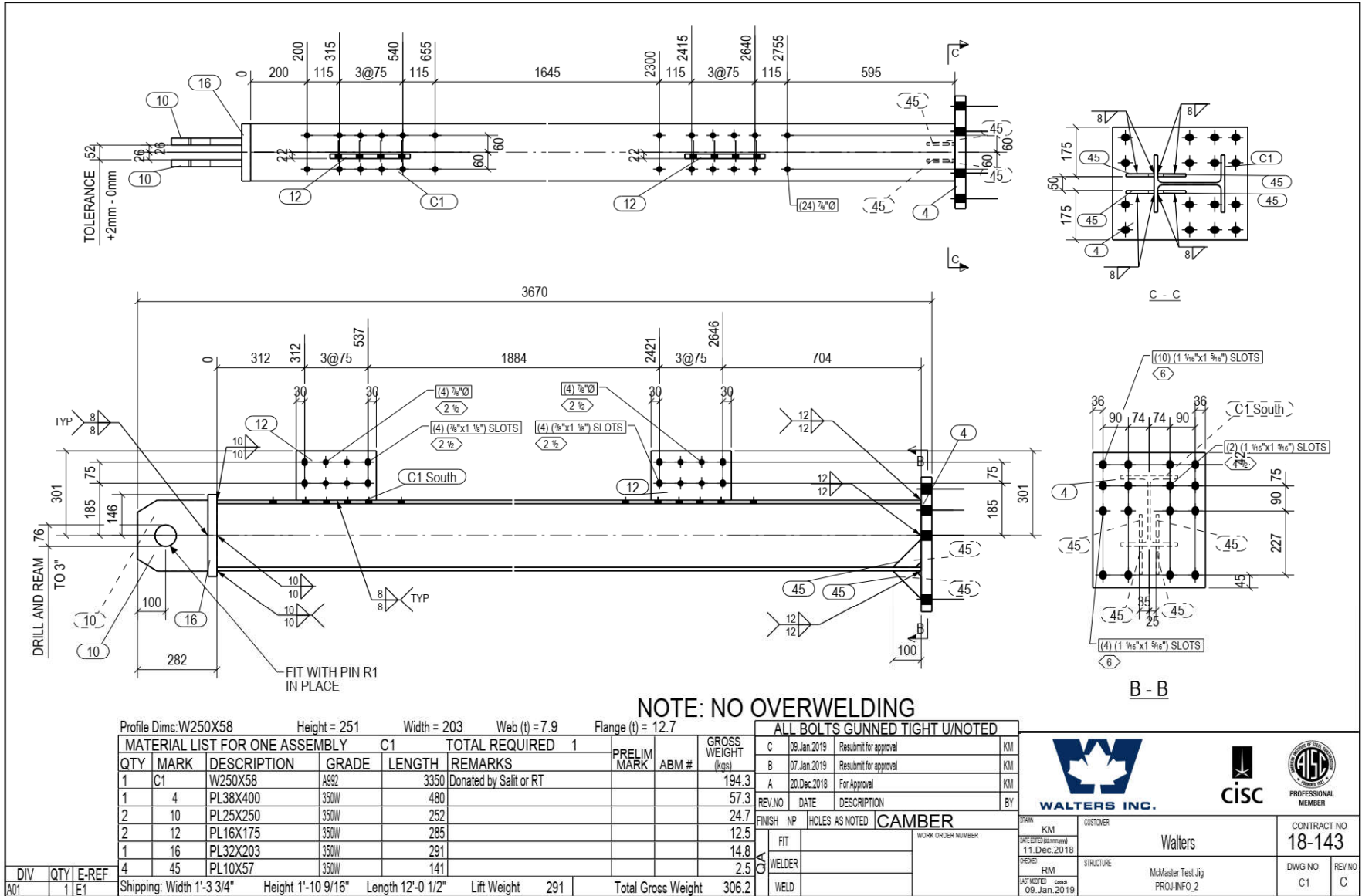
CONTRACT NO. 18-143

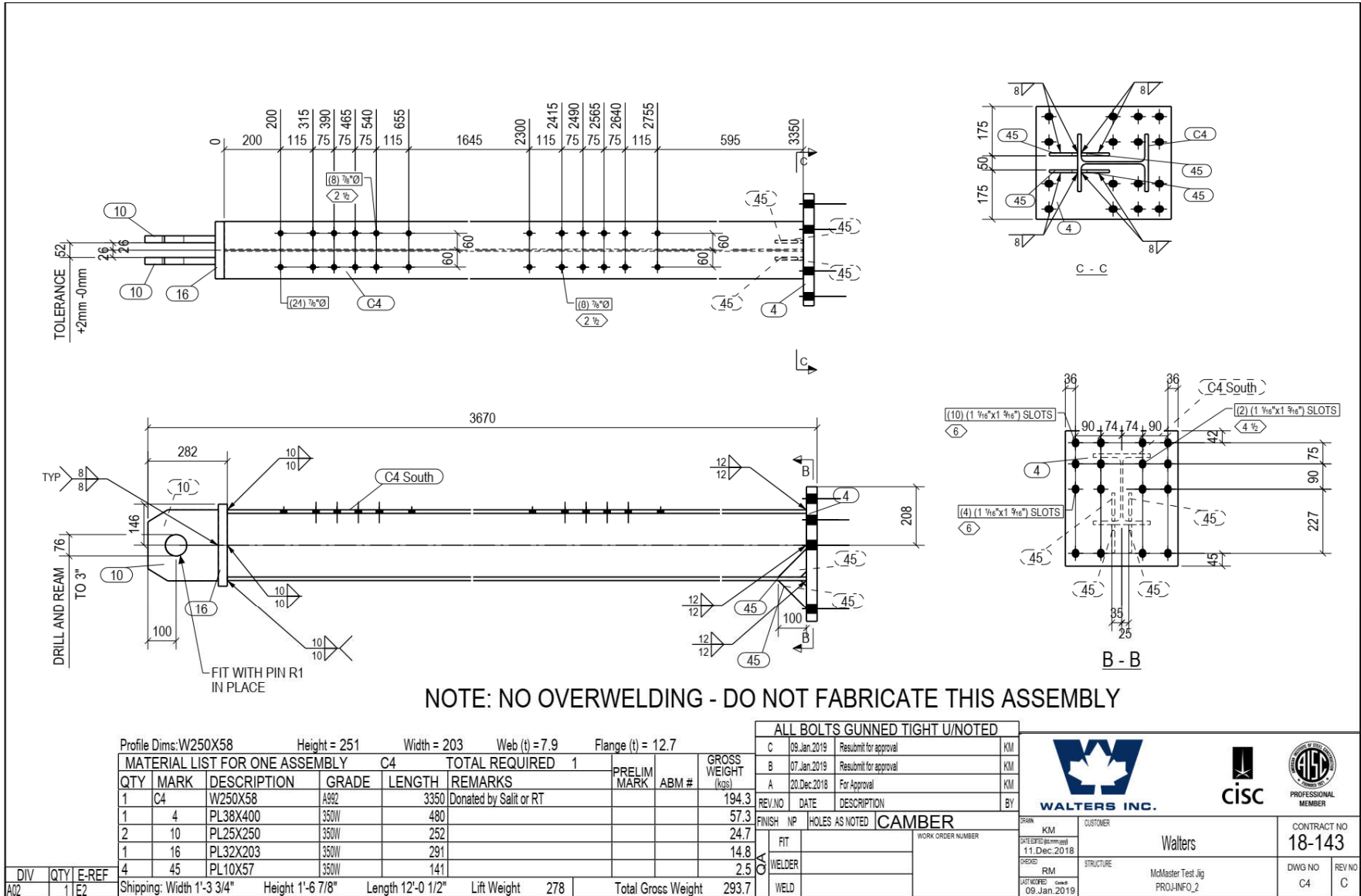
DATE: 11/26/2014

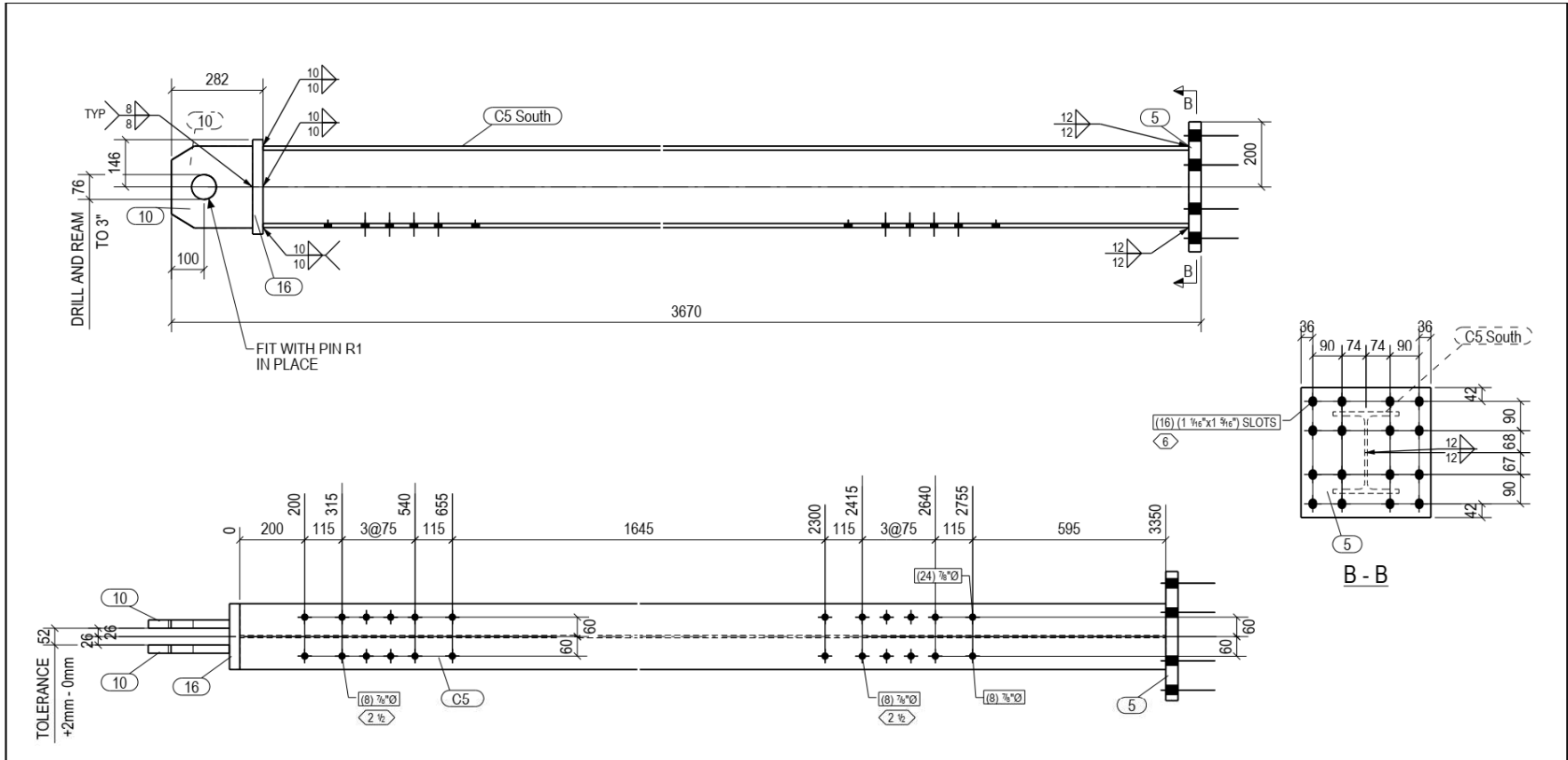
PROJECT: Water

DRAWN BY: J. C.

CHECKED BY: J. C.







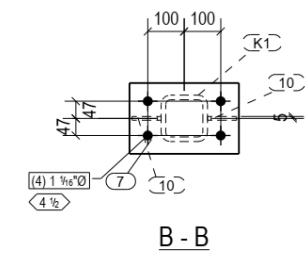
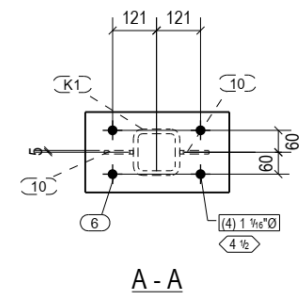
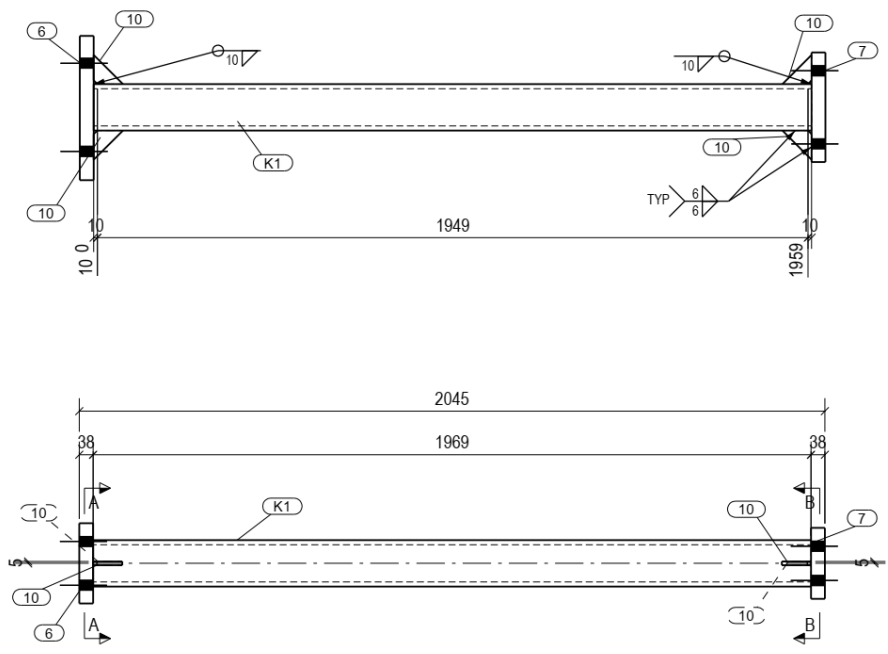
NOTE: NO OVERWELDING - DO NOT FABRICATE THIS ASSEMBLY

MATERIAL LIST FOR ONE ASSEMBLY		C5		TOTAL REQUIRED		1	
QTY	MARK	DESCRIPTION	GRADE	LENGTH	REMARKS	PRELIM MARK	ABM #
1	C5	W250X58	A992	3350	Donated by Salt or RT		
1	5	PL38X400	350W	400			
2	10	PL25X250	350W	252			
1	16	PL32X203	350W	291			

Profile Dims: W250X58	Height = 251	Width = 203	Web (t) = 7.9	Flange (t) = 12.7
Shipping: Width 1'-3 3/4"		Height 1'-3 3/4"		Length 12'-0 1/2"
Lift Weight	267	Total Gross Weight	281.6	

ALL BOLTS GUNNED TIGHT U/NOTED			
REV/NO	DATE	DESCRIPTION	BY
C	09.Jan.2019	Resubmit for approval	KM
B	07.Jan.2019	Resubmit for approval	KM
A	20.Dec.2018	For Approval	KM
FINISH: NP HOLES AS NOTED CAMBER			
WORK ORDER NUMBER			
FIT			
WELDER			
WELD			

 WALTERS INC.	 CISC <small>PROFESSIONAL MEMBER</small>
BRAN: KM CUSTOMER: Walters STRUCTURE: McMaster Test Jig PROJ: INFO_2	CONTRACT NO: 18-143 DWG NO: C5 REV NO: C



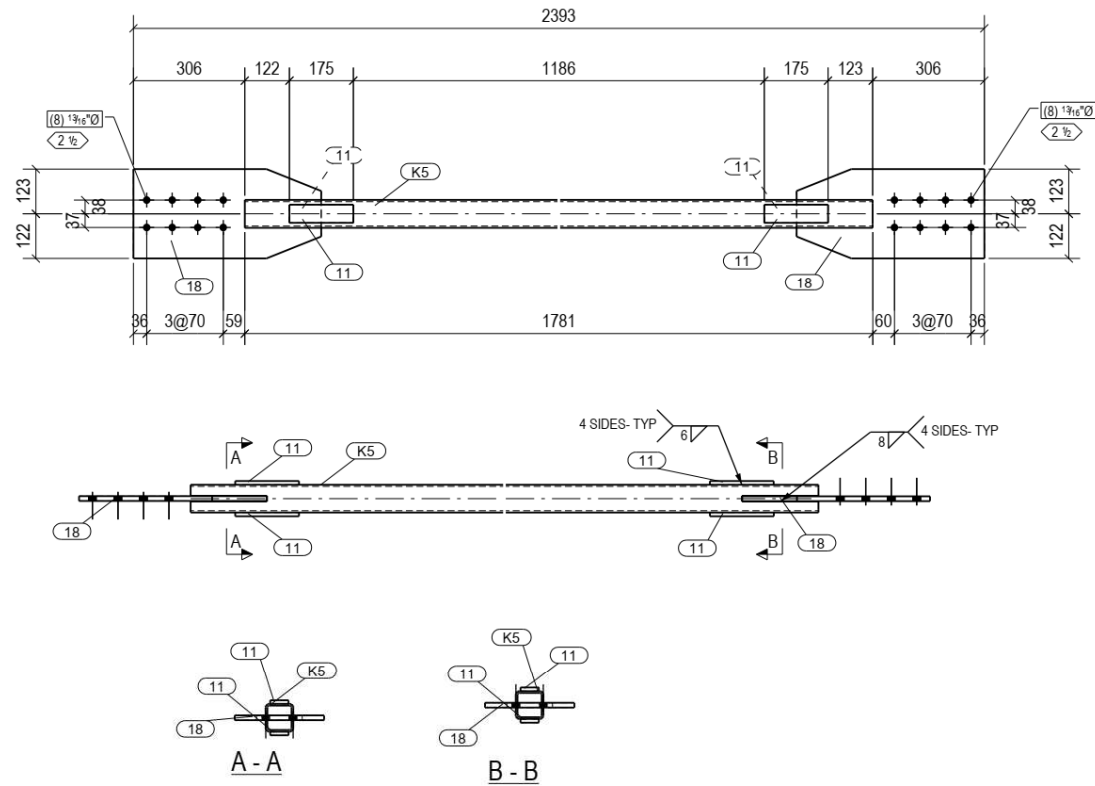
NOTE: NO OVERWELDING

MATERIAL LIST FOR ONE ASSEMBLY										K1		TOTAL REQUIRED		2	
QTY	MARK	DESCRIPTION	GRADE	LENGTH	REMARKS	PRELIM MARK	ABM #	GROSS WEIGHT (kgs)							
1	K1	HSS127X127X12.7	350W CLASS C	1969	Donated by Salt or RT			82.9							
1	6	PL38X220	350W	395				25.9							
1	7	PL38X194	350W	300				17.4							
4	10	PL10X49	350W	113				1.8							
Shipping: Width 1'-3 9/16"		Height 0'-8 11/16"		Length 6'-8 1/2"		Lift Weight 134		Total Gross Weight 127.9							

ALL BOLTS GUNNED TIGHT U/NOTED		
C	09.Jan.2019	Resubmit for approval
B	07.Jan.2019	Resubmit for approval
A	20.Dec.2018	For Approval
REV. NO	DATE	DESCRIPTION

FINISH		HOLES AS NOTED		CAMBER	
NP					
FIT					
WELDER					
WELD					

WALTERS INC.		CISC		PROFESSIONAL MEMBER	
BY	KM	CUSTOMER	Walters		
DATE	11.Dec.2018	STRUCTURE	McMaster Test Jig		
PROJECT	RM	PROJ-INFO_2			
LAST MODIFIED	20.Dec.2018	DWG NO	K1		REV NO
					C



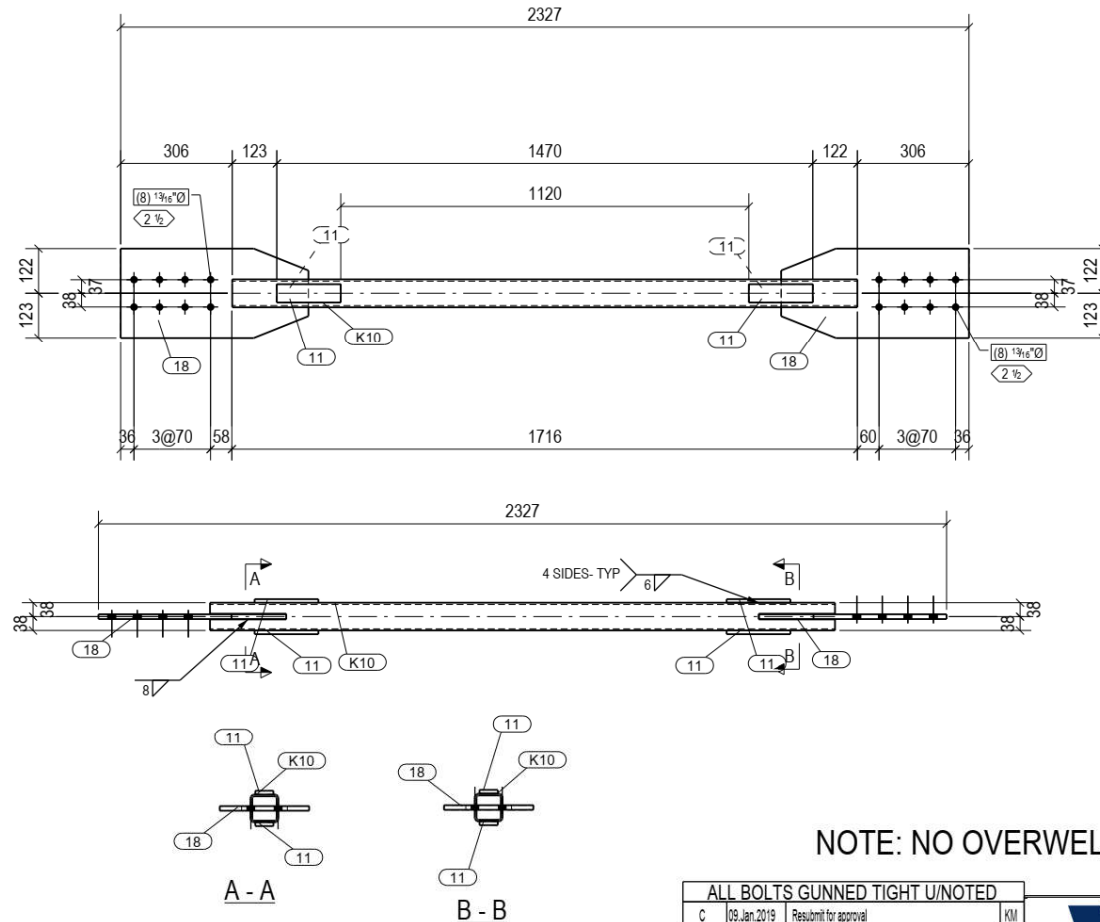
NOTE: NO OVERWELDING

MATERIAL LIST FOR ONE ASSEMBLY					K5	TOTAL REQUIRED				
QTY	MARK	DESCRIPTION	GRADE	LENGTH	REMARKS	PRELIM MARK	ABM #	GROSS WEIGHT (kgs)		
1	K5	HSS76.2X76.2X4.8	350W CLASS C	1781				18.2		
4	11	PL10X50	300W	175				2.7		
2	18	PL13X245	300W	515				25.8		
Shipping: Width 0'-9 5/8" Height 0'-3 13/16" Length 7'-10 3/16" Lift Weight					45	Total Gross Weight		46.7		

ALL BOLTS GUNNED TIGHT U/NOTED		
C	09.Jan.2019	Resubmit for approval
B	07.Jan.2019	Resubmit for approval
A	20.Dec.2018	For Approval
REV.NO	DATE	DESCRIPTION
FINISH	NP	HOLES AS NOTED
CAMBER		
WORK ORDER NUMBER		
FIT		
WELDER		
WELD		

 WALTERS INC.		 CISC <small>PROFESSIONAL MEMBER</small>	
BRAN: KM CUSTOMER: Walters		CONTRACT NO: 18-143	
DESIGNED: [Signature] 11.Dec.2018		STRUCTURE: McMaster Test Jig PROJ:INFO_2	
DRAWN: RM 20.Dec.2018		DWG NO: K5 REV NO: C	

DIV	QTY	E-REF
A03	4	E3



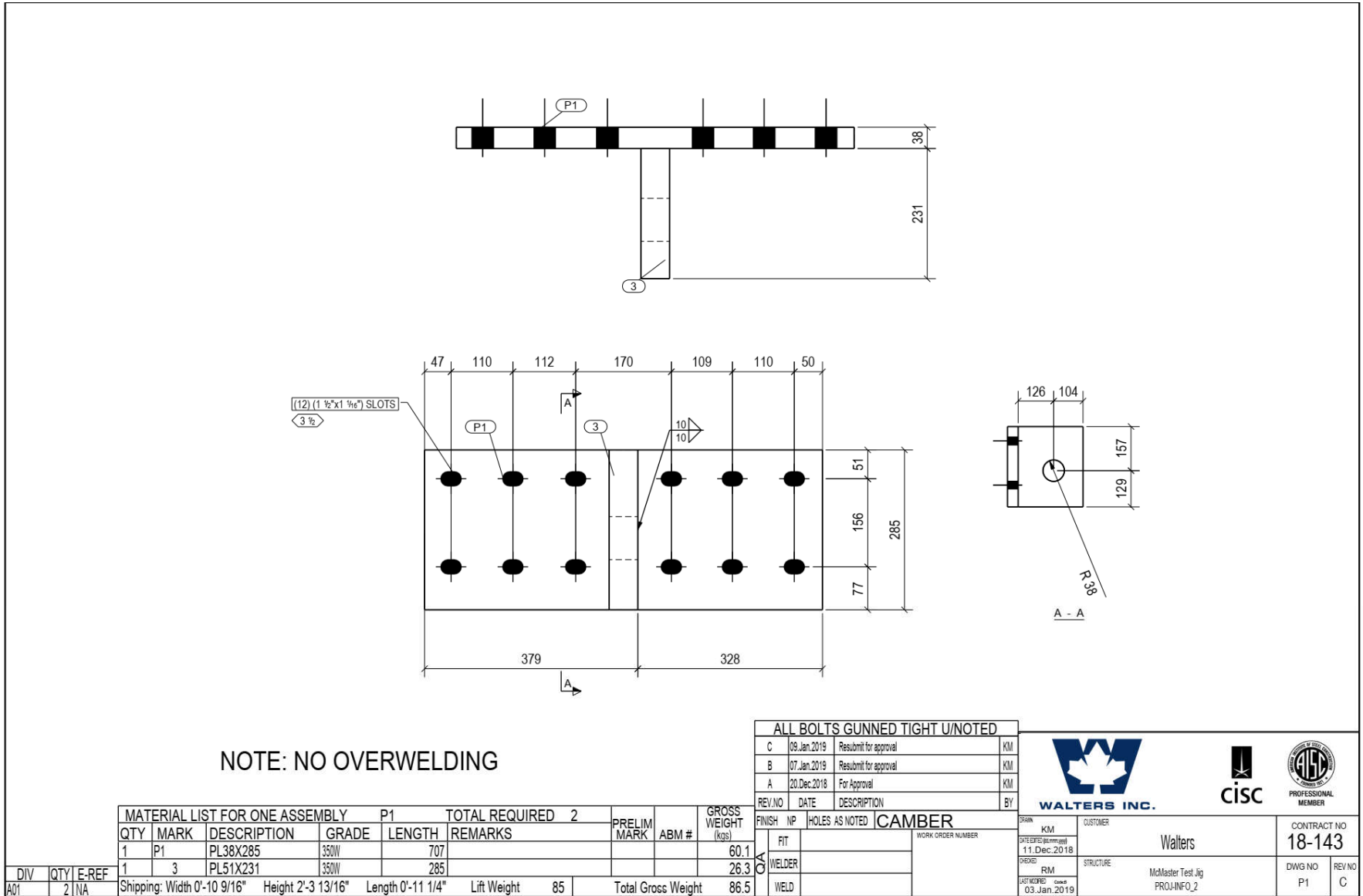
NOTE: NO OVERWELDING

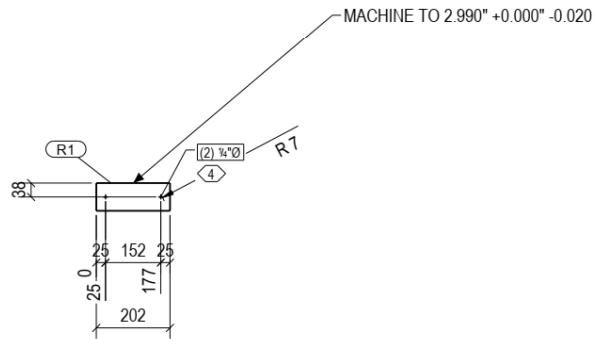
MATERIAL LIST FOR ONE ASSEMBLY						K10	TOTAL REQUIRED	4
QTY	MARK	DESCRIPTION	GRADE	LENGTH	REMARKS	PRELIM MARK	ABM #	GROSS WEIGHT (kgs)
1	K10	HSS76.2X76.2X4.8	350W CLASS C	1715	Donated by Salit or RT			17.5
4	11	PL10X50	300W	175				2.7
2	18	PL13X245	300W	515				25.8
Shipping: Width 0'-9 5/8" Height 0'-3 13/16" Length 7'-7 5/8" Lift Weight						45	Total Gross Weight	46.0

ALL BOLTS GUNNED TIGHT U/NOTED			
REV. NO	DATE	DESCRIPTION	BY
C	09.Jan.2019	Resubmit for approval	KM
B	07.Jan.2019	Resubmit for approval	KM
A	20.Dec.2018	For Approval	KM
FINISH	NP	HOLES AS NOTED	CAMBER
FIT			WORK ORDER NUMBER
WELDER			
WELD			

 WALTERS INC.		 CISC		 PROFESSIONAL MEMBER	
BRAN: KM CUSTOMER: Walters		STRUCTURE: McMaster Test Jig PROJ:INFO_2		CONTRACT NO: 18-143 DWG NO: K10 REV NO: C	
DRESSES (R/mm/yyyy): 11.Dec.2018 PENDER: RM LAST MODIFIED (mm.d/yyyy): 20.Dec.2018					

DIV	QTY	E-REF
A01	4	E1





NOTE: NO OVERWELDING

MATERIAL LIST FOR ONE ASSEMBLY							R1	TOTAL REQUIRED	2	PRELIM MARK	ABM #	GROSS WEIGHT (kgs)		
QTY	MARK	DESCRIPTION	GRADE	LENGTH	REMARKS									
1	R1	RND76	350W	202								7.0		
Shipping: Width 0'-3"							Height 0'-3"	Length 0'-7 15/16"	Lift Weight	7	Total Gross Weight			7.0

ALL BOLTS GUNNED TIGHT U/NOTED		
C	09.Jan.2019	Resubmit for approval
B	07.Jan.2019	Resubmit for approval
A	20.Dec.2018	For Approval
REV. NO	DATE	DESCRIPTION

					
Walters Inc.		CISC		PROFESSIONAL MEMBER	
FINISH	NP	HOLES AS NOTED	CAMBER		
DRN	KM	CUSTOMER	Walters		
DRAWN	11.Dec.2018	CONTRACT NO	18-143		
DRAWN	11.Dec.2018	STRUCTURE	McMaster Test Jig		
DRAWN	11.Dec.2018	PROJ. INFO	PROJ-INFO_2		
DWG NO	R1	REV NO	C		

Appendix C Experimental Study Instrumentations

This appendix describes what instruments were used, where they were located and what they were intended to measure. Three different types of gauges were used to make measurements in the experimental study presented in Chapter 4: linear variable displacement transducers (LVDT), string potentiometers (pots), and strain gauges.

The generalized location of instrumentation is shown in Figure C-1.

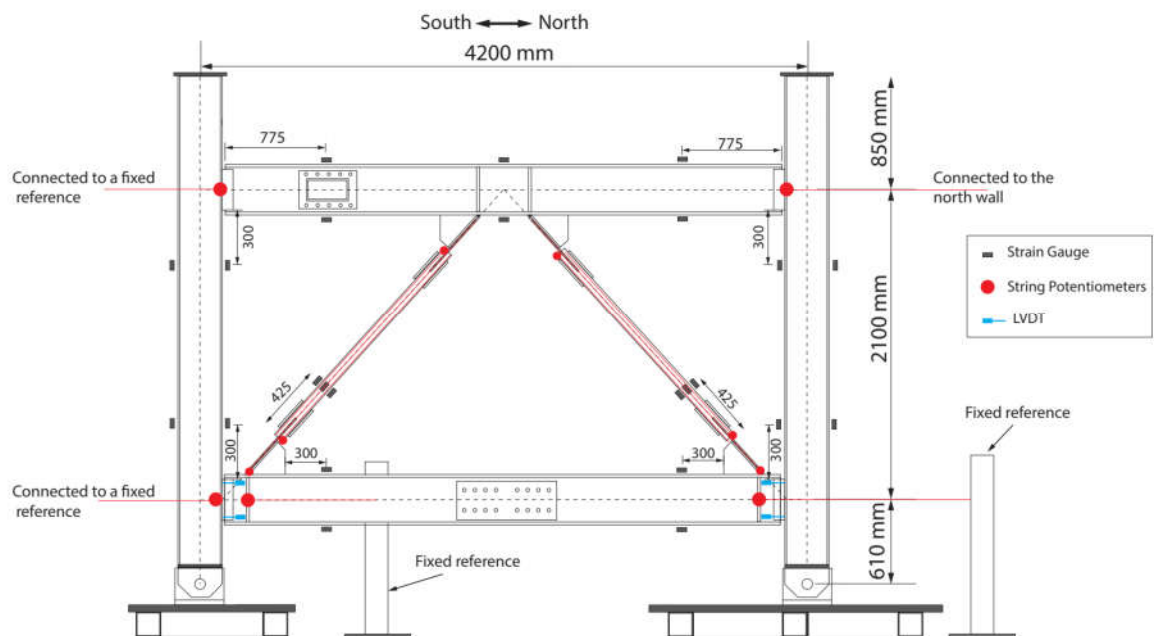


Figure C-1 Instrumentation setup (Dimensions are in mm)

The gauges and their respective purposes are summarized in Table C.1.

Table C.1 Type of instruments

Type	Range (Total, mm)	Required Numbers	Purpose
String pots	200	2	Top storey drift
String pots	50	3	Bottom storey drift
String pots	100	2	Brace elongation
String pots	200	4	Brace IP displacements
String pots	50	2	Horizontal Brackets (To monitor torsional movement, if it happens)
LVDT	50	4	Bottom storey beam-column connection rotation
LVDT	50	4	Hinge plate rotation
Strain gauges		26	Beam, column, brace strains

C.1 Hinge Plate Rotation

For every hinge plate, the rotation was determined using a LVDT mounted to the stiffener plate. Figure C-2 shows a picture of lower-south hinge plate connection. The hinge plate rotation was determined using the outputs of the LVDTs and normalizing them by their relative distance from either the center of the bolts or end of the support plate to the LVDT's tip, considering the fold line in the hinge plate.

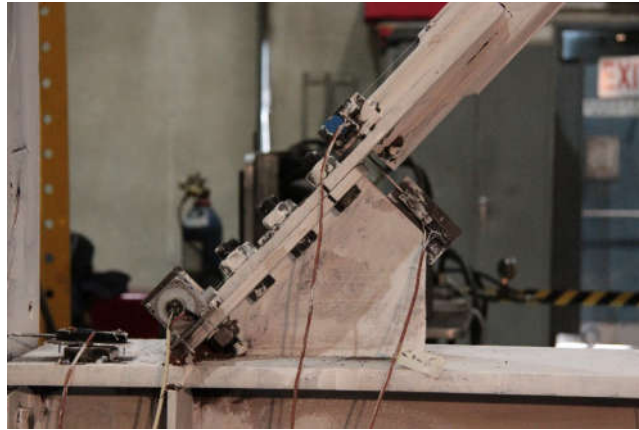


Figure C-2 Lower-south hinge plate connection

C.2 Brace Center Displacement

To measure the in-plane displacement of braces, two string pots were placed parallel to the brace. Each string pot was attached to one end of the brace and on the other end the string pot was tied off to a screw using fishing tacking line. At the center of the brace there was a pivot plate with two pivot screws coming out of it, as shown in Figure C-3. This plate was attached to the brace using two zip ties.



Figure C-3 Parallel brace displacement string pots and pivot plate setup

When the brace buckles, one string pot remains straight and can measure the brace shortening, and the other spring pot moves along with the brace. Therefore, the brace buckled displacement can be determined using the Pythagorean Theorem. Figure C-4 shows the relationships between the reading data from string pots.

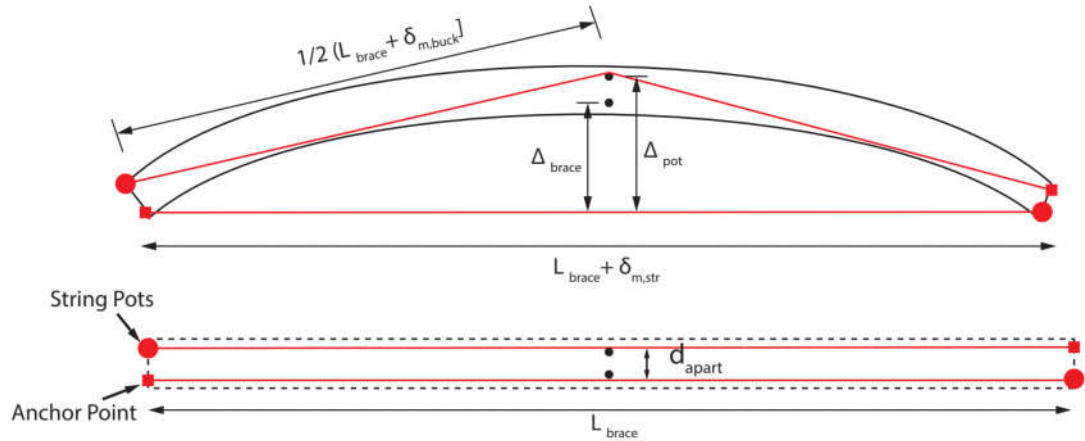


Figure C-4 Brace center displacement method

In Figure C-4, Δ_{brace} is the brace buckled displacement, $\delta_{m,bruck}$ and $\delta_{m,str}$ are the measurements recorded by the string pot for the buckling string pot and the straight string pot, respectively.

$$\Delta_{pot} = \sqrt{\left\{ \frac{1}{2} [L_{brace} + \delta_{m,bruck}] \right\}^2 - \left\{ \frac{1}{2} [L_{brace} + \delta_{m,str}] \right\}^2} \quad (C-1)$$

However, the brace displacement (Δ_{brace}) is not equal to the pot displacement (Δ_{pot}) because the brace displacement should be measured from a consistent reference point. Therefore:

$$\Delta_{brace} = \Delta_{pot} - d_{apart} \quad (C-2)$$

C.3 Frame Inter-Storey Drift

The frame inter-storey drift was measured using string pots. The inter-storey drift was measured by placing two string pots at each end of the top and bottom beams, as seen in Figure C-1.

C.4 Beam-to-Column Connection Rotation

The beam-to-column connection rotation on the lower beam was measured using two 50 mm LVDTs. The output from the two LVDTs could be subtracted and normalized by the distance between the two gauges to determine the connection rotation. Figure C-5 shows the exact detail of the placement of the LVDTs for the three considered connections.

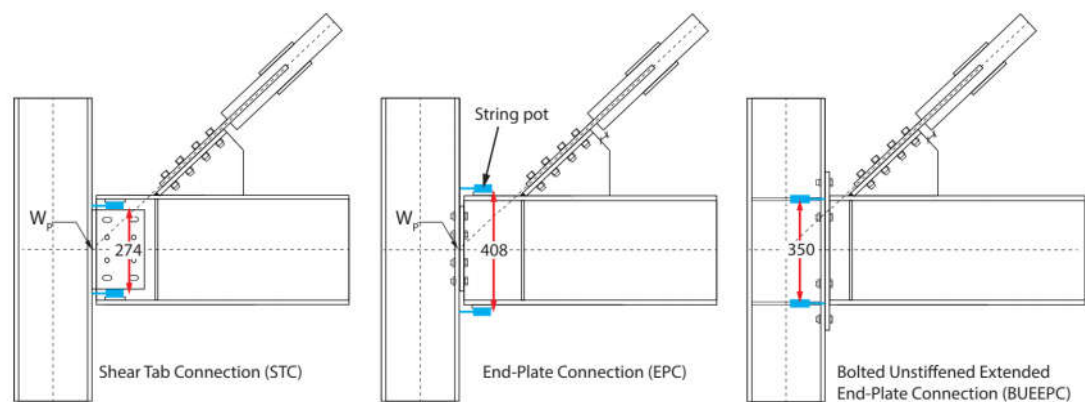


Figure C-5 Connection rotation setup

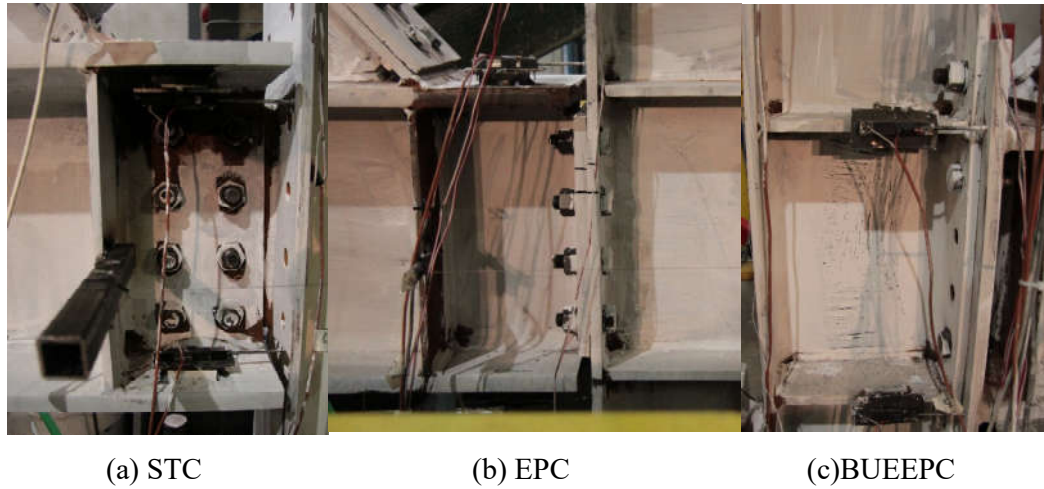


Figure C-6 Connection rotation setup pictures

C.5 Strain Gauges

Strain gauges were placed on the beams, columns and braces to determine shears, moments and axial forces. On the beams and columns, the strain gauges were placed in the elastic region as can be seen in Figure C-1. Strain gauges were also placed at the quarter-point of every brace in order to determine the brace force prior to brace yielding.

C.5.1 Brace Axial Force

The axial force in the braces was determined by averaging the strains measured in the four strain gauges using Equation C-3.

$$P_{brace} = \frac{\varepsilon_1 + \varepsilon_1 + \varepsilon_1 + \varepsilon_1}{4} EA \quad (C-3)$$

where ε is the strain recorded by strain gauge, E is the modulus of the elasticity and A is the cross sectional area of the brace.

C.5.2 Column Forces

The strain gauges were always mounted in sets of four, as shown in Figure C-7. The strain profile along the member depth could be determined at two different locations. This permitted to determine the column axial force, moments and shear forces.

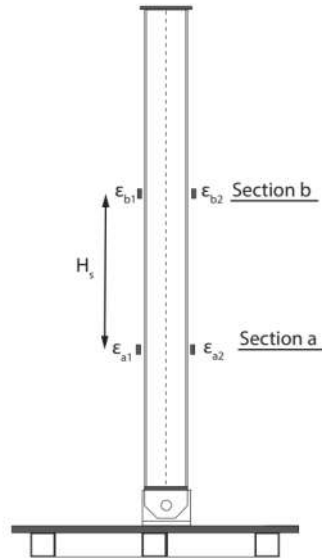


Figure C-7 Column force determination figure

$$P_{column} = \frac{\varepsilon_{a1} + \varepsilon_{a2} + \varepsilon_{b1} + \varepsilon_{b2}}{4} AE \quad (C-4)$$

$$M_a = \left(\frac{\varepsilon_{a1} - \varepsilon_{a2}}{d_c} \right) EI \quad (C-5)$$

$$M_b = \left(\frac{\varepsilon_{b1} - \varepsilon_{b2}}{d_c} \right) EI \quad (C-6)$$

$$V_{column} = \frac{M_b - M_a}{H_s} \quad (C-7)$$

C.6 Data Acquisition System

PI660 version 10 was used to control the Pacific Series 6000 data acquisition system. The 6035 modules and 6013 modules were used for strain gauges and potentiometers,

respectively. Each module has eight channels of programmable transducer signal conditioning amplifiers and digitizer. PI660 scanned data channels and converted measured voltage to appropriate physical quantities before being recorded to the data file. Measurements of voltage from the potentiometers were converted to units of mm by using an appropriate calibration factor corresponding to a given potentiometer. Strain gauges were configured using a two-wire quarter-bridge circuit and readings from the strain gauges were converted to units of micro strain using a built-in function of PI660. Readings from the instruments were recorded at 20 Hz during testing to a tab-delimited file. Data was then processed for analysis using Microsoft Excel and Matlab.

C.7 Actuator and Reaction Frame

A hydraulic actuator was used to apply the lateral load force and displacement history to each specimen. The actuator used in this experimental study had a nominal stroke of ± 250 mm and a nominal tensile and compressive capacity of 1000 kN. The actuator was connected to a loading frame that transferred the load to the top beam. The loading frame beams were connected by plates with slotted holes to the loading frame columns using detail shown in Figure C-8. This detail can accommodate the rotation of the beams relative to the columns in the loading frame under large drifts and transfer the load from the actuator to the specimen.

In order to control the stability of the stiff-strong beam, two out-of-plane hydraulic cylinders were used. As shown in Figure C-9 each cylinder had a load cell for measuring the force. Figure C-10 is showing the connection that were used for connecting the load cell to the beam on one side and to the strong vertical column on the other side. The connection was detailed to accommodate the expected displacement of the beam without providing any horizontal resistance in the plane of testing. Laser displacement transducers were used to measure the out-of-plane displacement and hold the beam at its initial position.



Figure C-8 Loading frame beam-column connections

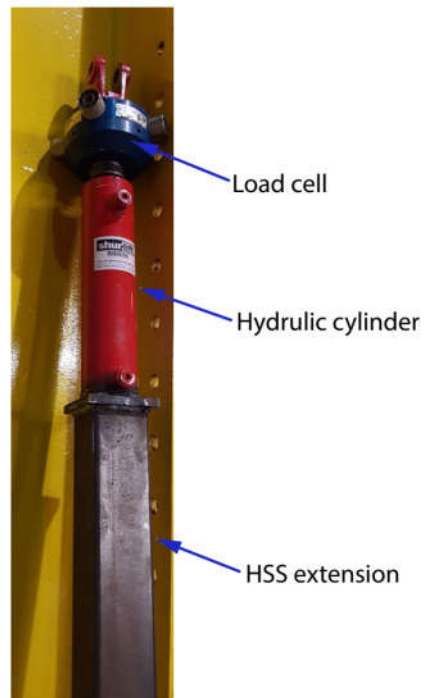


Figure C-9 Out-of-plane implement cylinder details



(a)



(b)

Figure C-10 End connection details of the out-of-plane implement cylinder